Enhanced Emission Prediction Modeling and Analysis for Conceptual Design

A Final Report to
NASA GLENN RESEARCH CENTER
21000 BROOKPARK ROAD
CLEVELAND OH 44135-3191

NASA Grant Number NNX07AO08A

Period of Performance:
18 August 2007 – 17 August 2010

Submitted by:

Dr. Dimitri Mavris, Principal Investigator

Aerospace Systems Design Laboratory
Daniel Guggenheim School of Aerospace Engineering
Georgia Institute of Technology
Atlanta, GA
www.asdl.gatech.edu

17 November 2010

Executive Summary

The combustor emissions prediction research reported herein was conducted from August 2007 through August 2010 under NASA grant number NNX07AO08A. The technical monitor was Mr. William Haller, NASA Glenn Research Center. The research is an outgrowth of a proof-of-concept study performed as part of the NASA/DoD University Research and Engineering Technology Institute (URETI) on Aero-propulsion and Power Technology (UAPT) during 2006-2007.

The goal of the present research is to develop an emissions prediction procedure for use in the conceptual design phase. The approach is to use simplified physics-based models to bridge the gap between the empirical and high fidelity approaches. The new approach will provide the capability to perform design trades at the conceptual level and to quickly predict emissions as the engine cycle and architecture are parametrically varied.

The emissions prediction approach is a modeling process consisting of three main elements: (1) an object-oriented one dimensional (1-D) flow model to provide a simple, common procedure for modeling different types of advanced combustors, (2) a chemical reactor network (CRN) model representative of the combustor flowfield, and (3) an emissions regression model to speed up the calculations when a large number of parametric variations are desired.

The research presented herein has successfully developed and demonstrated an emissions prediction capability for systems-level analysis during *conceptual design.* The new capability has infused more physics-based effects into the emissions predictions, such as unmixedness, droplet evaporation, rich burning, and lean burning. In addition, a library of NPSS elements has been developed to model combustors in more detail, explicitly taking into account the diffuser, the primary zone, the secondary or mixing zone, and the dilution zone. The new capability was demonstrated for three types of combustors: a conventional single annular combustor, a Rich-Quench-Lean type of advanced combustor, and a Lean-Burn type of advanced combustor. The new NPSS elements allow parametric modeling of these types of combustors.

Research Team

- Prof. Dimitri Mavris - PI
- Dr. Jimmy Tai – SRE
- Mr. Russell Denney – RE II
- Dr. Ping Yang – Post Doc
- William Bowden
    - Single Annular Combustor (third year)
- Alexis Brugere
    - 1-D flow model (first year)
- Haoyun Fu
    - Rich-Quench-Lean Regression Models
- Ian Gillis
    - Parametric Modeling
- Colin Leclercq
    - 1-D flow model (second year)
- Mark Nelson
    - Lean-Burn Combustor
- Reza Rezvani
    - URETI project
    - Single Annular Combustor (first and second years)
    - Rich-Quench-Lean Combustor
- Miguel Walter
    - Combustion Mechanism

Table of Contents

List of Figures

List of Tables

1 Introduction

The combustor emissions prediction research reported herein was conducted from August 2007 through August 2010 under NASA grant number NNX07AO08A. The technical monitor was Mr. William Haller, NASA Glenn Research Center. The research is an outgrowth of a proof-of-concept study performed as part of the NASA/DoD University Research and Engineering Technology Institute (URETI) on Aero-propulsion and Power Technology (UAPT) during 2006-2007.

Objective

Future stringent aircraft emissions regulations increase the need for an emissions prediction capability suitable for application during the aircraft/engine conceptual design phase, in order to support system level assessments with the capability to model various advanced combustor types with parametric variations in the combustor geometry as the engine architecture and/or the engine thermodynamic cycle is varied parametrically.

Current emissions prediction approaches depend upon empirical or semi-empirical relations which are unique to a specific combustor geometry and type and therefore are not useful for parametric design studies. The alternative to empirical models, high fidelity simulation based upon computational fluid dynamics (CFD), requires detailed simulation of the combustor 3-D geometry, the turbulent flowfield, and chemical kinetics. The run time and computing requirements for CFD are too great for parametric design studies. Thus neither approach is suitable for consideration of parametric variations as are needed for conceptual level analysis.

The goal of the present research is to develop an emissions prediction procedure for use in the conceptual design phase. The approach is to use simplified physics-based models to bridge the gap between the empirical and high fidelity approaches. The new approach will provide the capability to perform design trades at the conceptual level and to quickly predict emissions as the engine cycle and architecture are parametrically varied.

Approach

The emissions prediction approach is a modeling process consisting of three main elements: (1) an object-oriented one dimensional (1-D) flow model to provide a simple, common procedure for modeling different types of advanced combustors, (2) a chemical reactor network (CRN) model representative of the combustor flowfield, and (3) an emissions regression model to speed up the calculations when a large number of parametric variations are desired. These elements are illustrated in Figure 1 below.

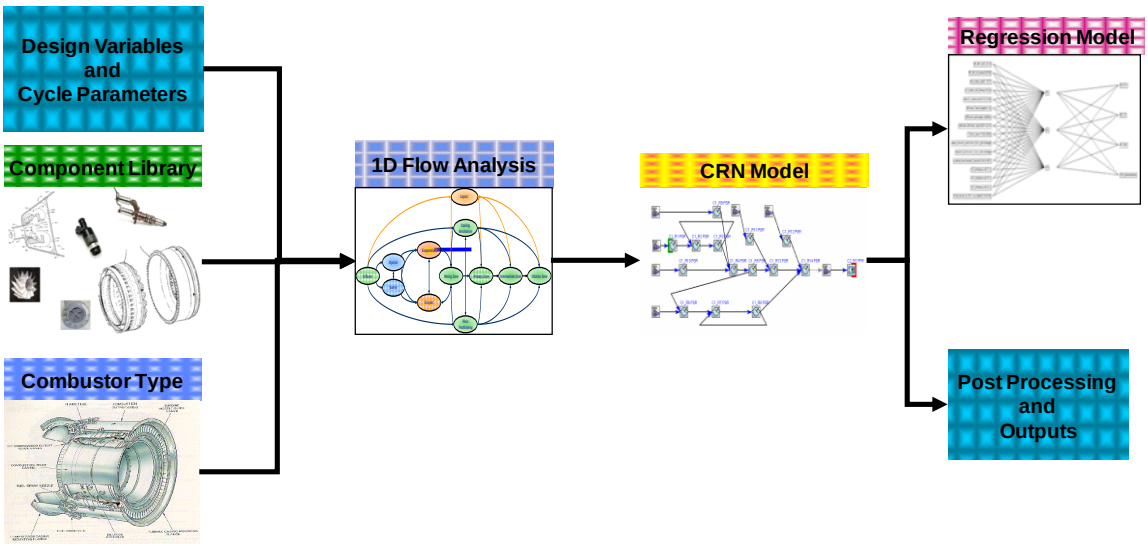

Figure 1: Combustor Modeling Overall Approach

The overall goal of this approach is to enable the modeling of any combustor type with a common methodology and minimal reprogramming. For example, the object-oriented 1-D flow model should permit the modeling of both single- and dual-annular combustors (see below):

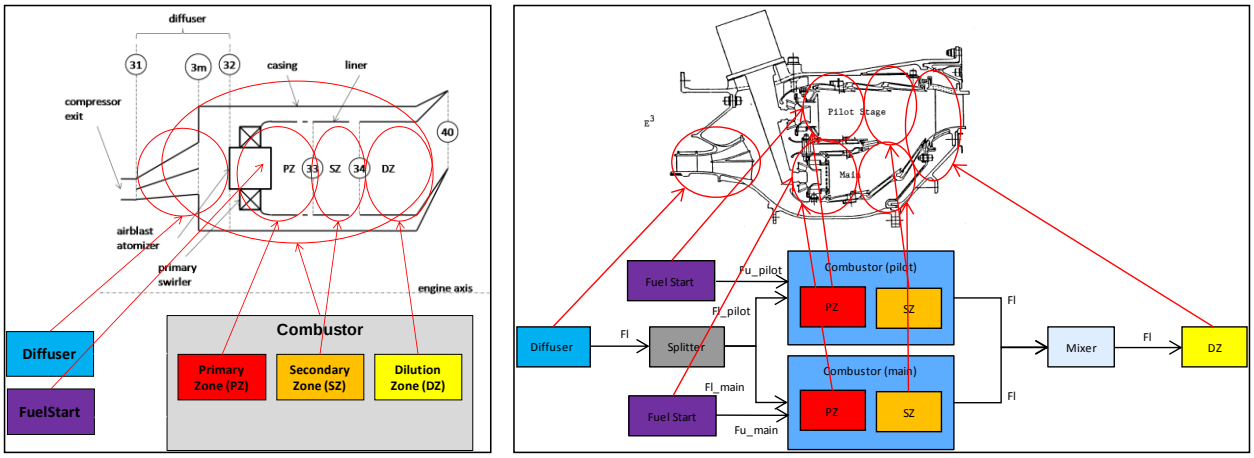

Figure 2: Notional SAC model (left) and DAC model (right)

The 1-D flow model and the regression model are developed using the NASA Numerical Propulsion System Simulation (NPSS) and the elements are intended to be incorporated directly into any NPSS turbine engine model. The 1-D flow model accepts inputs from the upstream components in the engine model, in addition to user inputs describing the combustor geometry, and provides outputs to the downstream engine components, the CRN, and the emissions regression model.

It may be helpful to think of the emissions prediction model in two different modes of operation, the "user mode" and the "developer mode". From the user's perspective, as illustrated in Figure 3, the usual Burner element in an NPSS model is replaced by the 1-D flow model, which comprises a new Diffuser element and a Combustor element. The Combustor element contains

sockets representing the different parts of the combustor, such as the primary zone (PZ), secondary zone (SZ), and dilution zone (DZ), as well as the regression model (neural net). The engine model in this configuration may be run as part of a parametric aircraft/engine conceptual design study.

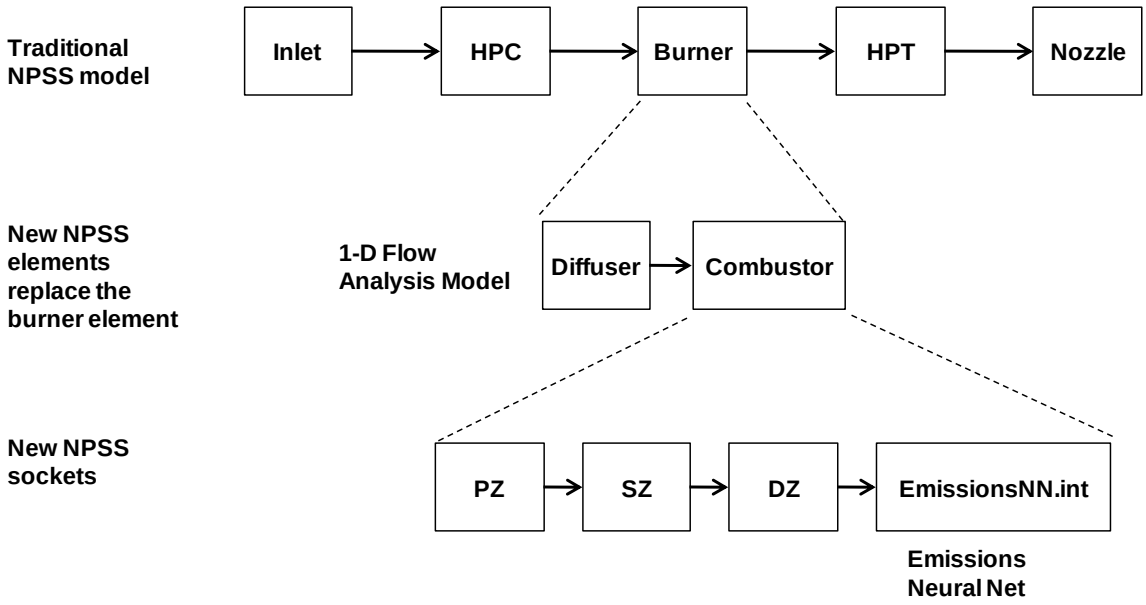

Figure 3: Emissions Prediction Model from the User's Perspective

From the developer's perspective, in order to first create the emissions regression model for a given design study, the emissions prediction model must be linked to the chemical reactor network and executed repeatedly using a design of experiments technique. In this case, the NPSS model is linked with CHEMKIN, which is used to model the chemical reactor network. The process for developing the emissions regression model is illustrated in Figure 4 below.

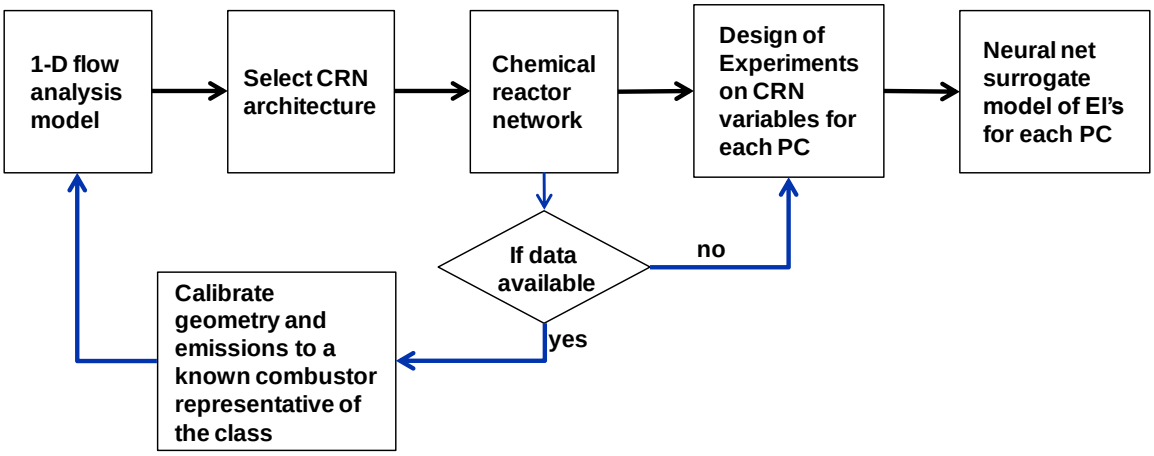

Figure 4: Emissions Prediction Model from the Developer's Perspective

Due to the complexity of the CHEMKIN model, fileWrappers are provided to link the two codes using ModelCenter, and NPSS elements are provided to automatically calculate and compile the required CHEMKIN inputs.

Methodology

To develop the emissions prediction model described above, three representative combustor architectures were selected for modeling: a conventional single-annular combustor, a Rich-Quench-Lean type of advanced combustor, and a Lean-Burn type of advanced combustor. Models for each combustor type were developed and validated against available data. Then, to demonstrate the parametric capability of the models, a combustor of each type was created to operate in the CFM56 engine cycle and size class. Finally, regression models were created for this representative CFM56-size engine application for each combustor type. Results are compared to published data. The methodology flowchart is presented in Figure 5 below.

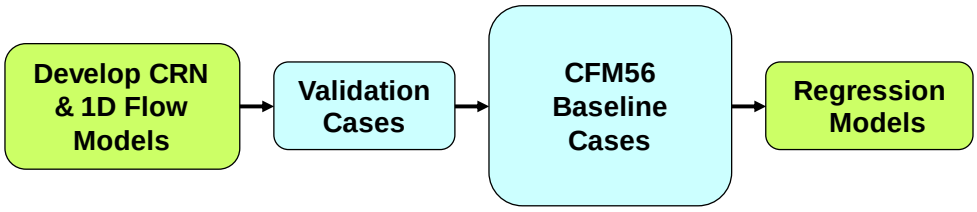

Figure 5: Modeling Methodology Flowchart

2 Combustors Modeled

Three representative combustor architectures were selected for modeling: a conventional single-annular combustor (SAC), a Rich-Quench-Lean (RQL) type of advanced combustor, and a Lean-Burn type of advanced combustor.SAC.

SAC

A typical conventional SAC is illustrated in Figure 6 below. In this type of combustor, the primary zone is designed for stoichiometric burning for maximum efficiency and flame stability. Unfortunately, burning at such high temperatures results in high NOx and CO emissions. Intermediate or secondary air is added downstream to complete the combustion process and reduce the CO emissions [28]. Finally, dilution air is added to control the temperature level and distribution entering the turbine.

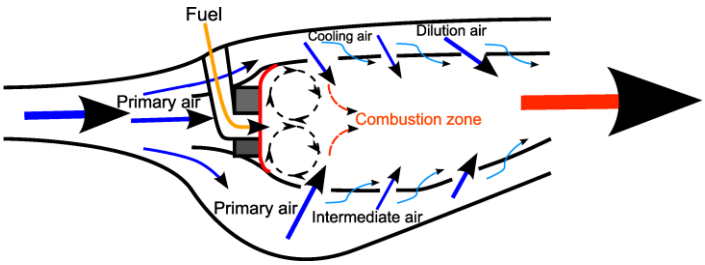

Figure 6: Conventional Single-Annular Combustor [24]

The SAC model for the present research is based on published data for the GE Energy Efficient Engine (E3) prototype combustor [5]. The E3 combustor is used for the validation case, and the CFM56-7B27 engine is used as the baseline case for emissions regression model.

RQL

The concept of the RQL combustor involves bypassing the high temperature stoichiometric burning region by initial burning at rich conditions followed by quick quenching of the hot gases and completion of burning at lean conditions. The combustion process is illustrated in Figure 7 below.

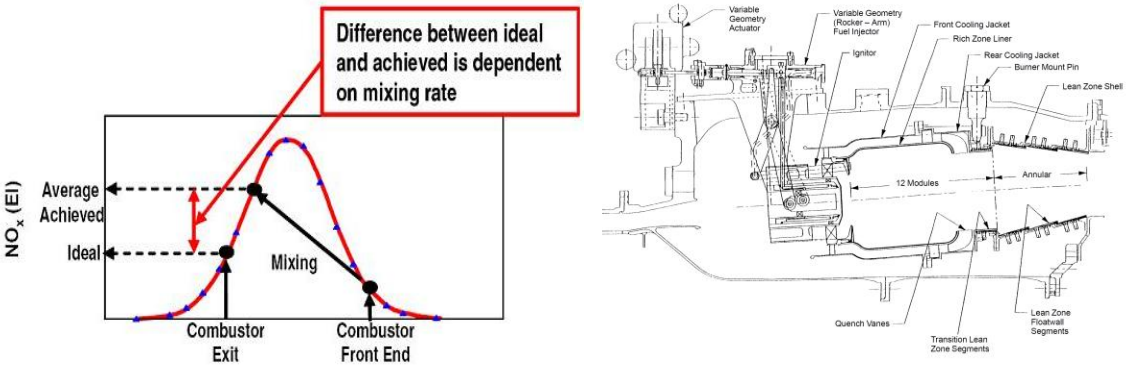

Figure 7: Example Rich-Quench-Lean Combustor [44]

Successful performance of the RQL concept depends upon good atomization, quick mixing, a uniform mixture, and avoidance of stoichiometric burning at all power settings. This last requirement may necessitate the use of variable geometry or fuel shifting concepts [44].

The RQL model considered in the present research is validated against published data from the NASA High-Speed Research (HSR) project [44]. The validated model is then adapted to the CFM56-7B27 engine operating conditions and this is used as the baseline case for the emissions regression model.

Lean-Burn

The Lean-Burn combustor investigated in this research is a notional combustor similar to the GE Twin-Annular Premixed Swirler (TAPS) combustor. The GE TAPS combustor is illustrated in Figure 8 below. In this combustor, the primary zone is lean to keep temperatures and NOx emissions low. This results in a challenging condition for flame stability. To promote stability, there are two co-annular swirling jets produced by the pilot and the main mixer. Also, fuel staging is used within the fuel nozzle to control the fuel distribution from 100% through the pilot at low power to 5-10% at max power. Cooling air is provided for the liner and combustor dome only.

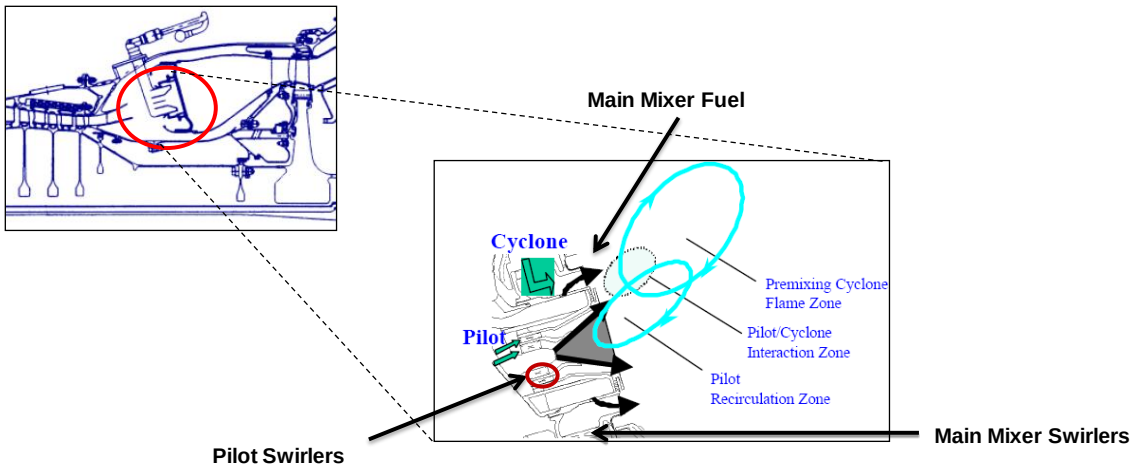

Figure 8: Example Lean-Burn Combustor [39]

The Lean-Burn combustor considered in the present study is validated against published data for the ONERA multi-point combustor [33]. The validated model, adapted to the CFM56-7B27 engine operating conditions, is then used as the baseline case for the emissions regression model.

3 Chemical Reactor Network Development

The combustor flow field is simulated by a network of idealized chemical reactors representing the different controlling reaction processes in the different combustion zones. The concept of network of reactors is based on partitioning the combustor flow-field into the regions in which the flow field and combustion has specified characteristics in such a way that each region can be replaced by a simple idealized chemical reactor. Common types of chemical reactors are the Perfectly Stirred Reactor (PSR) and the Plug Flow Reactor (PFR). [59]

Perfectly Stirred Reactor (PSR)

The perfectly stirred or well-stirred reactor is a zero dimensional ideal reactor in which perfect mixing occurs. In the PSR, combustion takes place uniformly in the control volume and there is no spatial or temporal variation of parameters. The dominant parameter in the PSR is residence time, which represents the available time that reactants have in reactor. A PSR may be used in those regions of the combustor where the turbulence intensity or mixing degree is high due to circulation i.e. mixing, primary and intermediate zones.

Plug Flow Reactor (PFR)

Like the PSR, there is no temporal variation in the PFR and the flow is steady. However the PFR is a one-dimensional reactor, which means the flow properties are changing in the axial direction while they remain uniform in the radial direction. Also there is no mixing taking place in the axial direction. Regions of the combustor where flow is one-dimensional, calm and turbulence intensity is low may be modeled with a PFR. Parts of the intermediate zone and the dilution zone are the best candidates to be modeled by a PFR.

In addition to the chemical reactor network, a chemical mechanism representing the fuel must be defined. For this study, the Kollrack mechanism [27, 32] was selected. More details on idealized chemical reactors and chemical mechanisms may be found in Appendix A.

In principle, the Chemical Reactor Network should be developed from a flowfield analysis (e.g., with CFD) to identify the appropriate regions which should be modeled by PSRs versus those that should be modeled by PFRs. In the early stages of this research program, it was believed that such an analysis would be a necessary step in the modeling process. However, it was decided instead to adapt reactor networks from the published literature. This is a more logical approach for two reasons: (1) at the conceptual design phase there is not likely to be sufficient detailed geometry information for a CFD analysis, and (2) the published reactor networks have already been validated against test data. Even with this decision having been made, it is still desirable to understand the dependence of the reactor network on the combustor flowfield to assist in the selection of a representative reactor network from the literature. Toward this end, two simple combustion flowfields were analyzed: the SPRF (Stagnation Point Reverse Flow) combustor developed at Georgia Tech and the LDI (Lean Direct Injection) combustor developed at NASA.

SPRF

The experimental data for the SPRF was collected in the Georgia Tech Ben Zinn Combustion Laboratory under the NASA/DoD URETI Project. The data analyzed for this study was for a gaseous methane fuel. The SPRF combustor geometry, thermocouple-measured temperature field, and PIV-measured velocity field are shown in Figure 9 below.

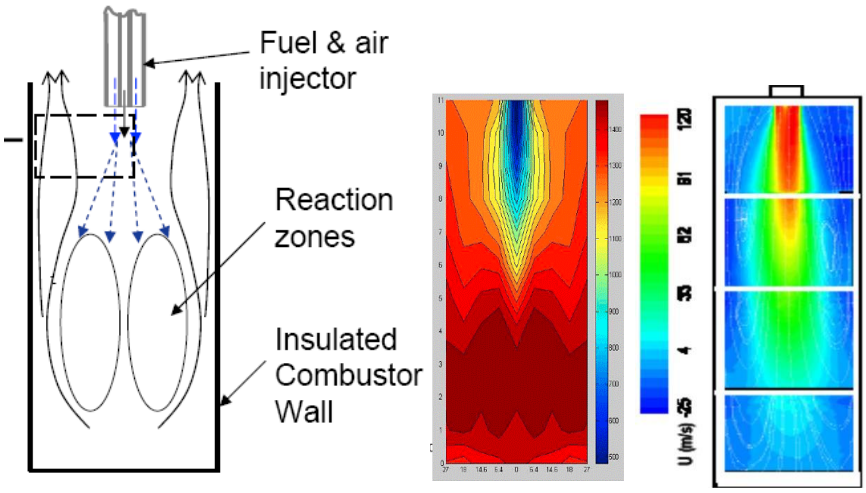

Figure 9: SPRF Combustor Geometry, Temperature Field, and Velocity Field

The CFD analysis of the SPRF combustor was carried out using Fluent. By symmetry, the flow was modeled initially as a 2-D, steady flow. The combustion reaction was simulated with a simple reaction mechanism. This allowed the temperature field to be predicted with a relatively short computation time, but did not allow for the accurate calculation of the chemical species. A grid convergence study was performed to find a grid-independent solution.

Given the temperature and velocity field information from the CFD results, the CHEMKIN chemical reactor network shown in Figure 10 was designed. The flowfield was discretized into several volumes, each with a relatively uniform temperature distribution. A recirculation zone was included to investigate the influence of any mixing between the inflow and outflow regions.

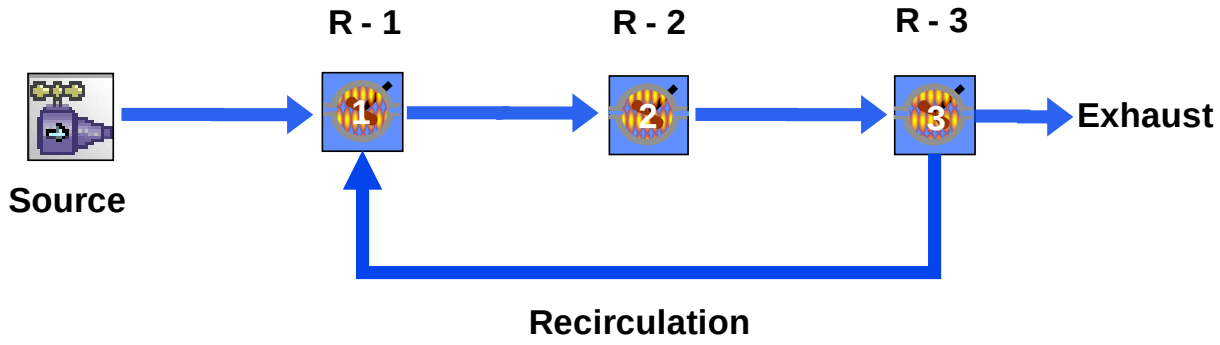

Figure 10: CRN for SPRF Combustor

The CHEMKIN results for the computed temperature and NOx are presented in Figure 11 below. It may be seen that, while the temperature is over predicted, the NOx predictions are generally in agreement.

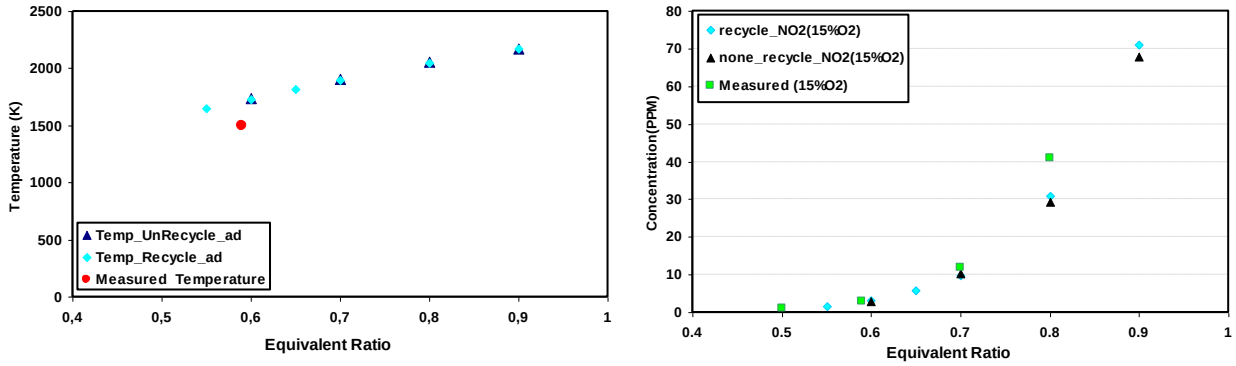

Figure 11: CHEMKIN Results for SPRF Combustor

LDI

The LDI test configuration is illustrated in Figure 12. In this case, no CFD was run but the test data was used directly to create a representative CRN.

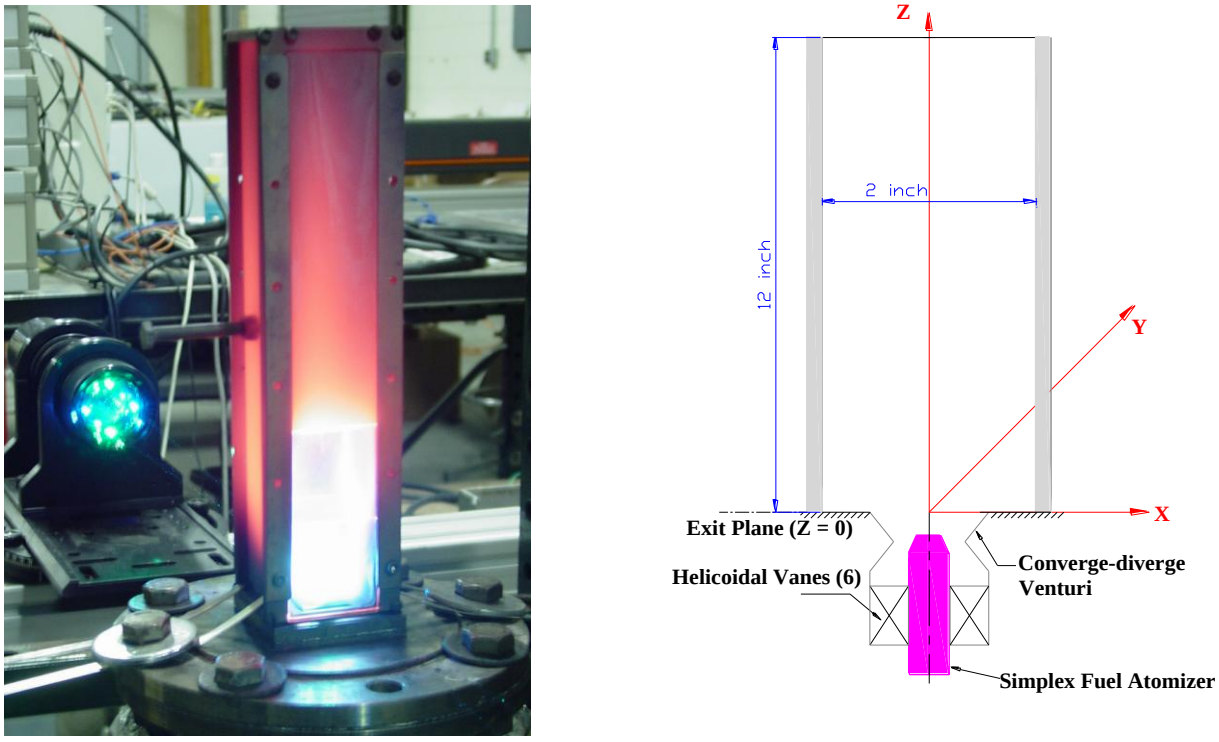

Figure 12: LDI Combustor Test Configuration [6]

As shown in Figure 13, based on the measured temperature and velocity profiles, PSRs are located where the temperature is relatively uniform with recirculation. A PFR is used to represent the downstream portion of the test section, where temperature is relatively constant and flow turbulence is relatively weak.

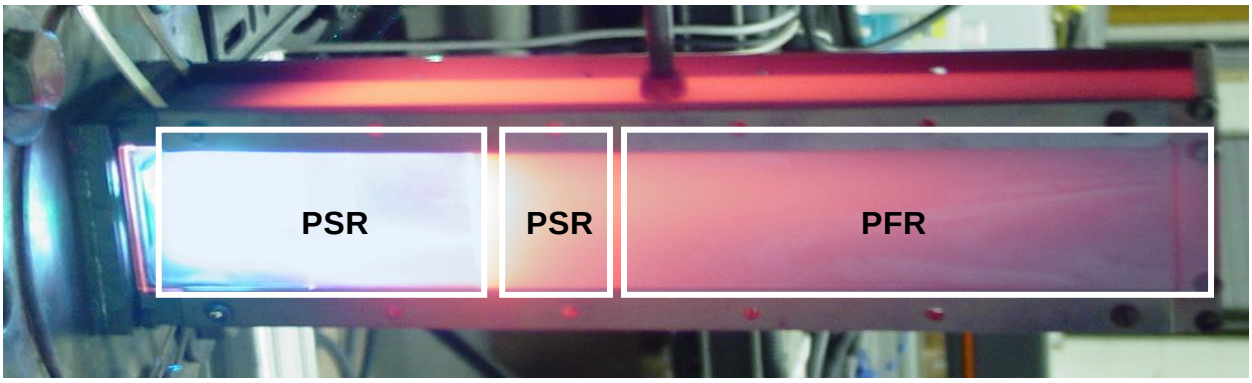

Figure 13: Flowfield Analysis of LDI Combustor

In addition, in order to simulate the unmixedness of the liquid fuel spray and air, the first PSR is divided into 3 branches at different equivalence ratios. The CRN thus developed for the LDI combustor is shown in Figure 14.

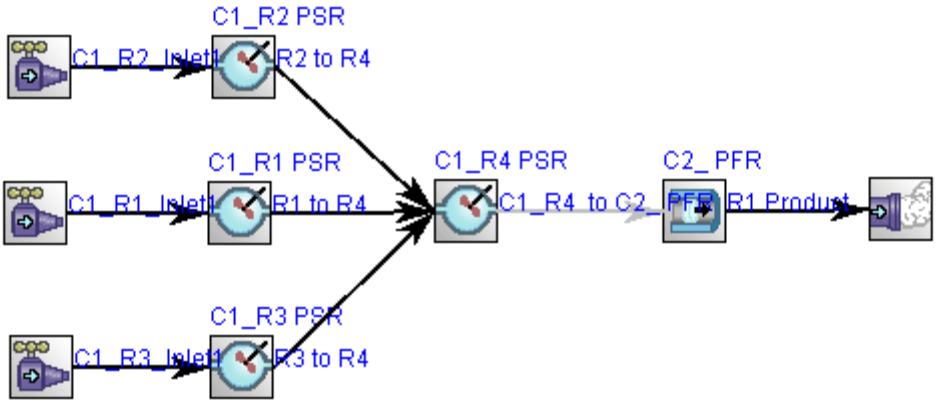

Figure 14: CRN for LDI Combustor

To summarize, a reasonable process for developing a CRN for a given flowfield was defined by analysis of two relatively simple combustors. The process of defining the CRN for an aircraft gas turbine type combustor follows the same general procedure; each of the combustion zones (primary, secondary, and dilution) may be modeled by PSRs and/or PFRs, as illustrated in Figure 15.

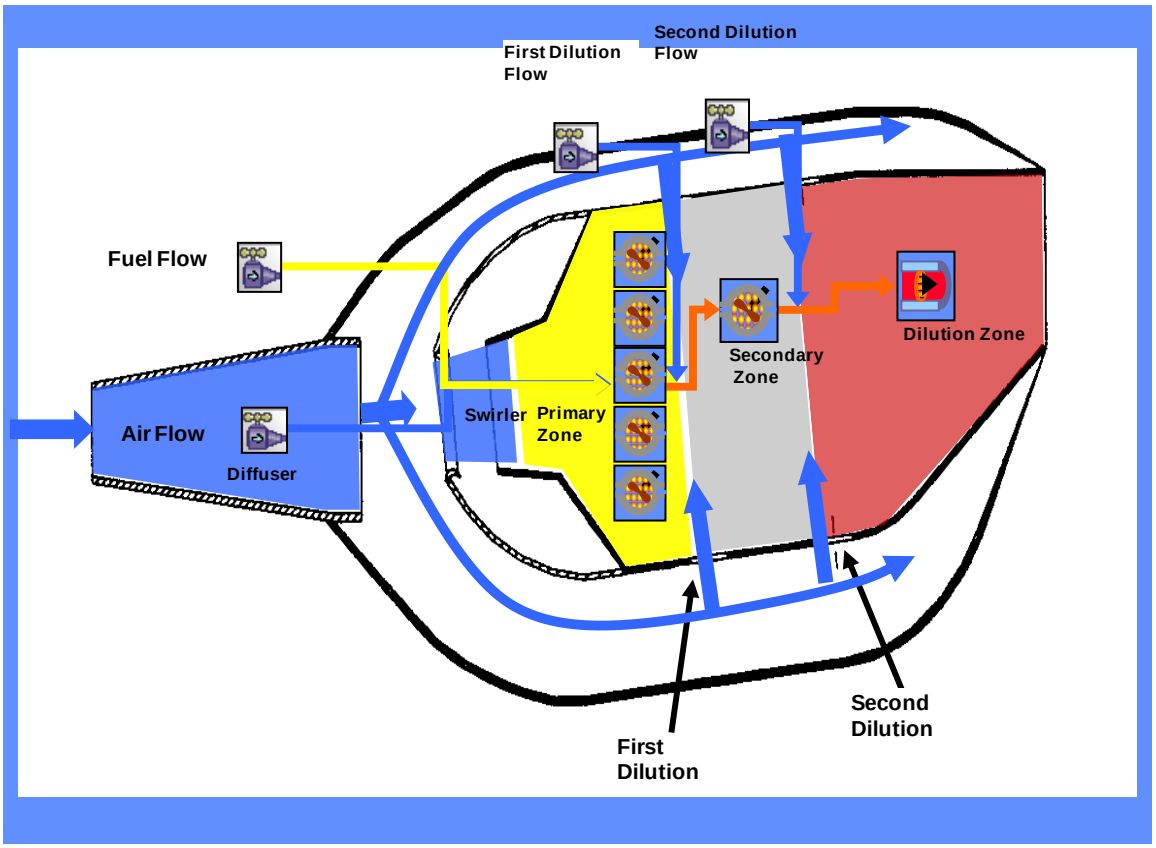

Figure 15: Example of CRN Development from Combustor Flowfield

In the following sections, the development of the Chemical Reactor Network models for the SAC, RQL, and Lean-Burn combustors are described.

SAC

Because detailed geometry was not available, the CRN for the SAC model was not based directly on flowfield analysis, but was taken from the literature. Several CRNs for SAC type combustors have been published (see for example references [2, 45-47]). Each of these architectures has been validated with experimental data and/or CFD analysis.

The architecture chosen is based on the work of Rizk et al [48] because it has several attractive features. For example, the primary zone model accounts for fuel atomization and incompletely vaporized fuel droplets, and unmixedness is modeled by dividing the primary zone into multiple PSRs with different equivalence ratios, determined by the unmixedness parameter S [22]. However, whereas the Rizk model maintained parallel streams throughout the CRN from the primary zone through the dilution zone, in the present study the several primary zone streams are collected into a single stream which is carried through the secondary and dilution zones. A similar CRN was used in research performed at MIT [1].

The network architecture and empirical unmixedness curve are presented in Figure 16 below. The empirical unmixedness curve was taken from Sturgess [58].

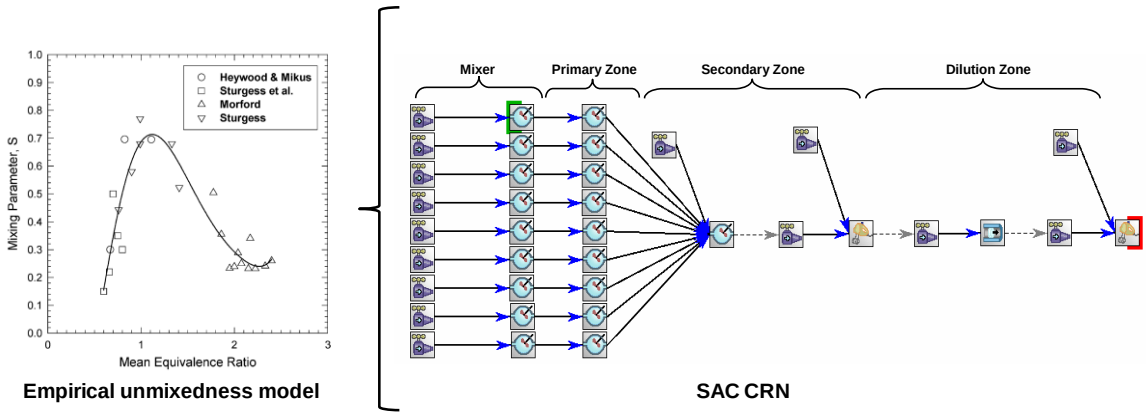

Figure 16: Chemical Reactor Network for Single-Annular Combustor

The inputs required by SAC CRN model are presented in Table 1 below. It is helpful in understanding the notation to refer back to Figure 16 above. Note that the Primary Zone is divided into 9 mixers and PSRs; the mass flow and fuel flow inputs for each of these reactors are determined from the specified Primary Zone equivalence ratio, which determines the unmixedness degree and the standard deviation of the distributions. In addition to these inputs, the fuel chemical mechanism and thermo properties tables must also be provided to CHEMKIN.

Table 1: Inputs Required for SAC Chemical Reactor Network

Variable	**Definition**
S_CreateChemKinInputs.Inlet_Phi (distribution)	Equivalence ratios for each PZ reactor
S_CreateChemKinInputs.Inlet_mdot (distribution)	Mass flow for each PZ reactor
S_CreateChemKinInputs.Inlet_T (distribution)	Temperature for each PZ reactor
S_CreateChemKinInputs.Inlet_Fuel (distribution)	Fuel flow for each PZ reactor
S_CreateChemKinInputs.Mixer_P (distribution)	Pressure for each PZ mixer
S_CreateChemKinInputs.Mixer_Vol (distribution)	Volume for each PZ mixer
S_CreateChemKinInputs.PZ_P (distribution)	Pressure for each PZ reactor
S_CreateChemKinInputs.PZ_Vol (distribution)	Volume for each PZ reactor
SZ_Volume(cm3)	Secondary zone volume
SZ_total_press(atm)	Secondary zone pressure
first_dilution_mdot(g/s)	Mass flow for first row of dilution holes
first_dilution_Tinlet(K)	Temperature of first dilution air
first_mixer_vol(cm3)	Volume of first mixer
first_mixer_total_press(atm)	Pressure of first mixer
second_dilution_mdot(g/s)	Mass flow for second row of dilution holes
second_dilution_Tinlet(K)	Temperature of second dilution air
DZ_total_press(atm)	Dilution zone pressure
DZ_cross_sect_area(cm2)	Dilution zone cross-sectional area
DZ_start_location	0.0
DZ_length(cm)	Dilution zone length
second_mixer_total_press(atm)	Pressure of second mixer
second_mixer_vol(cm3)	Volume of second mixer
cooling_air_mdot(g/s)	Cooling air mass flow
cooling_flow_temp(K)	Cooling air temperature

RQL

The CRN for the RQL combustor was created by modifying the SAC CRN, in consideration of the different processes occurring within the RQL. Only a few modifications are required. The SAC primary zone is replaced by a "Rich zone", which is essentially the same as the SAC primary zone, except that it runs at a rich equivalence ratio, and it uses the same evaporation and unmixedness models as in the SAC model. The SAC secondary zone is replaced by a "Quench/Mixing zone". Here, instead of a PSR, a partially stirred reactor (PaSR) is used to model the Mixing zone, and a Gas-Mixer Reactor is used to model the instant mixing of the remaining portion of quench air (mixed flow) with the hot gases. The lean zone and dilution zone are the same as in SAC model. The CRN for the RQL combustor is presented in Figure 17 below.

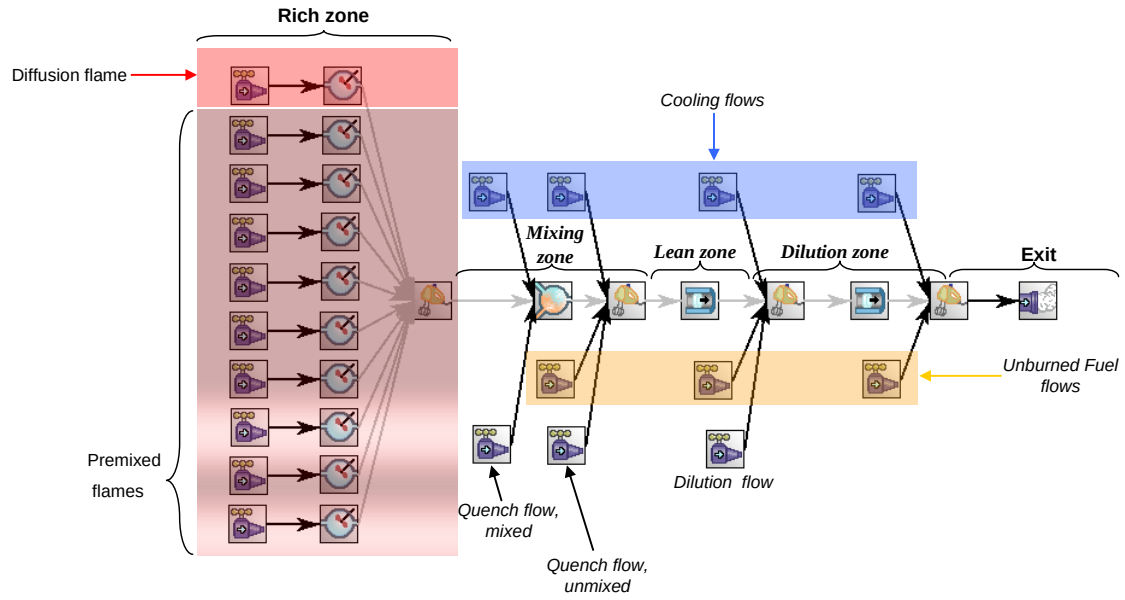

Figure 17: Chemical Reactor Network for RQL Combustor

Also the CRN has three mixers which are used to mix the dilution or the Mixing zone mixed flows with the core flow. The sensitivity analysis has shown that the emission levels are insensitive to the volume of the mixers. Also there are inputs for the unburned fuel. It was intended to calculate the amount of unburned fuel that goes to each zone (LZ, DZ and combustor exit) based on the defined zone efficiencies, however this feature has been deactivated for consistency with the other combustor models (SAC and Lean-Burn).

Table 2 shows the list of the input variables that are required by the CRN model. It is helpful in understanding the notation to refer back to the figure. All of the CRN inputs are calculated in the 1-D Flow Model.

Table 2: Inputs Required for RQL CRN model

Component	CRN Input Parameters	Units
Rich Zone	Inlet_Phi (Array of 9 elements)	-
	Inlet_Mdot (Array of 9 elements)	gr/s
	Inlet_T (Array of 9 elements)	K
	InletFuel Name (Array of 9 elements)	-
	PZ_Pt (Array of 9 elements)	atm
	PZ_Volumes (Array of 9 elements)	cm3
	PZ_eqRatio (Array of 9 elements)	-
Mixing Zone	MZ_Volume	cm3
	MZ_Pt	atm
	MZ_ResidenceTime	s
	MZ_SimulationTime	s
	MZ_MixingTime	s
	MZ_Mixing_model	-
	MZ_Mixing_model_factor	-
	MZ_Mixing_mode	-
	MZ_MonteCarlo_events_no	-
	MZ_MonteCarlo_time_step	s
Mixing Flow (First Dilution)	FirstDilution_Mdot_mixed	gr/s
	FirstDilution_T_mixed	K
	FirstDilution_Mdot_unmixed	gr/s
	FirstDilution_T_unmixed	K
Lean Zone	LZ_Pt	atm
	LZ_CrossSectionArea	cm2
	LZ_StartLocation	cm
	LZ_Length	cm
	LZ_eqRatio	-
First Mixer	FirstMixer_Volume	cm3
	FirstMixer_Pt	atm
	First_unburned_fuel_Mdot	gr/s
Second Dilution Flow	SecondDilution_Mdot	gr/s
	SecondDilution_T	
	Second_unburned_fuel_Mdot	gr/s
	SecondMixer_Pt	atm
	SecondMixer_Volume	cm3
Dilution Zone	DZ_CrossSectionArea	cm2
	DZ_StartLocation	cm
	DZ_Length	cm
Third Mixer	ThirdMixer_Pt	atm
	ThirdMixer_Volume	cm3
Cooling	CoolingAir_Mdot	gr/s
	CoolingAir_T	K
-	exit_unburned_fuel_Mdot	gr/s
-	Fuel_T	K

There are some important differences in the CHEMKIN model due to the use of a PaSR that should be noted. Since the PaSR performs a Monte Carlo simulation for a given number of

statistical samples for a range of time scales, it takes much longer time to execute the RQL model than the other models which do not use a PaSR. Other than the parameters that are described previously (residence time, mixing time, simulation time and time step) there are few additional parameters that are needed for the PaSR:

- Type of problem. The PaSR can handle "Mixing Only" problems (MIX), "Reacting" problems (CHEM) and "Equilibrium" problems (EQUIL). The "Mixing Only" case behaves like a "Gas Mixer" and the "Equilibrium" case is like a PSR. The fastest case is the "Mixing Only" and the slowest case is "Reacting" which is closest to the real mixing problem.
- Number of Monte Carlo Simulation samples (NPAR). This parameter defines the number of statistical samples that are randomly selected from a Joint Probability Distribution function to model the mixing. Usually values around 200 provide a reasonable balance between accuracy and execution time. After finishing the Monte Carlo simulation, the Probability Density function (pdf) of the species and temperature in the Mixing zone can be obtained.

Lean-Burn

The CRN for the Lean-Burn combustor was also made by modifying the SAC CRN. In this case, the primary zone is modeled by two branches representing the flowfields generated by the pilot and the main injector. The main injector is modeled by a PSR and PFR in series to represent a turbulent premixed flame [44]. The pilot injector is modeled by a set of PSRs in parallel, similar to the SAC primary zone. The secondary and dilution zone are represented by a PSR and PFR, respectively, the same as in the SAC. The Lean-Burn combustor CRN is presented in Figure 18 below.

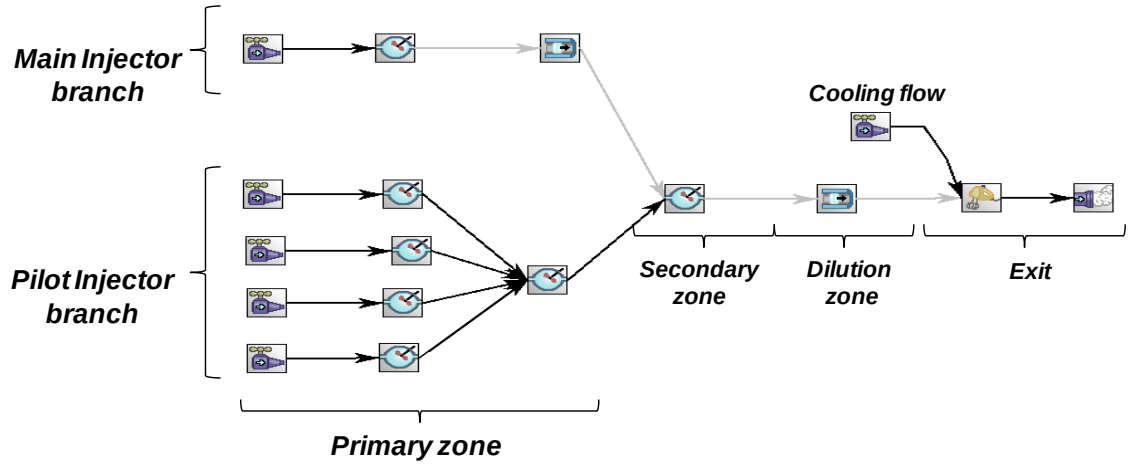

Figure 18: Chemical Reactor Network for Lean-Burn Combustor

The inputs required for the Lean-Burn CRN are summarized in Table 3 below. It is helpful in understanding the notation to refer back to the figure.

Table 3: Inputs Required for Lean-Burn CRN

Variable	Definition
S_CreateChemKinInputs.Main_Inlet_Fuel	Fuel type, e.g. C12H23
S_CreateChemKinInputs.Main_Inlet_mdotair	Airflow at Main inlet
S_CreateChemKinInputs.Main_Inlet_P	Pressure at Main inlet
S_CreateChemKinInputs.Main_Inlet_Phi	Equivalence Ratio at Main inlet
S_CreateChemKinInputs.Main_Inlet_T	Temperature at Main inlet
S_CreateChemKinInputs.Main_PZ_Vol	Main PZ volume
S_CreateChemKinInputs.Mixer_Vol	Main mixer volume
S_CreateChemKinInputs.Pilot_Inlet_Fuel (distrib)	Fuel type, e.g. C12H23
S_CreateChemKinInputs.Pilot_Inlet_mdotair (distrib)	Fuel flow to Pilot
S_CreateChemKinInputs.Pilot_Inlet_P (distrib)	Pressure at Pilot inlet
S_CreateChemKinInputs.Pilot_Inlet_Phi (distrib)	Equivalence Ratio of Pilot
S_CreateChemKinInputs.Pilot_Inlet_T (distrib)	Temperature at Pilot inlet
S_CreateChemKinInputs.Pilot_SZ_Vol	Pilot secondary zone volume
S_CreateChemKinInputs.Pilot_vol_x4 (distrib)	Volume of the four distributed PZ PSRs
S_CreateChemKinInputs.PZ_PFR_CrossSectArea_SI	Cross-sectional area of PZ plug flow reactor
S_CreateChemKinInputs.PZ_PFR_x_end_SI	Length of PZ plug flow reactor
S_CreateChemKinInputs.PZ_PFR_x_start	0.0
S_CreateChemKinInputs.SZ_Link_Vol	Volume of the PSR at the end of the PZ
S_CreateChemKinInputs.Wcool_SI	Cooling flow
DZ_total_press(atm)	Total pressure at Dilution zone
S_CreateChemKinInputs.DZ_PFR_CrossSectArea_SI	Cross-sectional area of DZ plug flow reactor
S_CreateChemKinInputs.DZ_PFR_x_end_SI	Length of DZ plug flow reactor
S_CreateChemKinInputs.DZ_PFR_x_start	0.0

4 1-D Flow Model Development

The main purpose of the 1-D Flow Model is to compute the inputs required by the CRN. These include the combustor cooling and mixing flow requirements, the air flow partitioning, and the volumes and residence times of the various combustion zones. In addition, the 1-D Flow Model computes geometry features of the combustor and other parameters that may be of interest to the combustor designer.

The 1-D Flow Model is intended to be a drop-in replacement for the NPSS Burner element. The model comprises new Diffuser and Combustor elements. The Combustor element contains sockets for the primary, secondary, and dilution zones. The elements and subelements of the 1-D Flow Model are described in detail in the following sections. More details and the specific equations used may be found in Appendices B and C and in references [28, 32].

4.1 Single Annular Combustor

A diagram of the overall SAC 1-D Flow Model is presented in Figure 19 below. This Figure indicates the several major elements and subelements of the model and their relation to the combustor flowfield.

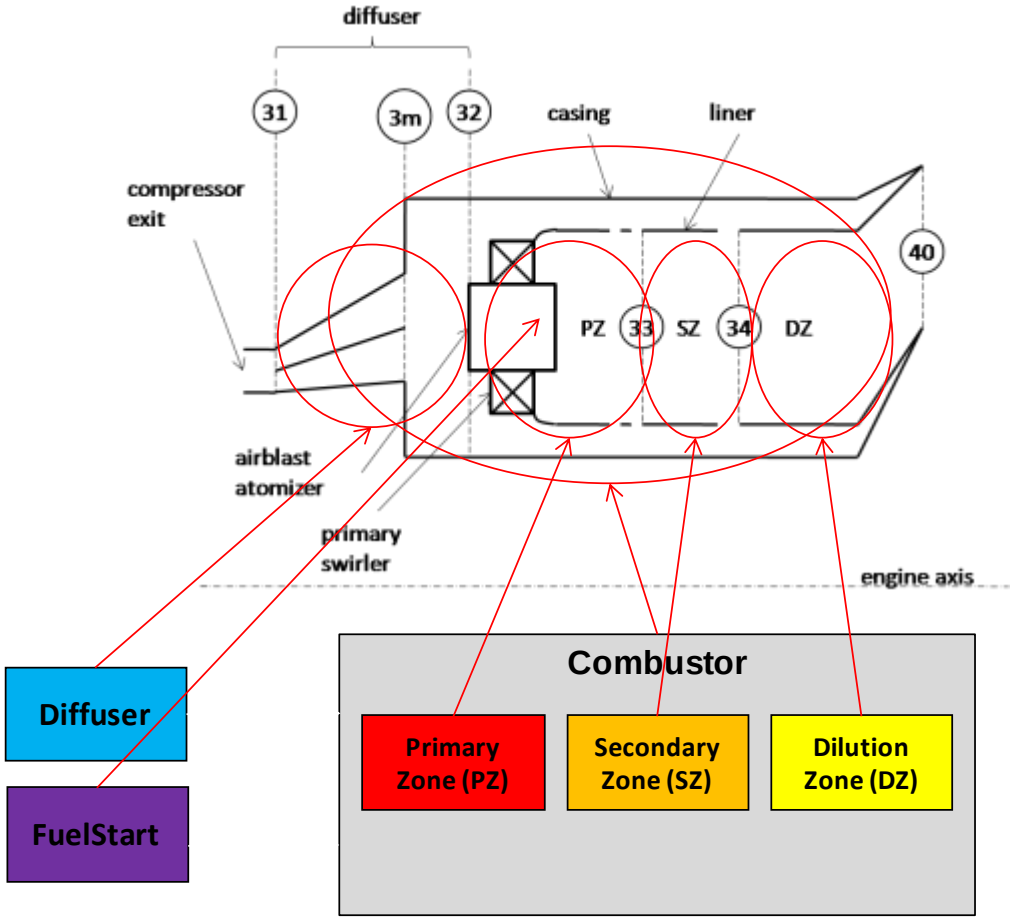

Figure 19: Overview of 1-D Combustor Flow Model for Single-Annular Combustor

Geometry Model

The geometry calculations are not collected into one single element or subelement, but appear as needed throughout the various parts of the model. However, before discussing each of the elements individually, it is helpful to consider the geometry calculations from an overview perspective. The geometry and nomenclature for the full combustor are indicated in Figure 20.

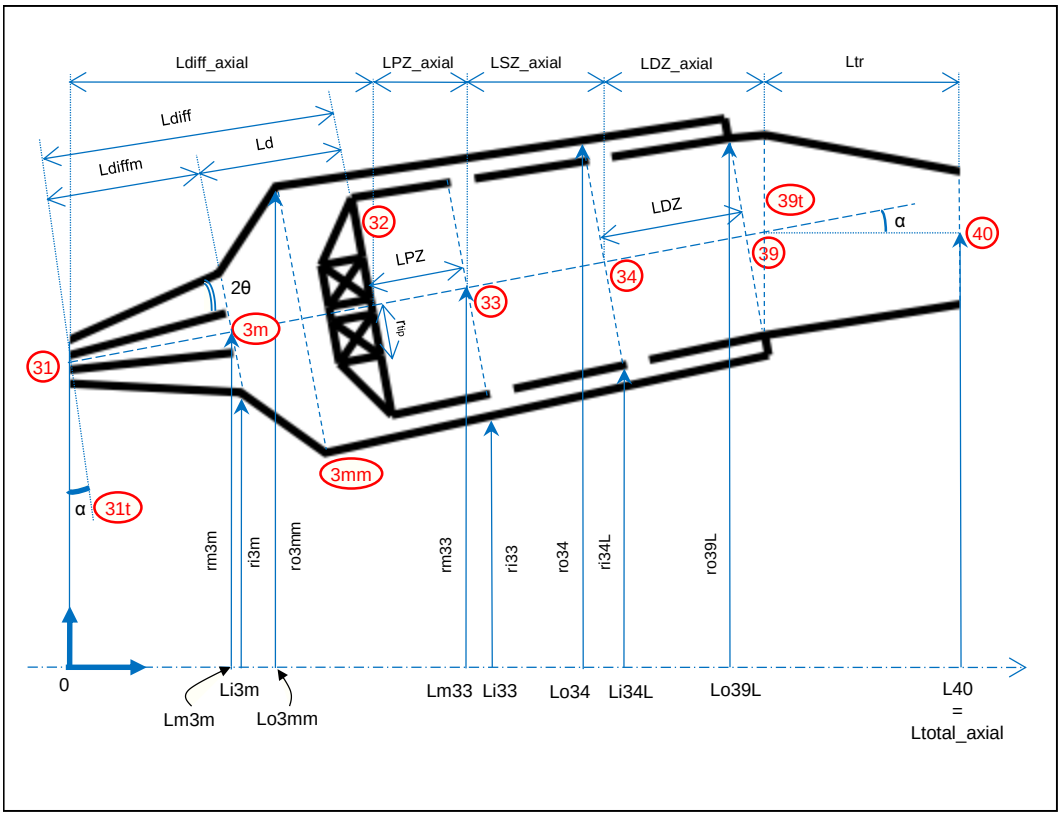

Figure 20: Combustor Geometry and Nomenclature

It is assumed that the combustor may be tilted from the diffuser inlet to the transition duct exit. The tilt angle α between combustor "meanline" and engine axis is constant from station 31t (located close to the HPC exit which is associated with flowstation 31) to station 39t (inlet flow station of the transition duct). In order to calculate the complete geometry, each point is parameterized by α. The liner and casing areas are assumed to be constant but the liner height varies with the mean radius of each station. The angle α is varied in the solver until the exit mean radius rm_{40} matches with the high pressure turbine mean radius. Equations for the geometry calculations are given in Appendix B.

Diffuser Element

A diagram of the diffuser element is presented in Figure 21. The diffusion process is assumed to be adiabatic (constant total temperature) but not isentropic. Pressure losses are related to the diffuser half-angle with an empirical relationship. The angle α between the combustor "meanline" and the engine axis is declared in the diffuser element and is propagated to the other elements. The diffuser element calculates the exit area of the diffuser that matches both target on-design Mach number (Mach32) and pressure losses. This is done by fixing the exit Mach number and varying exit total pressure until diffuser efficiency is matched (with calculated value from geometry only). The diffuser can have up to three passages to prevent stall for large diffuser angles. If the aspect ratio is higher than "sweet spot", a combined flat-wall/dump diffuser is added (flag_dump = 1). Subscript 3m refers to the flow station between the flat-wall diffuser and the dump diffuser. Station 3mm is a station located between 3m and 32 created for the only purpose of smoothing out the discontinuity in the wall profile from 3m to 32 in the case

of a dump diffuser. Off-design, the calculation keeps geometry the same (hence diffuser efficiency) and iterates on exit total pressure to match diffuser efficiency.

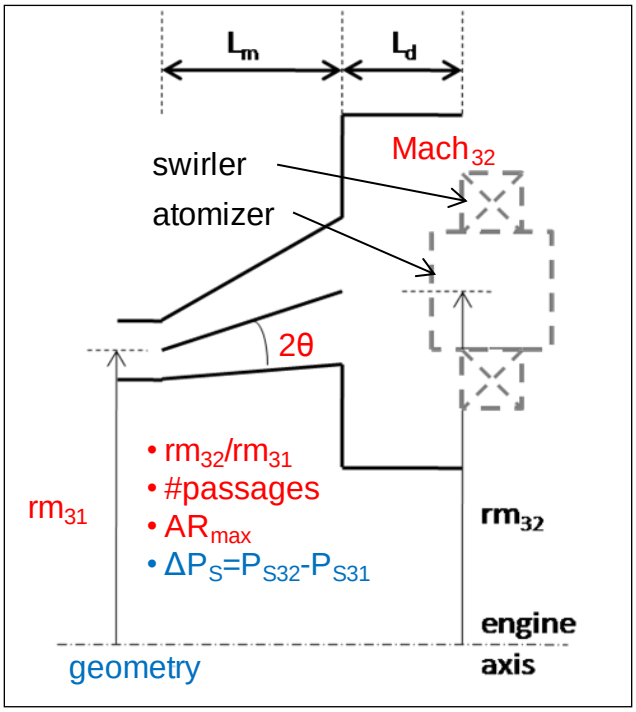

Figure 21: Diagram of Diffuser Element

The user-provided inputs to the diffuser element are summarized in Table 4.

Table 4: Diffuser Element Inputs

rm31	Mean radius at HPC exit
Mach32	Mach number at diffuser exit
theta	Diffuser passage half angle
alpha	Combustor "meanline" angle
passage_number	Number of diffuser splitter plates
sweet_spot	Maximum aspect ratio for a flat-wall diffuser

Combustor Element

The Combustor element represents the assembly of the liner (primary, secondary and dilution zones + transition duct) surrounded by a casing for annulus flow (secondary, dilution and cooling air). A diagram of the Combustor element is presented in Figure 22 below.

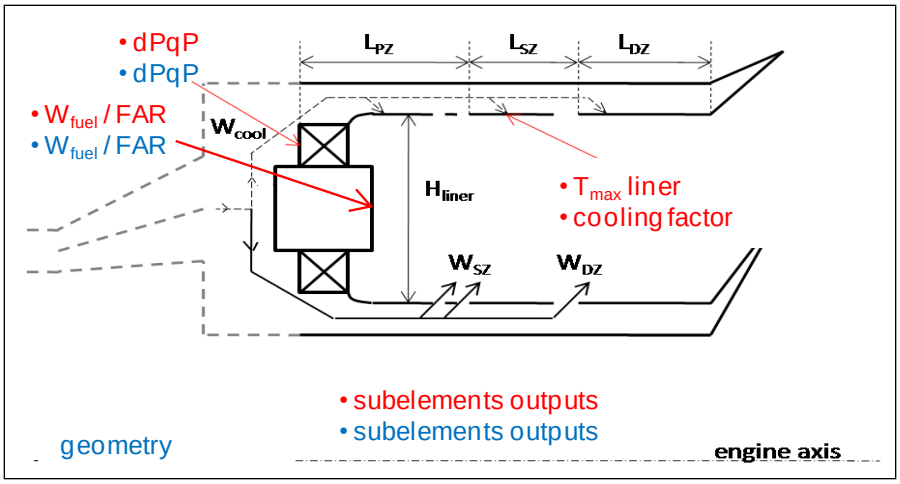

Figure 22: Diagram of Combustor Element

Total pressure is assumed to be constant in the liner and in the annulus. The relative difference between the annulus and liner total pressures is dPqP. Liner and casing cross-section areas are also assumed constant. The liner dynamic pressure is considered negligible compared to the liner total pressure. This hypothesis, together with the constant total pressure assumption in the liner and casing yields a constant velocity for every jet flowing from the casing into the liner (i.e., through the primary zone swirlers, secondary holes and dilution holes).

The Combustor element, as a "parent" element, is intended to facilitate transfer of variables between the different "objects" constituting the combustor. The different zones (PZ, SZ, DZ) are hence represented by subelements plugged into the Combustor element. Each subelement calculates the airflow required for its associated zone, the geometry of the zone and exit flow station properties. Any variable declared in the Combustor element is readable and writable by any subelement plugged in. Specific calculations in the Combustor element are related to cooling flow.

On design, pressure losses (dPqP) and either FAR or WFUEL (fuel weight flow) are specified by the user, with the other of the two calculated as an output. Airflow sent to the primary zone depends on the PZ equivalence ratio (eqratio_PZ, user input) and the global equivalence ratio (eqratio_40). Airflow sent to the secondary zone is calculated such that total temperature does not vary between the primary and secondary zones. Cooling flow is calculated depending on the maximum temperature the liner can withstand (MaxTempLiner), the type of cooling used (CoolMechanism_factor) and PZ & SZ total temperature. The remainder of air is dumped into the dilution zone. It should be noted that while eqratio_PZ is greater than 1, the combustion process is assumed to take place in stoichiometric conditions to compute the maximum possible temperature for purposes of sizing the cooling flow. However, the airflow through the combustor itself is calculated using the input value of eqratio_PZ .

Off design, the combustor pressure drop is assumed to be constant (dPqP). Again, either FAR or WFUEL is specified. Primary zone airflow depends on the geometry (LINtoCASE_areaRatio), assuming dPqQ is constant (also calculated on design). Secondary and dilution zones airflows are calculated based on the geometry (using mass conservation). Cooling airflow is calculated as the remainder of air.

The user-supplied inputs required for the Combustor element are summarized in Table 5 below.

Table 5: Combustor Element Inputs

MaxTempLiner	Maximum allowable liner temperature
CoolMechanism_factor	Cooling mechanism factor
dPqP	Burner pressure drop
switchBurn	Burner mode; input either “FAR” or “WFUEL”
switchPower	Power setting for use by regression model
injector_Ploss_design	Injector pressure loss (percent)

FuelProperties Subelement

To simplify the user interface, all the fuel property data needed for calculations is handled in the FuelProperties subelement. These parameters are used for the fuel droplet evaporation model and/or are passed along to the CRN for use in the detailed chemical mechanism calculations. The FuelProperties inputs are summarized in Table 6 below.

Table 6: Fuel Properties Subelement Inputs

fuel_density	Fuel density in kg/m3
fuelTemp	Fuel temperature in deg R
fuelFormula	Fuel chemical formula, e.g. C12H23
numCarbon	Number of carbon atoms in fuel formula
numHydrogen	Number of hydrogen atoms in fuel formula

FuelDropletEvaporationModel Subelement

The purpose of the FuelDropletEvaporationModel subelement is to compute the ratio of fuel vapor to total fuel. The fuel droplet evaporation model is described in Appendix A.

PZ Subelement

The PZ subelement represents the combustor primary zone. The purpose of the PZ subelement computes the swirler number and geometry, the primary zone required air, PZ geometry, and PZ exit temperature. A diagram of the PZ subelement is presented in Figure 23 below.

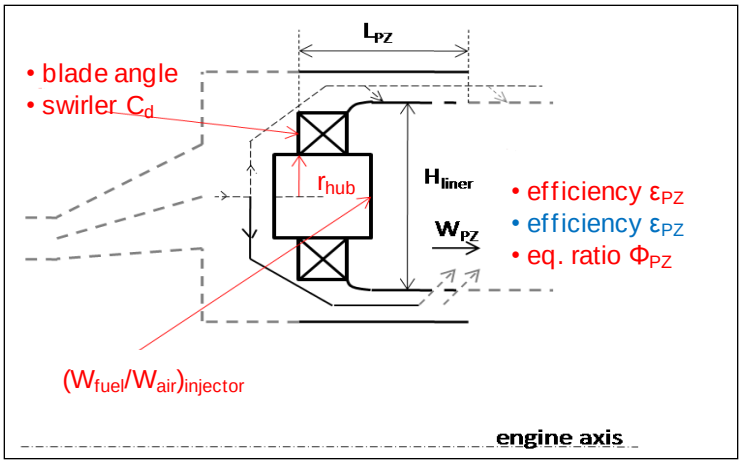

Figure 23: Diagram of PZ Subelement

An adiabatic flame temperature calculation is performed using the NPSS burn function (limited to lean or stoichiometric mixtures depending on which NPSS ThermoPackage is selected). The inputs are the combustion efficiency (ratio of fuel burned over fuel injected) and equivalence ratio.

The swirlers are designed with the conditions that the swirl number be large enough (greater than 0.6) and that all the swirlers fit in the liner dome (checking both azimuthal and radial space constraints). The swirler blade angle and number of nozzles are iterated on while hub radius and discharge parameters are inputs.

The primary zone length is calculated as the length of the recirculation bubble (based on swirler geometry and swirl number).

The user-supplied inputs required for the PZ subelement are summarized in Table 7

Table 7: PZ Subelement Inputs

sw_angle	Swirler blades angle (desired value)
swirler_discharge_parameter	Swirler discharge coefficient
r_hub	Swirler hub radius
Wair_nozzletoWfuel	Air/Fuel ratio of each fuel injector
eff_PZ	PZ combustion efficiency
eqratio_PZ	PZ equivalence ratio
mixer_PZ_vol_rat	Mixer to PZ volume ratio

SZ Subelement

The SZ subelement represents the combustor secondary zone. A diagram of the SZ subelement is presented in Figure 24 below.

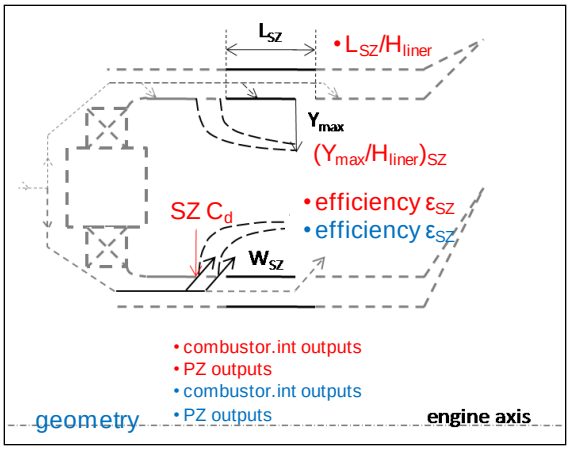

Figure 24: Diagram of SZ Subelement

On design, the amount of air to be added in the secondary zone through the secondary holes (frac_SZ) is calculated such that total temperature remains unchanged from the PZ (iterates on the fuel to air ratio). The number and diameter of the secondary zone dilution holes are calculated using conservation laws (mass & momentum), together with the Boussinesq assumption (density varies with temperature only) and empirical relationships (jet penetration as a function of dynamic pressure ratios). Jet penetration over liner height is a user input in this procedure. The SZ length and volume are fixed by the user when choosing the aspect ratio (SZ length to liner height ratio).

The required user-supplied inputs for the SZ subelement are summarized in below.

Table 8: SZ Subelement Inputs

SZ_discharge_coeff	SZ holes discharge coefficient
SZ_length_ratio	SZ aspect ratio (length/liner height)
SZ_penetration_ratio	SZ jets penetration ratio (Y_{max}/liner height)
eff_SZ	SZ combustion efficiency

DZ Subelement

The DZ subelement represents the combustor dilution zone. A diagram of the DZ subelement is presented in Figure 25 below.

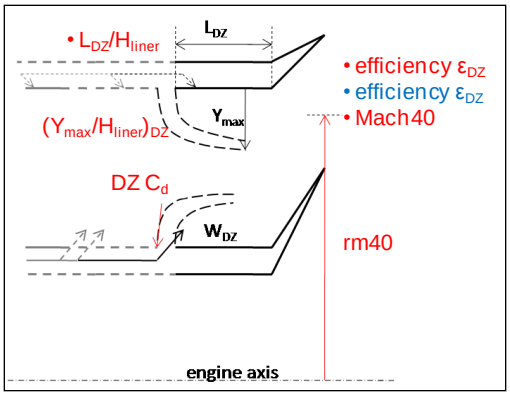

Figure 25: Diagram of DZ Subelement

On design, the air flowing through the dilution holes is simply the remainder of air after flow was partitioned between the cooling flow and the primary and secondary zones. In the dilution zone the adiabatic flame temperature is calculated using the overall efficiency and equivalence ratio of the entire burner, to be consistent with the NPSS cycle calculations using the standard NPSS Burner element.

The number and diameter of the dilution holes are calculated similarly to the secondary zone, but with unique values for the discharge coefficient and jet penetration ratio (both user inputs). As in the secondary zone, the dilution zone length and volume are fixed with the aspect ratio of the zone (user input). A transition duct is added to provide a good pattern factor at the HPT inlet (no hot spots). The length of this duct is fixed with an aspect ratio variable. It is assumed that no combustion occur in this zone, just mixing. The exit area is varied until the desired HPT inlet Mach number (Mach40) is matched.

The required user-supplied inputs for the DZ subelement are summarized in Table 9 below.

Table 9: DZ Subelement Inputs

DZ_discharge_coeff	DZ holes discharge coefficient
DZ_length_ratio	DZ aspect ratio (length/liner height)
tr_length_ratio	Transition duct aspect ratio (length/liner height)
DZ_penetration_ratio	DZ jets penetration ratio (Y_{max}/liner height)
eff_DZ	DZ combustion efficiency
Mach40	HPT inlet Mach number
rm40	HPT inlet mean radius

CombPerfParams Subelement

The CombPerfParams subelement is provided for the user to calculate any additional performance parameters of interest for the combustor which may not affect any of the combustor sizing and flow partitioning calculations. Currently the element is used to compute the unmixedness parameter from an empirical relationship [58]. The unmixedness parameter is needed for the CRN.

CreateCHEMKINInputs Subelement

The CreateCHEMKINInputs subelement is provided to gather or compute the necessary variables that are needed as inputs to the CHEMKIN model, such as the volumes of each of the elementary reactors (PSRs and PFRs) used in the CRN. Many of the parameters computed in this subelement are related to the unmixedness model, which is described in Appendix A.

4.2 Rich-Quench-Lean Combustor

The RQL 1D-Flow model is an extension of the 1D-Flow model of the SAC. An overview of the RQL 1-D Flow Model is presented in Figure 26. The RQL 1-D Flow Model comprises the Diffuser, the Rich Zone, the Mixing Zone, the Lean Zone, and the Dilution Zone. The Diffuser and Dilution Zone are identical with those elements of the SAC model.

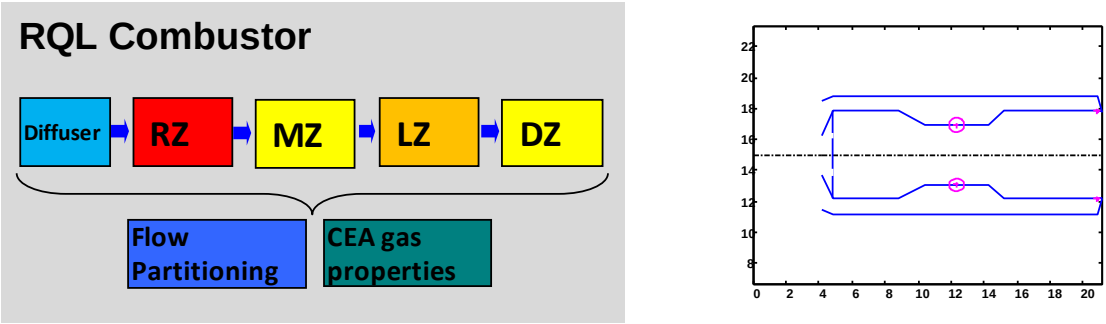

Figure 26: Overview of 1-D Flow Model for RQL Combustor

The following sections outline the major differences between the RQL model and the SAC model. More details and equations may be found in Appendix C.

RZ Subelememt

An important point in computing the Rich zone properties is that, since the Rich zone combustion occurs at conditions above stoichiometric, the normal GasTbl or AllFuel property tables in NPSS are not appropriate. A higher fidelity combustion model, such as chemical equilibrium analysis (CEA) is required to determine the flame temperature and flow properties at Rich conditions. The CEA Package is based on the NASA Chemical Equilibrium Analysis FORTRAN code that has been implemented in NPSS.
Rich zone

An additional feature is added to the Rich zone model which is the configuration option. Since some of the validation cases are performed for the a tubular type RQL combustor, it became necessary to include the tubular option (in addition to already available option of annular configuration) to the Rich zone, Mixing zone, Lean zone and Dilution zone models. The major difference between these two configurations is in the equation used to calculate the liner and casing heights for each component.

MZ Subelement

The Mixing zone is specific to the RQL combustor, where the annulus air must mix quickly with the fuel rich hot gases coming out from the Rich zone section. Different mixing methods may be used, but this research is limited to the Wall-Jet mixing method.

The main purpose of the MZ subelement is to determine the fraction of the air that should be added to the hot gases to bring it from Rich regime to Lean regime. In the SAC model the flow of the secondary zone is calculated based on the amount of increase in efficiency from PZ to SZ zone with the gas temperature kept constant from PZ to SZ. In the RQL model, the amount of flow that goes into the Mixing zone is based on the defined LZ equivalence ratio (in On-Design) or the quench orifice size and pressure drop (in Off-Design).

The Mixing zone component is linked to the Rich zone component through the flow station FS33. Similar to the Rich zone, the configuration may be "Annular" or "Tubular". The cross section area at the mixing zone is reduced by the user-defined factor "MZtoPZ_areaRatio". The number and size of the orifices at design condition is calculated and the maximum penetration is determined using empirical relations.

For determining the Mixing zone exit temperature, the "Burn" function is not used. Assuming the ideal case of the perfect mixing and absence of any reaction, the exit temperature of the Mixing zone is simply the sum of the sensible enthalpies of air and core flows divided the total flow. A more accurate exit temperature is determined later in the Chemical Reactor Network model.

CreateCHEMKINInputs Subelement

The CreateCHEMKINInputs subelement collects and/or comptues all the inputs required by the Chemical Reactor Network (CRN) model. The droplet SMD and evaporation modeling are the same as for the SAC model, as are the Rich zone unmixedness and corresponding distribution of equivalence ratio in the Rich zone.

The significant difference with the SAC model is the additional equations added to take into account the unmixedness in the Mixing zone. A simplified model is developed to model the macro-mixing and its quality in the mixing zone. The assumption for developing this model is that the perfectly mixed model (zero unmixedness) will burn in the Lean zone right at the Lean zone equivalence ratio (which is well below one). As the Mixing zone unmixedness increases from zero to one, more and more of the mixture will burn at the unity equivalence ratio and the rest will burn at an equivalence ratio that is determined by the remaining air and fuel. The unmixedness value is an input from the Mixing zone object. A linear relationship is assumed between the Mixing zone unmixedness value and the equivalence ration between the Lean zone equivalence ratio and one.

Additional parameters are related to the PaSR (Partially Stirred Reactor) model. First is the residence time of the Mixing zone, based on half the Mixing zone volume because the mixing flow enters the zone at the halfway point. The PaSR simulation time should be long enough so the solution of the PaSR reaches the steady state condition but not so long to make the simulation very slow. It is defined to be 5 times the calculated residence time. Also, the time step of

statistical samples that is required in the Monte Carlo simulation in the PaSR is set to one tenth of the Mixing zone residence time. The design inputs for the RQL 1-Df Flow Model are summarized in Table 10.

Table 10: Inputs to RQL 1-D Flow Model

Component		Inputs	Units
Diffuser		Inlet Mean Radius	in
		Inlet Mach Number	-
		Exit Mach Number	-
		Half Angle	-
		Orientation Angle (guess)	deg
		Passage Number	-
		Sweet Spot	-
BURNER		dP_injector	Psia
		Fuel Density	Kg/m3
		dP/P	-
		T_liner_max	R
		Cooling Mechanism Factor	-
		T_fuel	R
		Configuration	-
	Rich Zone	Swirl Angle	deg
		Swirler Discharge Coefficient	-
		Swirler_hub	in
		W_nozzle_air/w_fuel	-
		Burning Efficiency	-
		Equivalence Ratio	-
		Vol_Mixer/Vol_RZ	-
	Mixing Zone	Discharge Coefficient	-
		Length Ratio	-
		Area_MZ/Area_RZ	-
		Mixing Model	-
		Mixing Model Factor	-
		Mixing Mode	-
		Monte Carlo Sample Number	-
	Lean Zone	Burning Efficiency	-
		Equivalence Ratio	-
		Length Ratio	-
	Dilution Zone	Burning Efficiency	-
		Discharge Coefficient	-
		Jet Penetration Ratio	-
		Transition Length Ratio	-
		Length Ratio	-
		Exit Mean Radius	in
		Exit Mach Number	-

4.3 Lean-Burn Combustor

The Lean-Burn combustor considered in this study is intended to be representative of a GE Twin Annular Premixing Swirler (TAPS) type of combustor. The TAPS combustor is characterized by two co-annular swirling jets produced by a pilot and a main mixer [39]. The swirl in the pilot is primarily responsible for the recirculation zone around the axis of the combustor. All the fuel of the pilot injector and some of the main mixer, in the pilot/main interaction zone, are received by this recirculation zone. The resulting high fuel-air ratio in this zone leads to long residence time and high temperature which in turn give the necessary stability to the combustor. The remainder of the fuel from the main injector travels along the border of the recirculation zone and is consumed there [21], [33]. The pilot and main swirling jets are separated by a step height. This allows for the fuel injected into the main burner to be thoroughly mixed before it is consumed by the combustor flame downstream. This combustor utilizes an advanced fuel injection method to optimize the fuel mixture for low emissions products while maintaining the system design requirements. To ensure the combustor maintains a flame at both low and high power settings, fuel injection occurs at multiple sites in the fuel injector assembly.

The TAPS fuel injection system is what allows the combustor to reduce the NOx produced. There are two main sites of fuel injection; the first is the pilot injector. The pilot injector utilizes a similar fuel injection method as the SAC model. A fuel injector is surrounded by two swilrers that help to atomize the fuel. The second fuel injection site is referred to as the main mixer which contains a swirler situated parallel to the incoming airflow and a fuel injector.

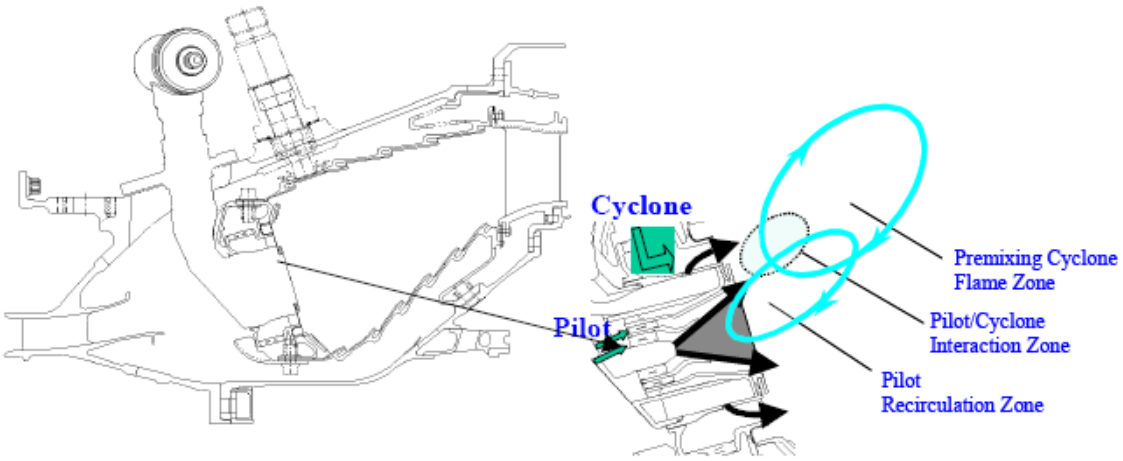

Figure 27: Overview of 1-D Flow Model for Lean-Burn Combustor

To create the 1-D Flow Model for the Lean-Burn combustor, the previously constructed SAC model is used as a starting point. Several changes are made to the model in order to more closely resemble the TAPS fuel injection method.

It is assumed that all of the air entering the combustor is used to create the lean conditions in the primary zone. As a result, there is no remaining air to be introduced through secondary or dilution zone jets (it is noted that there are still cooling holes). Therefore all of the calculations

in the SAC model that deal with air jets and jet hole sizing are omitted in the Lean-Burn combustor model.

The most significant difference between the two combustor models is the fuel injection system. The Lean-Burn injection system incorporates both a pilot injector and a main injector. The pilot injector is sized the same as the SAC injector and the physical geometry of the main injector is assumed to be a percentage of the pilot swirler size. This assumption is made because the main injector swirlers are parallel to the flow and so do not affect the sizing of the primary zone.

In addition, fuel- and air-schedules were added to the model. These schedules change the amount of fuel that enters the pilot injector and the main injector zones as a function of engine power setting, from 100% fuel flow through the pilot at idle to 15% fuel flow through the pilot at max power.

Other than the changes discussed above the 1-D Flow Model remained the same as the SAC model. The same program structure was kept so that there was continuity between all of the created advanced combustor models.

5 ModelCenter Integrated Environment

Due to the complexity of the CHEMKIN model, fileWrappers are provided to link the two codes using ModelCenter. As described above, a special NPSS subelement called CreateCHEMKINInputs was created to compile the inputs needed by CHEMKIN (and to convert them to SI units) through a special viewOut file. An example screen-shot of the ModelCenter environment created for the SAC model is shown in Figure 28.

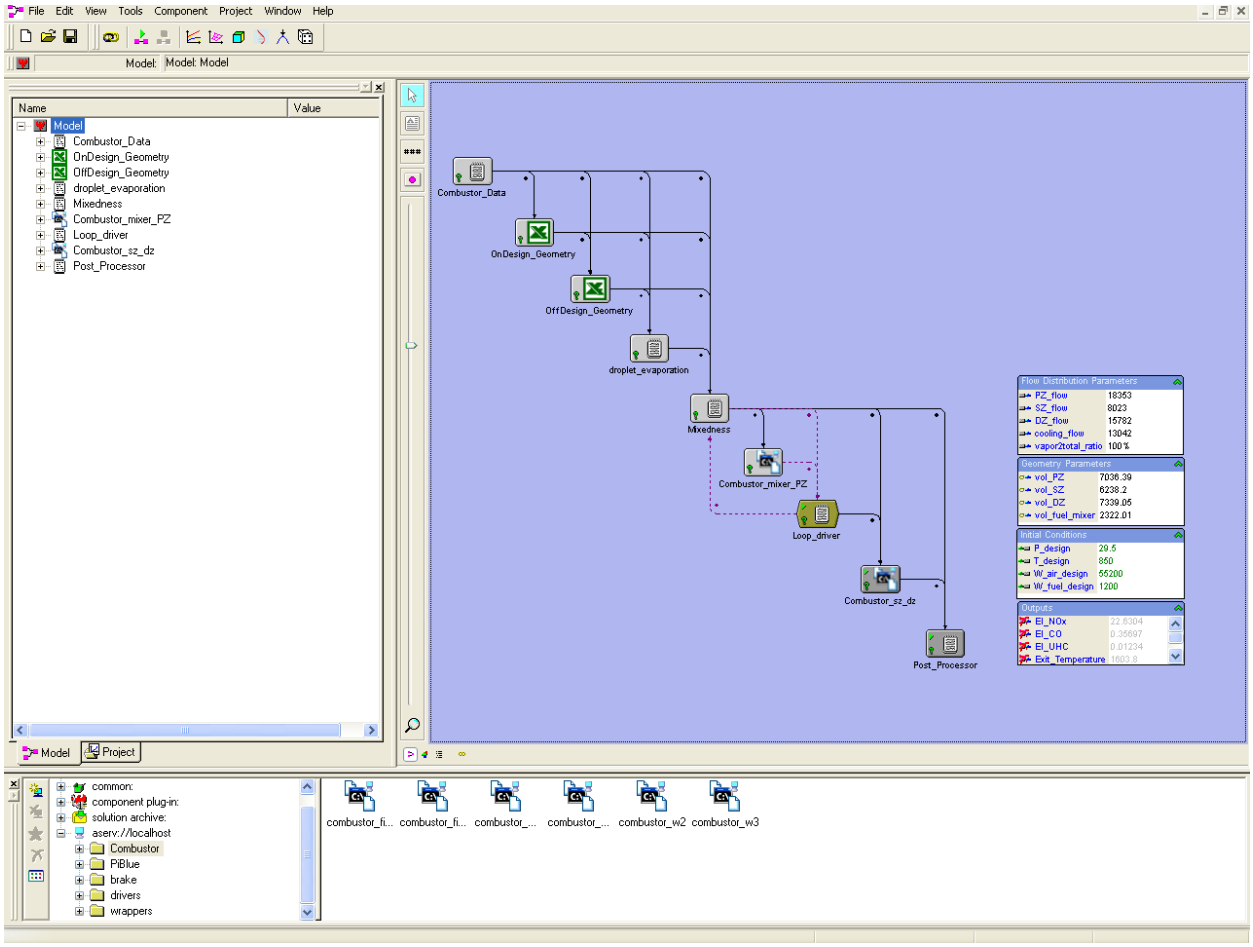

Figure 28: ModelCenter Environment for SAC Combustor Model

In this example, each data point is run one at a time, and the user may either specify the inputs via a DOE table or he may manually input the values in the window on the left-hand side of the screen.

Figure 29 shows an example screen-shot ModelCenter environment created for the RQL model. In this example, the process for running all four ICAO power settings to compute LTO emissions has been completely automated, and so four instances of the model appear in the right-hand window of the screen.

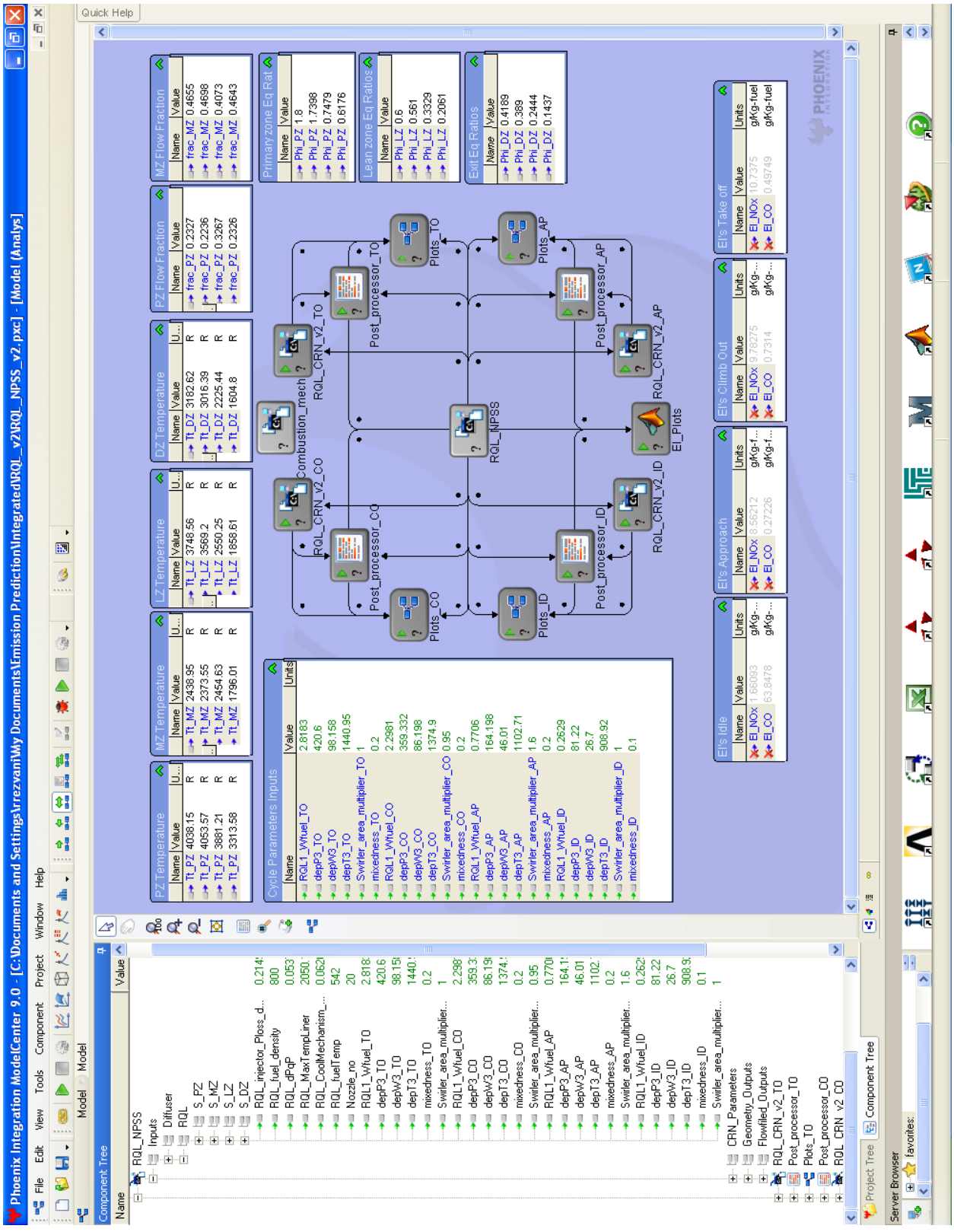

Figure 29: ModelCenter Environment for RQL Combustor Model

6 Validation Cases

Each combustor model (1-D Flow Model and CRN) was validated against published test data. The SAC was validated against the GE Energy Efficiency Engine (E^3) single-annular combustor [5], the RQL was validated against a NASA HSR combustor [44], and the Lean-Burn combustor was validated against an ONERA multi-point combustor [33]. The results are described in the following sections.

SAC

Figure 30 presents a comparison of the E^3 model results to the data published in the E^3 report. On the left, it may be seen that the EINOx is predicted very accurately. On the right, it may be seen that the EICO matches at high power but the model under-predicts at lower power.

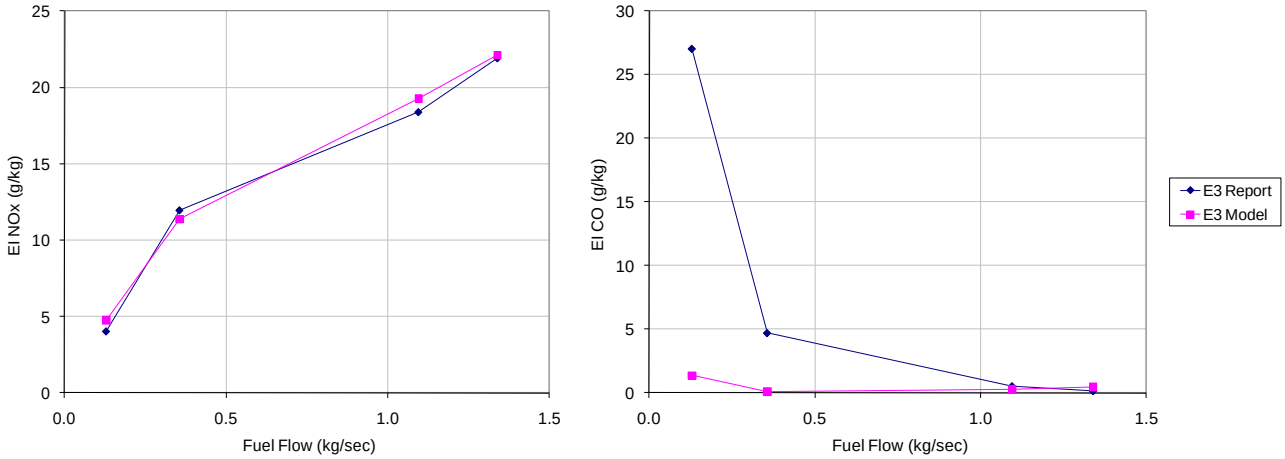

Figure 30: SAC Model Emissions Predictions vs. Validation Data

RQL

Several test conditions were reported in the HSR report; however only one condition included emissions data (see Table 11). The EINOx and EICO were matched at this point. The other conditions were evaluated and the trends were judged to be acceptable.

Table 11: HSR Combustor Test Results [44]

Test Conditions	**T3 (R)**	**P3 (psia)**	**FAR**	**Wa (lb/s)**	**Wf (lb/s)**	**EI NO_x**	**EI CO**
Subsonic Cruise	1090	80	0.02	22.2	0.44	?	?
Supersonic Cruise	1660	150	0.03	39.6	1.18	13.6	5-20
100% Thrust	1379	301	0.0329	79.2	2.6	?	?
65% Thrust	1200	212	0.0248	39.6	0.98	?	?
34% Thrust	1048	134	0.0187	38.4	0.72	?	?
15% Thrust	906	82	0.0141	25.8	0.36	?	?
5.8% Thrust	755	45	0.0113	?	?	?	?

Lean-Burn

The Lean-Burn model predictions were compared to experimental measurements on the ONERA multi-point combustor by Grisch *et al.*[21], and Matuszewski *et al*. [33]. NOx measurements were reported at Idle and Takeoff conditions. These results were matched, as shown in Table 12.

Table 12: ONERA Multi-Point Combustor Results [21, 33]

	P (bar)	Inlet T (K)	Airflow (kg/sec)	Fuel Flow (g/sec)	Overall Φ	EI NOx (Data)	EI NOx (Model)
Idle	45	480	0.344	5.03	0.215	0.8	1.75
Takeoff	22	730	1.255	38.17	0.433	12.6	12.65

7 CFM56-class Baseline Cases

To create a meaningful demonstration of a parametric design space, it is desirable to compare the three combustor types applied to the same engine cycle. The CFM56-7B27 engine cycle was selected for this purpose, since an existing, validated NPSS model was already available. The CFM56 engine model was developed previously as part of the FAA Environmental Design Space (EDS) project; the required engine cycle values taken from EDS engine model run at ICAO flight conditions and power settings are presented in Table 13. Geometry information needed for the 1-D Flow Model was determined from a CFM56 engine cross-section drawing.

Table 13: CFM56-7B27 Engine Cycle Parameters

Cycle Parameter	Unit	Takeoff	Climb	Approach	Idle
Pt3	psia	420.6	359.3	164.2	81.1
Tt3	°R	1441	1375	1103	908.9
Φ	-	0.42	0.39	0.245	0.144
Wair	lbm/sec	98.2	86.2	46.0	26.7

In the following Figures the baseline model for each combustor type (SAC, RQL, and Lean-Burn) are compared to the ICAO data. In each case, all the ICAO data for applicable single-annular CFM56-5 and CFM56-7 engines with the same combustor design was plotted, in order to give an indication of the experimental error in the ICAO data.

Figure 31 shows a good match of the SAC baseline model to the ICAO NOx and CO emissions index data for the family of CFM56 engines.

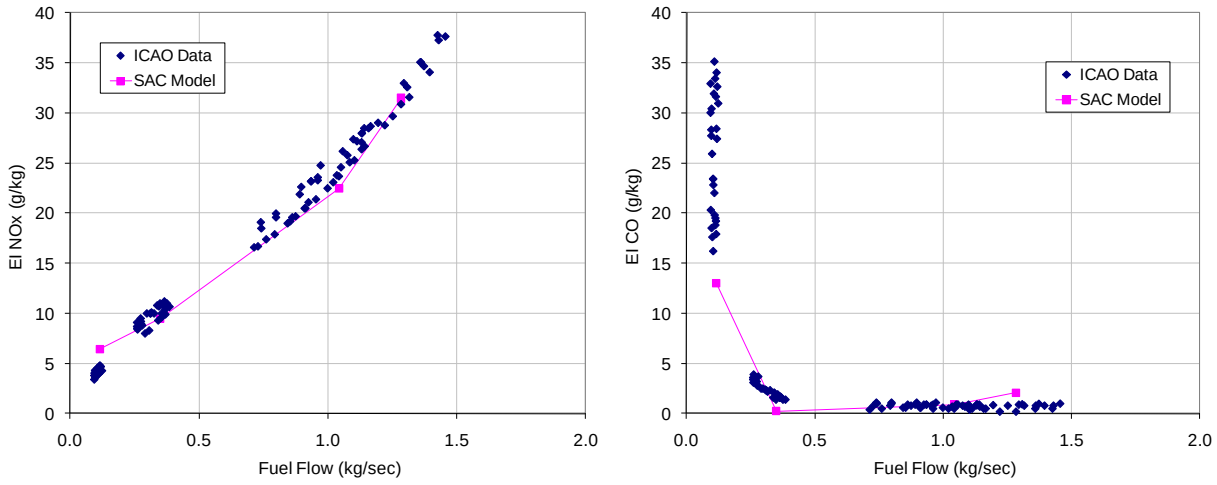

Figure 31: Comparison of SAC Model to CFM56 Baseline Data

Figure 32 presents the results for the RQL baseline model. In this case, the RQL 1-D Flow Model was "scaled up" to the CFM56 engine operating conditions. Fixed geometry fuel scheduling was assumed. Note that a 66% improvement in NOx is predicted; this is consistent with estimates given in the published literature.

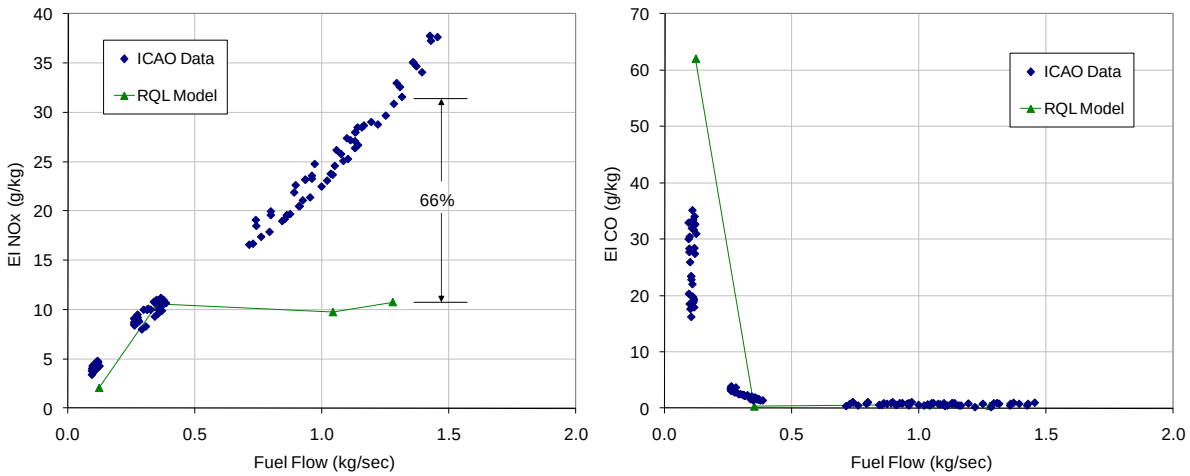

Figure 32: Comparison of RQL Model to CFM56 Baseline Data

The horizontal characteristic of the EINOx plot is of particular interest. The NOx production appears to be independent of the engine power setting over a wide range. This may be explained by the fact that the PZ equivalence ratios are greater than unity except in idle case. Since NOx production increases with reaction temperature, and reaction temperature increases as the PZ equivalence ratio is nearer to stoichiometric. Figure 33 shows that indeed the PZ reaches stoichiometric conditions at Approach power.

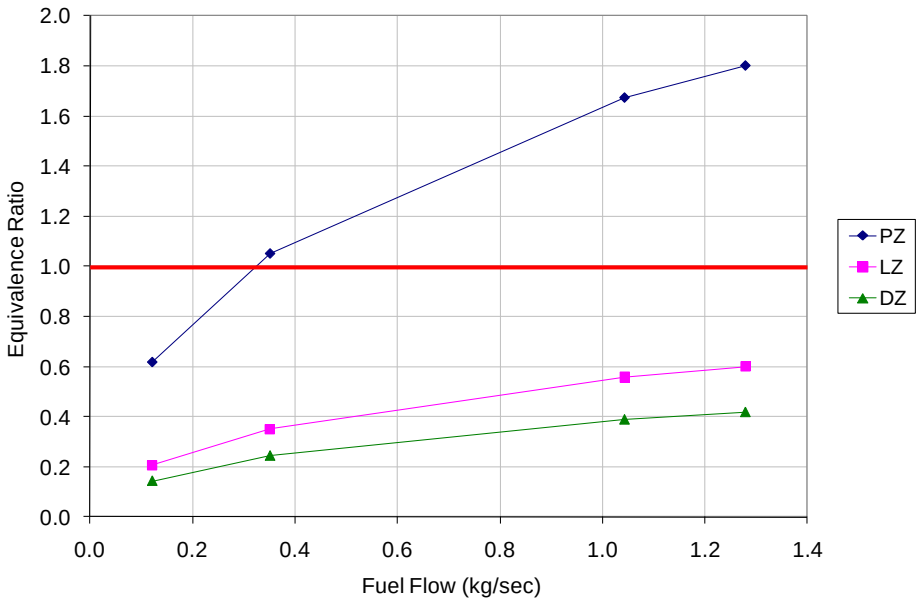

Figure 33: Variation of Equivalence Ratio with Power Setting in RQL Combustor

For the Lean-Burn baseline model, Figure 34 shows 37% improvement in NOx, again consistent with the published literature.

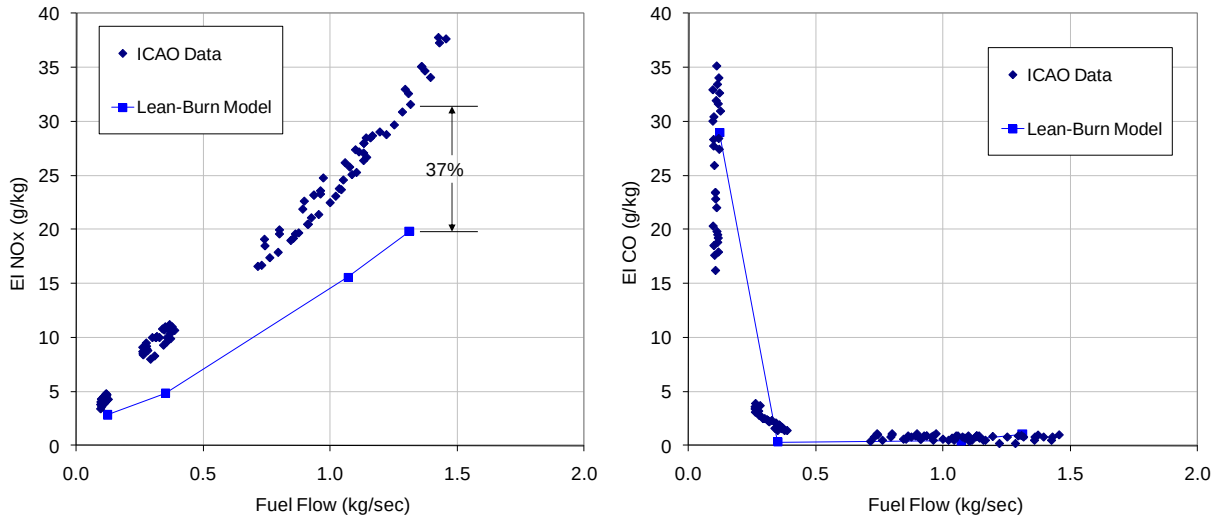

Figure 34: Comparison of Lean-Burn Model with CFM56 Baseline

Finally, one additional "sanity check" of the baseline models may be made to pusblished data with known combustor types (ref. Mongia [38]) on an overall (NOx Dp/F00) basis. In Figure 35, the SAC baseline model exactly coincides with the CFM56-7B27 engine at an OPR of around 29, as expected. At the same OPR, the RQL baseline model gives the lowest Dp/Foo NOx and plots very near a Talon X data point. Also the Lean-Burn model at the same OPR plots "in the neighborhood" of a CFM56 TAPS data point. All in all, the baseline models are judged to be good baseline points about which to build the regression models.

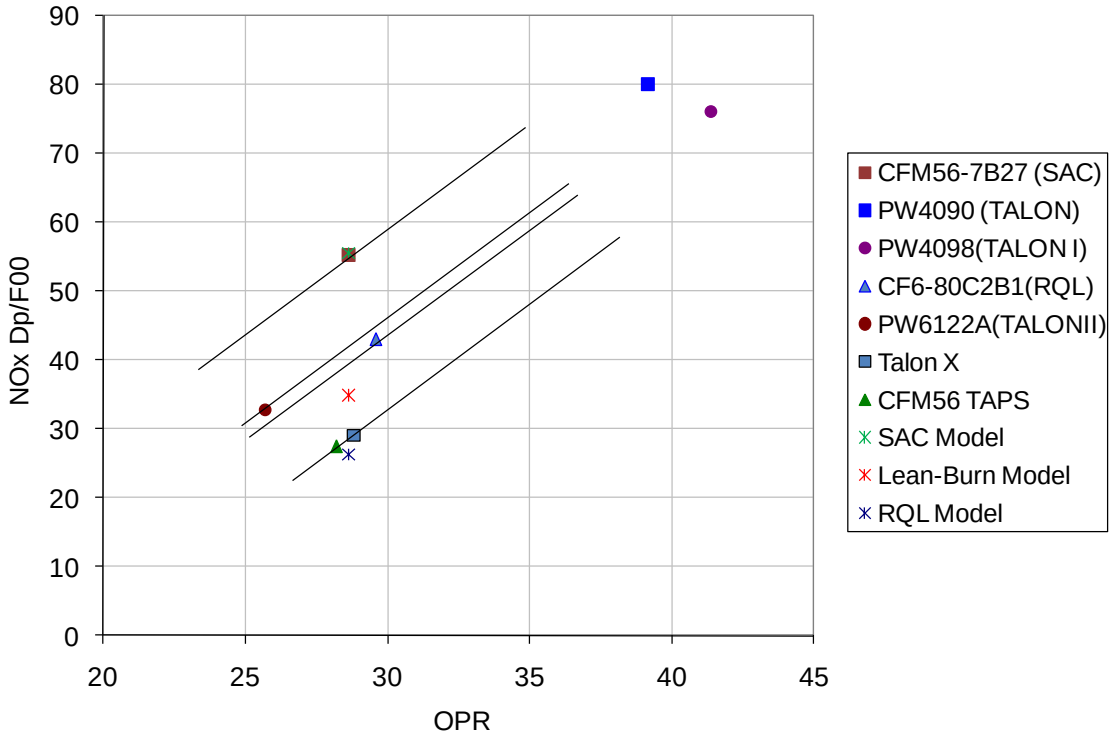

Figure 35: Comparison of Combustor Models to Existing Engines

8 Regression Models

The time required to execute the CHEMKIN Chemical Reactor Network models may hinder a comprehensive parametric analysis. This is especially true for the RQL combustor due to its use of the Partially Stirred Reactor (PaSR). Thus it is desirable to replace the CRN with a regression model. A regression model is not needed for the 1-D Flow Model because it runs quickly enough, even though the CEA gas properties do slow down the RQL model calculations.

The general steps in creating the regression model are summarized below:

- Establish baseline (center-point) values and ranges for independent variables
- Create space-filling Latin hypercube DOE
  - Approx. 15 independent variables based on CRN
  - 3000 cases run for each of the four ICAO power settings
- Generate training data by executing the models in ModelCenter
- Fit models to responses using Neural Network
  - EICO is transformed with log function
  - Hold back some of the data for validation

The baseline points for each of the three regression models (SAC, RQL, and Lean-Burn) were described in the previous section. In each case, the dependent variables (outputs) to be regressed are the EINOx and EICO for each of the four ICAO power settings. The independent variables depend upon the specific CRNs, and are summarized in previous sections.

The Neural Network method was chosen to create the regression models due to the non-linear nature of the problem. The goodness-of-fit was evaluated by examining the Model Fit Error (MFE) and the Model Representation Error (MRE). 3600 data points were used to train the Neural Networks, and 20% of the data was held back for evaluating the Model Representation Error.

The Model Fit Error evaluates the regression model against the data that was used to train the Neural Network; it indicates how well the regression model reproduces the training data. The mean and the standard deviation of the error (residual) are computed and plotted. The mean should be near zero. A histogram of the error distribution and a plot of the residuals vs. the predicted data should indicate that the error is normally distributed, and the standard deviation should be less than one. In addition, a plot of the predicted results vs. the training data should be a straight line with a value of correlation coefficient R^2 near one.

The same criteria are applied to the Model Representation Error, which compares the regression model to the data points which were not used for training the Neural Network. The Model Representation Error indicates how well the regression models perform at points for which the models must interpolate.

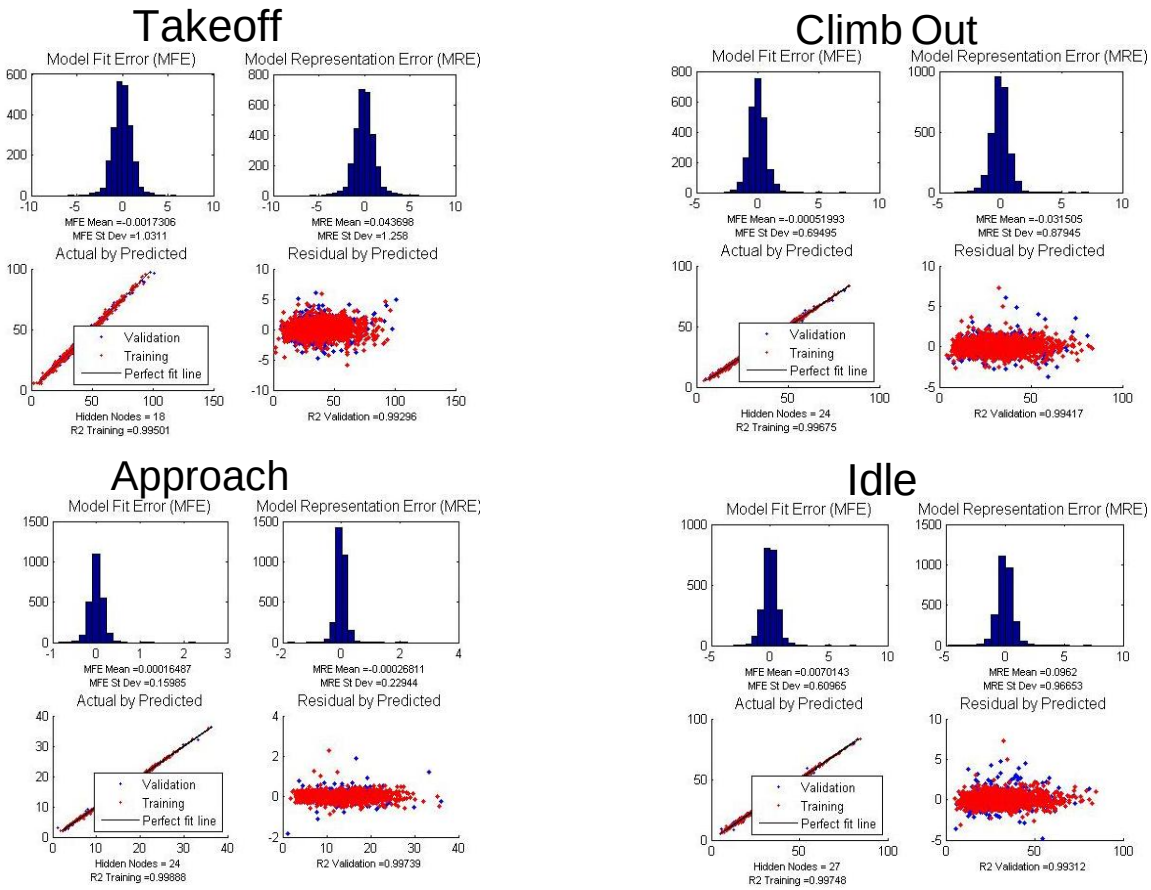

Figure 36: Goodness-of-Fit Results for Regression Model of SAC NOx

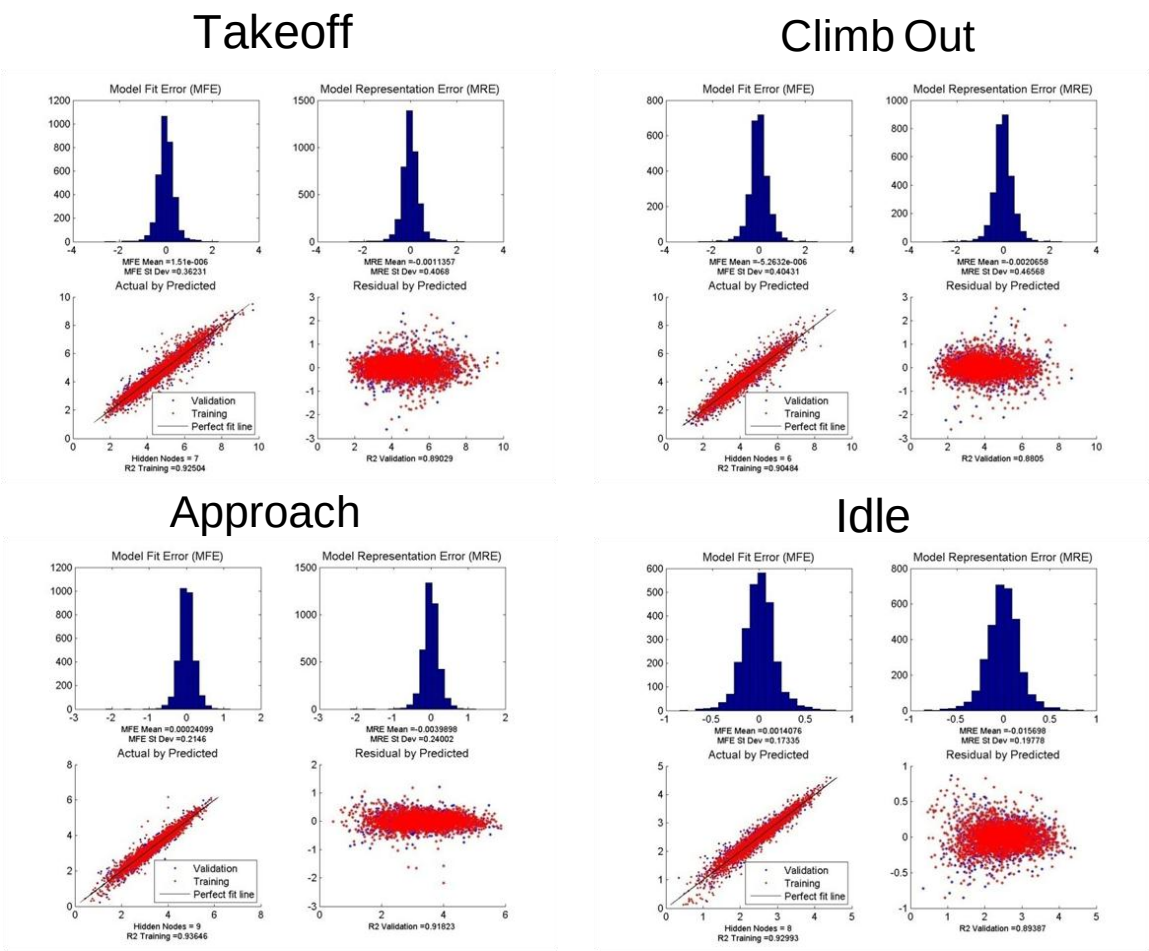

Figure 37: Goodness-of-Fit Results for Regression Model of RQL NOx

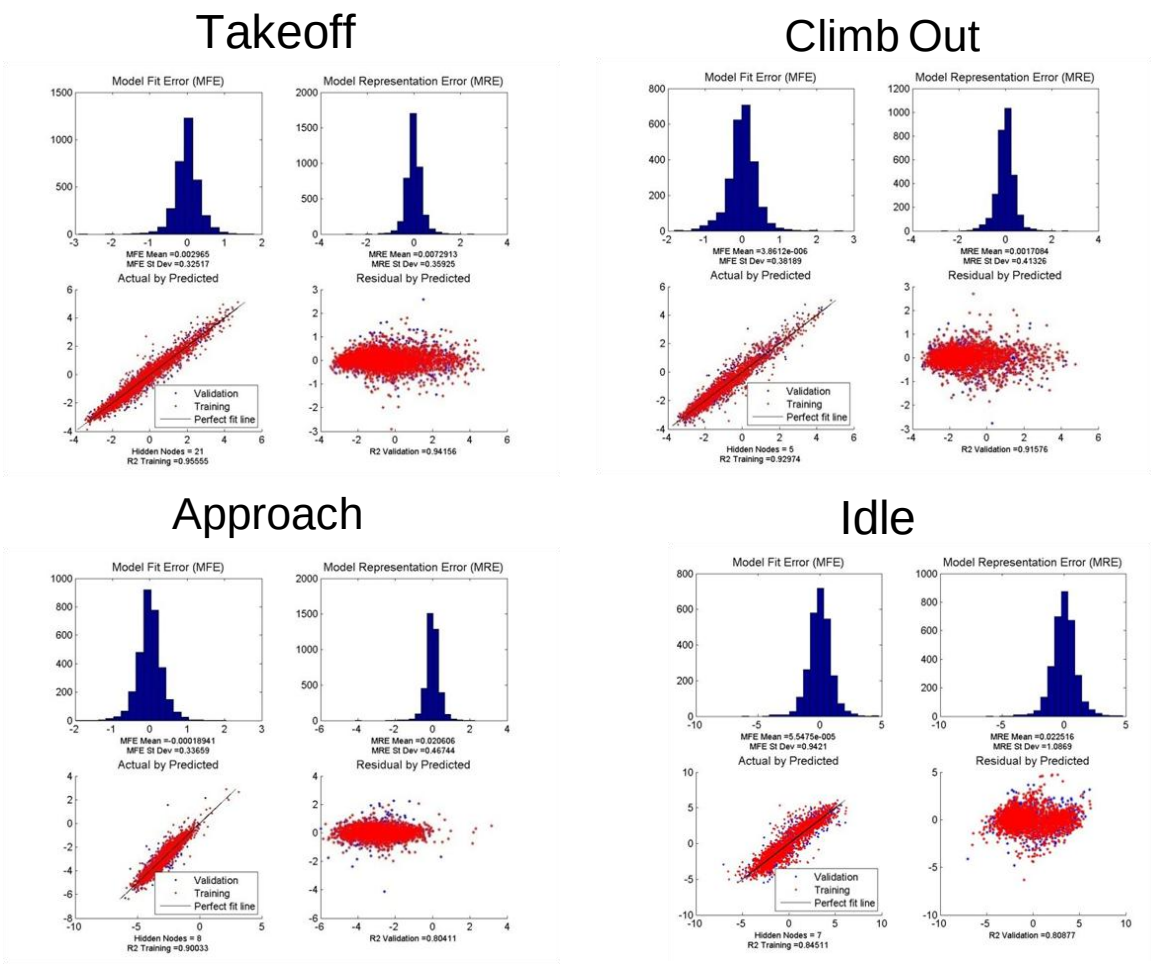

Figure 38: Goodness-of-Fit Results for Regression Model of RQL CO

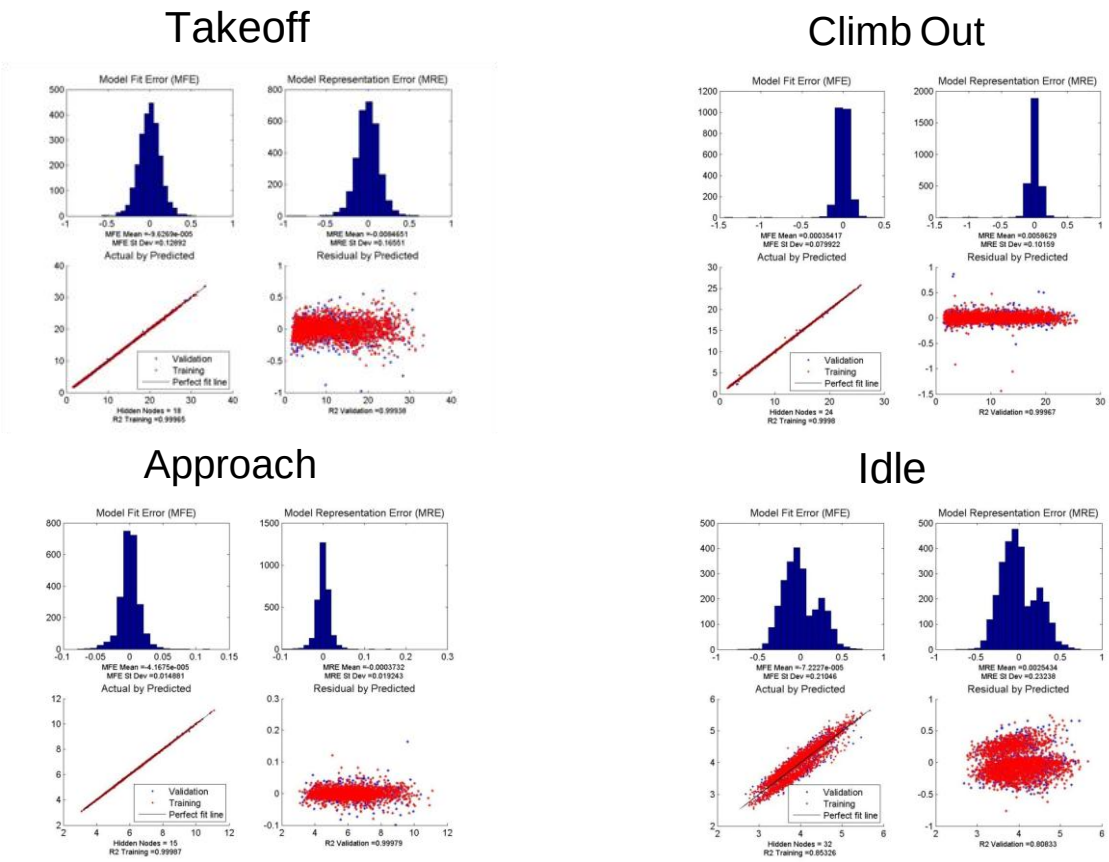

Figure 39: Goodness-of-Fit Results for Regression Model of Lean-Burn NOx

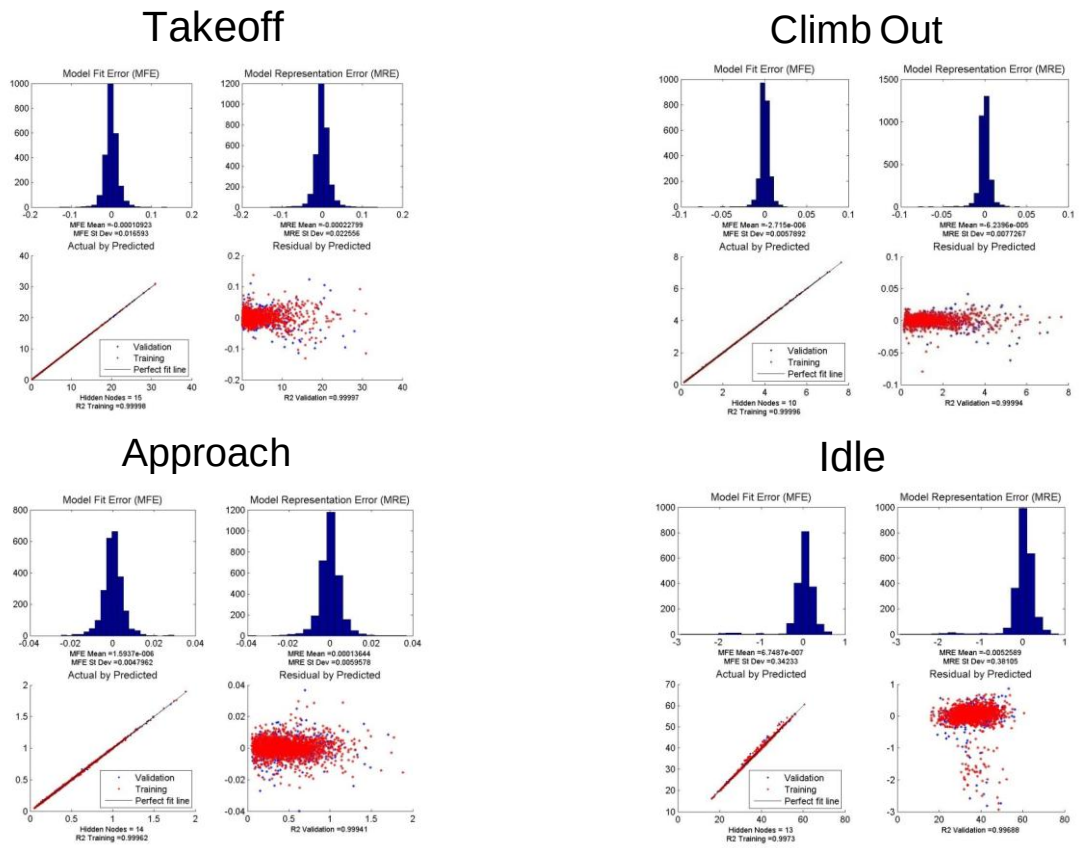

Figure 40: Goodness-of-Fit Results for Regression Model of Lean-Burn CO

The goodness-of-fit results are presented in the Figures above. It may be seen that all the regressions meet the criteria, although the Lean-Burn model displays a curious bi-modal characteristic in the NOx prediction at idle (see Figure 39). The cause for this behavior could not be verified, but it is believed to be related to the main- and pilot-zone equivalence ratios.

EmissionsNN Subelement

The regression models are incorporated into the NPSS models through a combustor subelement called EmissionNN. This subelement contains the neural network equations for EINOx and EICO for the four LTO cycle power settings. There is a different subelement for each of the three combustor types.

9 Conclusions and Recommendations

The research presented herein has successfully developed and demonstrated an emissions prediction capability for systems-level analysis during *conceptual design.* The new capability has infused more physics-based effects into the emissions predictions, such as unmixedness, droplet evaporation, rich burning, and lean burning. In addition, a library of NPSS elements has been developed to model combustors in more detail, explicitly taking into account the diffuser, the primary zone, the secondary or mixing zone, and the dilution zone. The new capability was demonstrated for three types of combustors: a conventional single annular combustor, a Rich-

Quench-Lean type of advanced combustor, and a Lean-Burn type of advanced combustor. The new NPSS elements allow parametric modeling of these types of combustors.

Recommendations for Future Research

1. While the resulting model did match well with the limited data available, it is difficult to fully assess the model accuracy without more data. It is recommended that the model be calibrated with real combustor data.
2. The Kollrack chemical mechanism described in Appendix xx was not intended for emissions prediction. In particular, the Kollrack mechanism contains only the thermal NOx mechanism which is dominant in conventional stoichiometric combustors. Other NOx and CO production processes may be more important for rich and lean conditions. Some of the limitations of the Kollrack mechanism may be reflected in the relatively poor matches to EINOx and EICO for the advanced combustors at idle conditions. It is recommended that additional reduced mechanisms be investigated. These mechanisms should be tailored for emissions prediction with Jet-A and alternative fuels.
3. The fuel injector, swirler, and unmixedness models make use of empirical relationships which were created for existing conventional combustors. Advanced combustors depend upon advanced swirler configurations for improved atomization and mixing. A more physics-based model of the fuel injection system would permit the effects of atomizer/swirler design on fuel-air distribution (unmixedness) to be evaluated. It would also permit improved flow partitioning and pressure loss variation with power.
4. The capability of the model should be increased to provide emissions predictions throughout the engine operating envelope. This capability depends mostly on the ability of the regression model to predict over a wide range of operating conditions.
5. Finally, the capability of the model should be extended to the use of alternative fuels (biofuels) and for the prediction of other species (e.g., SOx, soot). These capabilities depend upon having the appropriate chemical mechanisms and adequate models for other related combustion processes.

10 Acknowledgements

This research was performed under NASA grant number NNX07AO08A. Several members of the research team were supported by related FAA research programs. The research team would like to thank Nan-Suey Liu and Dan Bulzan from NASA Glenn Research Center for the LDI data, and John Crane of Georgia Tech for the SPRF data. The research team would also like to thank Dr. Vigor Yang, chair of the Daniel Guggenheim School of Aerospace Engineering at Georgia Tech, for his review of the project leading into the final year of research.

Appendix A: Combustion Theory

Appendix A provides relevant background information on aircraft gas turbine combustors and combustion modeling.

Parts of the Combustor

A brief explanation of the combustor elements that are used in the component modeling approach is provided here. Figure 41 illustrates the major parts of a typical gas turbine combustor.

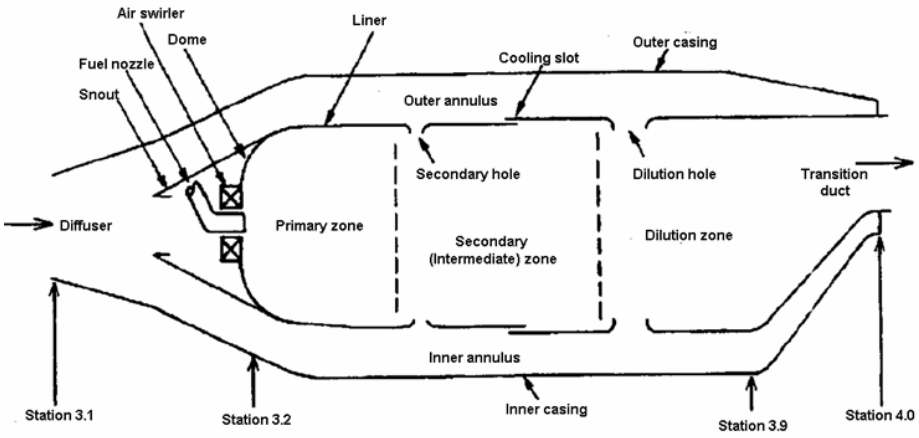

Figure 41: Parts of a Typical Gas Turbine Combustor

Diffuser

The purpose of the diffuser is to slow down the air flow coming from the compressor, to provide smooth and well-distributed flow to the combustor core and annulus, and to increase the static pressure with a minimum total pressure loss, flow distortion or swirl. Diffusers may have a flat or curved wall, with gradual or sudden expansion, and single or multiple passages.

Atomizer

Fuel atomization and spray droplet size have important effects on combustor performance and emission levels. When liquid fuel such as Jet-A is injected to the combustor core, the stream of fuel forms droplets with various sizes through aerodynamic and hydraulic instabilities [10, 59]. The heat that exists in the vicinity of the droplets evaporates most of them quickly, but the size of some of droplets is such that they enter the flame zone before they completely evaporate. Existence of droplets in the flame region creates what is called a *diffusion* flame [51].

In contrast to the *premixed* flame, where the fuel and oxidizer (air) are mixed together before burning, in the diffusion flame the fuel and air are separate and they encounter the flame from opposite directions through the diffusion process. The flame front is located at a place between the incoming air and fuel streams where the fuel to air ratio is stoichiometric and it always produces the maximum flame temperature. Thus the existence of droplet burning and consequentially the diffusion flame has a significant effect on the level of pollutants. While high temperature diffusion flames can burn off Carbon Monoxide (CO) and Unburned Hydro Carbons

(UHC), at the same time they will enhance one of the NO_x formation mechanisms and result in a higher level of NOx emissions [48].

The droplet size distribution depends on many factors such as atomizer type, flow-field around the fuel jet and upstream fuel line conditions (see Figure 42).

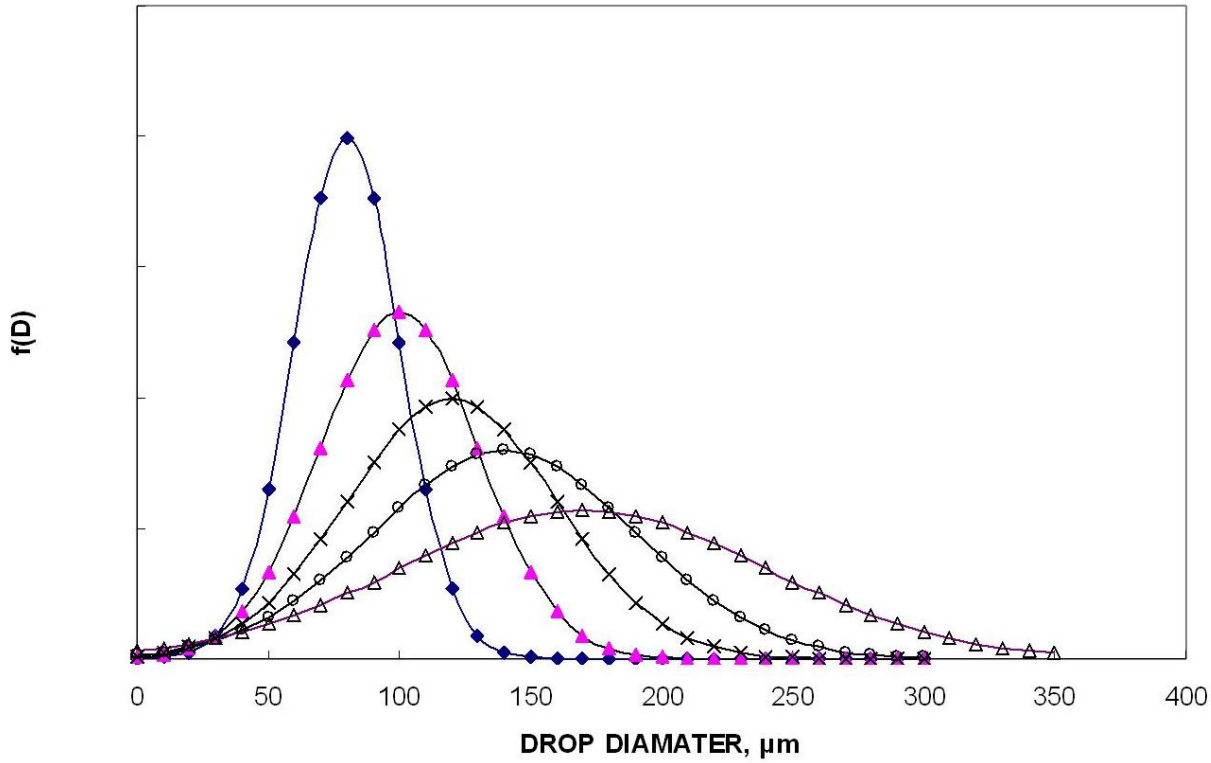

Figure 42: Example Droplet Size Distribution

It is convenient to work with mean droplet diameter instead of droplet distribution. Among many different definitions available for mean diameter, the Sauter Mean Diameter or SMD is widely used in combustion applications and is defined as the diameter of a droplet whose ratio of volume to surface is the same as whole fuel spray. The SMD can be looked at as an average or mean value diameter of all droplets that are present in the spray. Droplet models are usually defined in term of the droplet SMD as a function of atomizer type. Lefebvre [28] and Mellor [37] have provided droplet models for simplex and air blast atomizers.

Swirler

The other element that has a direct effect on the structure of the flame, emissions levels and overall combustor efficiency is the swirler. The main purpose of the swirler is to impose a tangential motion to the flow and create a flow recirculation that brings the hot gases back to the flame front. This increases the flame stability and prevents flame blow-off. At the same time the toroidal motion of the flow reduces the flame length [9]. The amount of swirling that a swirler imposes to the flow is quantified by the *Swirl* number (*S*) which is shown in the equation below [11].

$$S = \frac{G_\phi}{G_x \, r_0} \qquad (1)$$

where G_φ is the axial flux of angular momentum, G_x is the axial flux of momentum (axial thrust) and r_0 is the outer radius of the swirler. Flow recirculation is obtained for strong Swirl number greater than 0.6.

Another purpose of the swirler is to enhance the mixing of the fuel with air [9]. Swirlers may be axial, radial or a combination of both (Figure 43).

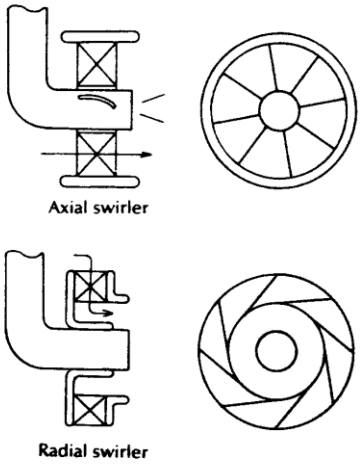

Figure 43: Axial and Radial Swirlers

Primary, Secondary and Dilution Zones

The number of zones in a core section of a combustor depends on the number of rows of dilution holes. Depending on the combustor type there are one, two or three rows of holes and each region between the rows is considered as one zone. Often the combustor core section is divided into three major axial parts. These parts are distinguished from each other by introducing additional air that comes from the annulus in the form of jets through dilution holes and crossing the main core flow.

There are specific tasks that should be accomplished in each zone. The Primary Zone is where the flame is anchored. In this region, the flow is characterized as turbulent flow with high intensity. The main purpose of the Primary zone is to keep the flame burning at all conditions. A swirler induced recirculation is contained in the primary zone to recirculate part of the hot gases back to the flame region to prevent flame blow-off or extinction. In conventional combustors the primary zone fuel to air ratio is close to the stoichiometric value to have a stable flame.

To burn off the unburned fuel and hydrocarbons coming from the Primary Zone, additional air from the annulus is introduced to the core section through the first row of dilution holes. The region between the first and next set of dilution holes is called the Intermediate or Secondary Zone. The Primary and Secondary zones have the most significant contribution to the total NO_x and CO emissions [20, 40].

The addition of additional air from annulus to the core section through the second row of dilution holes identifies the beginning of the Dilution Zone, which ends at the combustor exit plane. The flow in this post-flame region is relatively calm. The purpose of the Dilution zone and its dilution holes is to provide a desired exit temperature and velocity profile for the first stage of the turbine. The exit profiles are tailored to the needs of the turbine vanes and blades in terms of life and thermal and mechanical stress management.

Simplified Droplet Evaporation and Burning Model

Droplet burning in the combustor is the major source of NO_x emissions and it is important to find a way to consider it in the emissions prediction model. Since the fuel is sprayed into the combustion area in liquid form, it is important to investigate whether all the fuel evaporates before combustion or if some of the droplets will survive to enter the flame zone. The presence of fuel droplets in the flame zone creates a diffusion flame in addition to the premixed flame, which result in a high local flame temperature and a high NOx emissions level. A complete and detailed model for droplet evaporation and burning is computationally intensive and time consuming; however, for the current task, a faster model is required to determine the quantity of evaporated fuel and the effect of fuel droplets on the species concentrations without considering fine details of the process.

The droplet Sauter Mean Diameter (SMD) equation will be used to calculate the size of the droplets. Many SMD models are provided for the different types of injectors which can be used for this purpose [28, 37]. Flow and evaporation time scale analysis determines the fraction of droplets that evaporate before ignition. The physical properties of fuel and air mixtures can be obtained from aviation fuel properties handbooks [3, 12, 22, 53].

The SMD model of a pressure-swirl atomizer is given below as an example [28].

$$SMD = 2.25\sigma_L^{0.25}\mu_L^{0.25}\dot{m}_L^{0.25}.\Delta P_L^{-0.5}\rho_A^{-0.25} \qquad (2)$$

σ_L: Fuel (Jet-A) surface tension (N/m)
μ_L: Fuel (Jet-A) dynamic (absolute) viscosity (Poise, Pa.s)
$\dot{m}_L$: Fuel flow rate (Kg/s)
ΔP_L: Pressure drop across atomizer (Pa)
ρ_A: Gas density (Kg/m3)

In order to find the amount of vaporized fuel in a given volume (mixer volume) before entering into flame zone, following equation is derived from the droplet evaporation D^2 law and mass conservation principle:

$$\frac{\dot{m}_{f_{vaporized}}}{\dot{m}_{f_{total}}} = \left(\frac{\sqrt{SMD^2 - K.\tau_{mixer}}}{SMD}\right)^3 = \left(1 - \frac{K.\tau_{mixer}}{SMD}\right)^{\frac{3}{2}} = \left(1 - \frac{\tau_{mixer}}{\tau_{evaporation}}\right) \qquad (3)$$

K: Mean fuel evaporation constant
τ_{mixer}: Mixing characteristic time
$\tau_{evaporation}$: Evaporation characteristic time
SMD: Droplet Sauter mean diameter

Evaporation time in mixer (τ_{mixer}) is obtained from Equation (4):

$$\tau_{mixer} = \frac{\rho_{Air} . V}{\dot{m}_{Air}} \qquad (4)$$

The part of the fuel flow that remains in liquid form is considered to be burned at stoichiometric ratio to resemble the diffusion flame; therefore an adequate amount of air will be assigned to liquid fuel flow to make the equivalence ratio equal to one. The rest of the airflow and vaporized fuel flow will be assumed to be mixed before ignition. The air and fuel mixture is not uniform in the combustor and this non-uniformity should be modeled because it has a significant effect on flame temperature and pollutant levels.

Non-Uniform Fuel and Air Mixture Model

To compensate for the non-uniformity and equivalence ratio dispersion that exist in the combustor, the mixing parameter *S*, also known as the unmixedness degree, is used. The unmixedness degree, as defined in Equation (5), determines the distribution of flow fraction over an interval of equivalence ratio [22, 56].

$$S = \frac{\sigma}{\overline{\varphi}} \qquad (5)$$

σ: Standard deviation
$\overline{\varphi}$: Mean equivalence ratio

As shown in Figure 44, there is one unique value of the unmixedness degree for each given mean equivalence ratio which corresponds to various engine power settings.

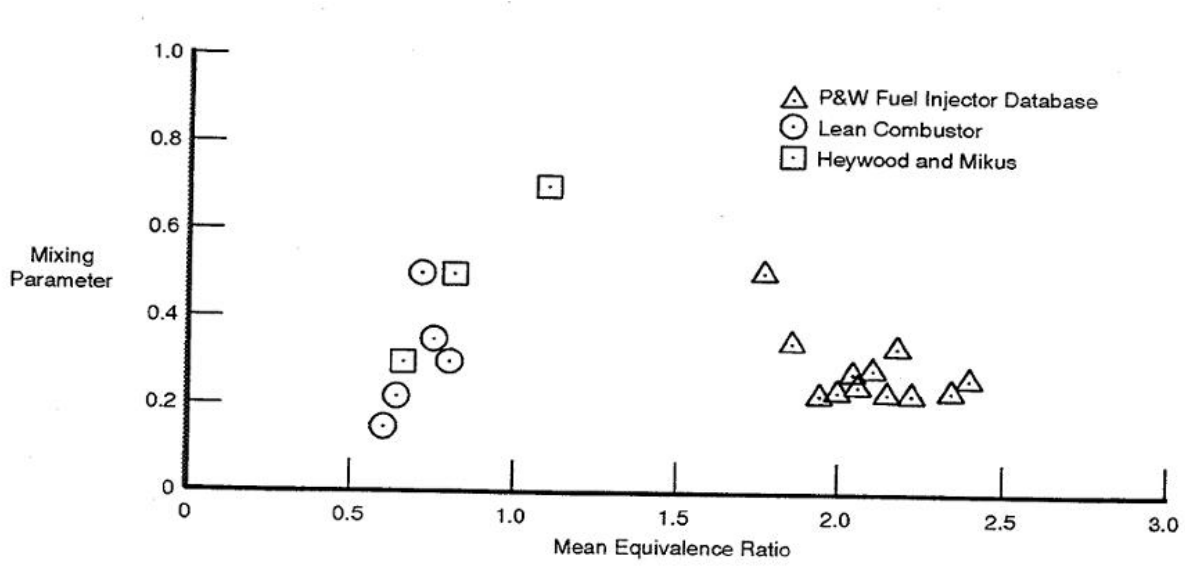

Figure 44: Heywood Unmixedness Parameter [56]

Knowing the value for *S* and the mean equivalence ratio ($\overline{\varphi}$), the value for the standard deviation, σ is determined and the Gaussian (Normal) distribution of equivalence ratio is obtained as in Equation (6).

$$f(\varphi) = \frac{1}{\sqrt{2\pi\sigma^2}} e^{-\frac{(\varphi-\bar{\varphi})^2}{2\sigma^2}} \qquad (6)$$

It should be noted that each combustor model may have its own S-$\bar{\varphi}$ diagram which should be obtained through experiment and tuning of the model to match the known data.

Idealized Chemical Reactors

Idealized chemical reactors are used to simplify combustion reaction calculations. The most common types of reactors are the perfectly stirred reactor and the plug flow reactor. In this research the partially stirred reactor is also considered.

Perfectly Stirred Reactor (PSR)

The perfectly stirred reactor (PSR) is an ideal reactor that neglects mixing processes in a reaction [59]. In a combustion system, there exists a characteristic flow mixing time τ_{flow} and a characteristic chemical time τ_{chem}. A non-dimensional parameter, the Damkohler number *Da*, can be introduced to characterize this system:

$$Da = \frac{\tau_{flow}}{\tau_{chem}}$$

When Da $\ll 1$, it suggests either the mixing rates are very high or the chemical reaction rates are very slow, and the burning rate is almost completely dominated by the chemical kinetics of the mixture and the mixing process can be ignored.

Inside a perfectly stirred reactor (PSR), it is assumed that the Damkohler number is essentially zero and thus the mixture is considered perfectly stirred. Mixing has no effect on the system and is neglected. This assumption allows for a large reduction in the complexity of the governing equations.

Conservation Equations for the PSR

The conservation equations for the perfectly stirred reactor may be written as follows. The control volume for the analysis is shown in following figure:

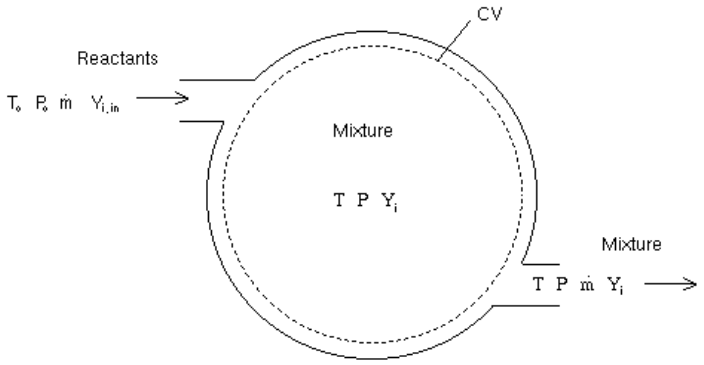

Figure 45: Diagram of a Perfectly Stirred Reactor [59]

Mass conservation for an arbitrary species *i* may be written as

$$0 = \dot{m}_i''' \forall + \dot{m}_{i,in} - \dot{m}_{i,out}$$

where $\dot{m}_i''' \forall$ is the rate of generation or destruction of mass of the i^{th} species inside the control volume $\forall$,
and $\dot{m}_{i,in}$ and $\dot{m}_{i,out}$ are the mass flow of the i^{th} species into and out of the control volume, respectively.

The generation or destruction of a species is written as

$$\dot{m}_i''' = \dot{\omega}_i MW_i$$

where $\dot{\omega}_i$ is the net production rate of the i^{th} species in mol/m and MW_i is the molecular weight of the i^{th} species in kg/mol.

The mass flow of the i^{th} species into the control volume is:

$$\dot{m}_{i,in} = \dot{m} Y_{i,in}$$

where $Y_{i,in}$ is initial mass fraction of i^{th} species; and similarly, the mass flow out of the control volume is

$$\dot{m}_{i,out} = \dot{m} Y_{i,out}$$

The conservation of energy for the PSR is:

$$\dot{Q} = \dot{m}(h_{out} - h_{i,in})$$

Also, $\dot{Q}$ can be expressed by individual species:

$$\dot{Q} = \dot{m}(\sum_{i=1}^{N} Y_{i,out} h_i(T) - \sum_{i=1}^{N} Y_{i,in} h_i(T_{in}))$$

where h_i is the specific enthalpy of the i^{th} species, and

$$h_i(T) = h_{f,i}^o + \int_{T_{ref}}^{T} c_{p,i}(T) dT$$

where $h_{f,i}^o$ is the enthalpy of formation of the i^{th} species and $c_{p,i}(T)$ is specific heat of i^{th} species

Plug Flow Reactor (PFR)
A plug flow reactor is an ideal reactor filled with ideal gas mixture, and assumes it has steady, one-dimensional inviscid flow properties. It implies that there is no mixing in the axial direction of PFR. The control volume for the conservation equations refers to following figure.

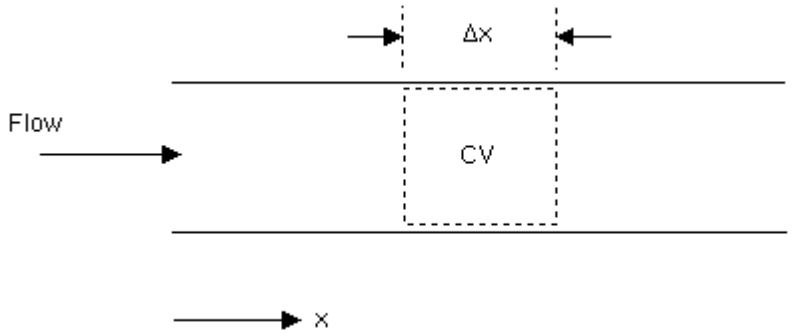

Figure 46: Diagram of a Plug Flow Reactor [59]

Conservation equations for PFR:

Conservation of Mass:

$$\frac{d(\rho u_x A)}{dx} = 0$$

Conservation of Momentum:

$$\frac{dp}{dx} + \rho u_x \frac{du_x}{dx} = 0$$

Conservation of Species:

$$\frac{dY_i}{dx} - \frac{\dot{\omega}_i MW_i}{\rho u_x} = 0$$

Conservation of Energy:

$$\frac{dT}{dx} = \frac{u_x^2}{\rho c_p}\frac{d\rho}{dx} + \frac{u_x^2}{c_p}\left(\frac{1}{A}\frac{dA}{dx}\right) - \frac{1}{u_x \rho c_p}\sum_{i=1}^{n} h_i \dot{\omega}_i MW_i = 0$$

Where ρ is the mass density and u_x is axial velocity of the mixture flow, while A is local cross area of the PFR.

Partially Stirred Reactor (PaSR) [7]
When the turbulent mixing rate is not fast compared to chemical kinetics, the degree of mixing can have a profound impact on the reactor characteristics. The PaSR focuses on the influence of an unmixed state on the reactor properties. The mean thermo-chemical properties inside a PaSR are assumed to be spatially homogeneous, but imperfectly mixed at the molecular level.

A PaSR addresses the interaction between chemical reactions and turbulence [8, 13]. It allows fluid dynamics to control the extent of the molecular mixing and consequently the chemical reactions, by means of an additional parameter: the scalar mixing time, τ_{mix}, which is proportional to the turbulent eddy turnover time:

$$\tau_{mix} = C_D \frac{\kappa}{\varepsilon}$$

C_D is a constant for certain flow configuration, κ is turbulent kinetic energy and ε is turbulent dissipation rate.

One of the crucial issues of modeling chemical reaction in turbulent flows is the chemical closure problem. Due to the highly nonlinear dependence of chemical reactions on temperature, using the mean temperature and mean species concentrations for calculations of mean chemical reaction rates can cause significant errors. To avoid the closure problem associated with non-linearities in the equations governing turbulent flow, a transport equation for the joint PDF of flow variable scalars, $P_\phi(\psi, \vec{x}, t)$, is introduced, irrespective of the complexity and nonlinearity of the reaction mechanism.

To solve the PDF transport equation practical for general turbulent reactive flows with large dimension, Pope [43] developed a Monte Carlo algorithm. The dependent variable in the simulation is represented by an N-member ensemble:

$$\phi^{(1)}, \phi^{(2)}, ..., \phi^{(n)}, ..., \phi^{(N)}$$

Here each of the members of the ensemble is referred to as a "particle". Each particle is ascribed a unique number, $1 \le n \le N$, no ordering is implied. Operations are performed either on all particles or particles selected at random. The ensemble average of any function $Q(\phi)$ is defined by

$$\langle Q(\phi) \rangle \equiv \frac{1}{N} \sum_{n=1}^{N} Q(\phi^{(n)})$$

In the limit of large N, Pope [43] showed that the ensemble average $\langle Q(\phi) \rangle$ converges to the corresponding density-weighted average, i.e.,

$$\langle Q(\phi) \rangle \to \widetilde{Q}(\phi) = \int Q(\psi) \widetilde{P}_{\bar{\phi}}(\psi) d(\psi)$$

For the general multiple reactive scalars, the transport equation for the joint PDF in the PaSR is derived by integrating the governing equation of the single-point joint scalar PDF over the reactor volume. The resulting PDF transport equation for the PaSR is:

$$\frac{\partial \widetilde{P}_{\bar{\phi}}(\overline{\psi}, t)}{\partial t} = -\sum_{\alpha=1}^{K_{tot}} \frac{\partial}{\partial \psi_\alpha} \left\{ S_\alpha(\overline{\psi}) \widetilde{P}_{\bar{\phi}}(\overline{\psi}, t) \right\} + \frac{1}{\tau_R} \sum_{i=1}^{M} \left\{ \widetilde{P}_{\bar{\phi},i}(\overline{\psi}, t) - \widetilde{P}_{\bar{\phi}}(\overline{\psi}, t) \right\} -$$
$$\sum_{\alpha=1,\beta=1}^{K_{tot}} \frac{\partial^2}{\partial \psi_\alpha \partial \psi_\beta} \left\{ \left\langle \varepsilon_{\alpha\beta} \middle| \bar{\phi} = \overline{\psi} \right\rangle \widetilde{P}_{\bar{\phi}}(\overline{\psi}, t) \right\}$$

The first two terms on the right hand side of the above equation represent the effects of chemical reaction and the through-flow on the joint PDF, respectively. The last term represents the effect of micro-scale mixing on the PDF, which requires the use of a finite rate mixing model. Two widely used mixing models are employed as options in the current PaSR model: the modified

Curl's mixing model [26] and the linear-mean-square-estimation (LMSE) model [18] their mathematical formulas are listed below:

The modified Curl's mixing model:

$$-\sum_{\alpha=1,\beta=1}^{K_{tot}} \frac{\partial^2}{\partial\psi_\alpha \partial\psi_\beta}\left\{\left\langle \varepsilon_{\alpha\beta} \middle| \bar{\phi}=\overline{\psi}\right\rangle \widetilde{P}_{\bar{\phi}}(\overline{\psi},t)\right\}=$$

$$\frac{1}{\tau_{mix}}\left\{\iint_{\psi',\psi''} \widetilde{P}_{\bar{\phi}}(\psi',t)\widetilde{P}_{\bar{\phi}}(\psi'',t)H(\psi',\psi'''|\overline{\psi})d\psi' d\psi'' - \widetilde{P}_{\bar{\phi}}(\overline{\psi},t)\right\}$$

where H is the transitional probability defined as $H(\psi',\psi''|\overline{\psi})=1/|\psi''-\psi'|$ for $\psi\in[\psi',\psi'']$ otherwise 0.

The Interaction-by-Exchange-with-the-Mean (IEM) or the Linear-Mean-Square- Estimation (LMSE) model is:

$$-\sum_{\alpha=1,\beta=1}^{K_{tot}} \frac{\partial^2}{\partial\psi_\alpha \partial\psi_\beta}\left\{\left\langle \varepsilon_{\alpha\beta} \middle| \bar{\phi}=\overline{\psi}\right\rangle \widetilde{P}_{\bar{\phi}}(\overline{\psi},t)\right\}=\frac{C_\phi}{2\tau_{mix}}\frac{\partial}{\partial\psi_\alpha}\left\{(\overline{\psi}-\widetilde{\phi})\widetilde{P}_{\bar{\phi}}(\overline{\psi},t)\right\}$$

Where C_ϕ is a constant parameter for the model.

The unmixedness is a parameter used to quantify the unmixed nature, which is bounded by 0 and 1, and represent completely segregated and perfectly mixed state, respectively.

The theoretical values of the unmixedness at the statistically stationary state for the two mixing models are:

Modified Curl's model

$$unmixedness=\frac{1}{1+\tau_{res}/3\tau_{mix}}$$

LMSE (IEM) model

$$unmixedness=\frac{1}{1+C_\phi\tau_{res}/3\tau_{mix}}$$

Reactor Equations

The PaSR consists of an adiabatic chamber having *M* steady flows inlet streams and one outlet. The reactor pressure is assumed to be constant, no surface reaction. In order to represent the evolution of the PDF properly by a stochastic scheme, PaSR addresses all problems in a transient manner. The overall mass balance for the gas mixture inside the PaSR is

$$\frac{d\langle M\rangle}{dt}=\frac{d(\langle\rho\rangle V)}{dt}=\sum_{i=1}^{M}\dot{m}_i-\dot{m}_o=0$$

where $\dot{m}_i$ is the mass flow rate of the i^{th} inlet and is the through-flow mass flow rate. The average properties of the PaSR are obtained from the ensemble of particles inside the reactor. Each particle is treated as an independent PSR and interacts with others only through the molecular mixing process. Therefore, the conservation of energy and species is applied to an individual particle rather than to the reactor.

$$\frac{dY_k^{(n)}}{dt} = \frac{1}{\dot{m}_o \tau_R} \sum_{i=1}^{M} \left\{ \dot{m}_o (Y_{i,kt} - \langle Y_k \rangle) \right\} + \frac{W_k \dot{\omega}_k^{(n)}}{\rho^{(n)}}$$

The energy equation for a particle is:

$$\frac{dT^{(n)}}{dt} = \frac{1}{C_p^{(n)} \dot{m}_o \tau_R} \sum_{i=1}^{M} \dot{m}_i \left(\sum_{k=1}^{k_g} Y_{i,k} (h_{i,k} - \langle h_k \rangle) \right) - \sum_{k=1}^{k_g} \frac{W_k \dot{\omega}_k^{(n)} h_k^{(n)}}{\rho^{(n)} C_p^{(n)}}$$

In the above equations, the angled bracket ($\langle \ \rangle$) indicates the ensemble average that we use to approximate the density-weighted average in the simulation. The average residence time of the reactor, τ_R , is calculated as

$$\tau_R = \frac{\langle \rho \rangle V}{\dot{m}_o}$$

Stochastic Simulation

A time marching scheme with a time-step size of Δt is used to solve τ_R and the stochastic simulation is carried out by the following sequential procedures with *N* statistical particles:

First, we set the properties of these N_c particles from the stochastic ensemble, the properties of the inlet mixture. The number of correct particles in a time step is chosen as:

$$N_c = N \times \Delta t / \tau_R$$

Second, particles are chosen to mix with each other, with the modified Curl's mixing model,

$$N_m = C_m N \times \Delta t / \tau_{mix}$$

C_m is a parameter for the modified Curl's model. If the IEM (LMSE) model is used, IEM (LMSE) Equation is solved to determine the statistics over a period of Δt.

At last, we compute chemical kinetics for each particle by integrating the species and energy equations over a period of Δt .

These three procedures are repeated for the next time step until the end of the simulation time is reached.

Chemical Kinetic Mechanisms

Although it is generally perceived that the reaction of fuel with air can be written as a single line of chemical equation at which on the left there are reactants and at the right there are products with coefficients to conserve the number of atoms at both sides; however, this is just overall picture of what really happens and does not tell the whole story. This type of chemical equation which is called the *global reaction,* gives the end products of chemical reaction without mentioning intermediates steps. In fact, the creation of product molecules is not the direct result of fuel and air molecules collision; it is more probable that there are many intermediate molecular and atomic collisions and reactions that are responsible for forming the final product. These reactions are called *elementary reactions* and they represent what really happens in combustion process in molecular scale (Figure 47).

$$CO + O_2 \underset{k_r}{\overset{k_f}{\Leftrightarrow}} CO_2 + O$$

$$O + H_2O \underset{k_r}{\overset{k_f}{\Leftrightarrow}} OH + OH$$

$$CO + OH \underset{k_r}{\overset{k_f}{\Leftrightarrow}} CO_2 + H$$

$$H + O_2 \underset{k_r}{\overset{k_f}{\Leftrightarrow}} OH + O$$

$$O + N_2 \underset{k_r}{\overset{k_f}{\Leftrightarrow}} NO + N$$

$$N + O_2 \underset{k_r}{\overset{k_f}{\Leftrightarrow}} NO + O$$

Figure 47: Example of Elementary Reactions

Each elementary reaction can have forward or forward/reverse reaction. Each direction as is shown in Figure 47 has forward and reverse reaction rates k_f and k_r which are used to find the rate of production or destruction of species present in the reaction. For example the production rate of CO in the above mechanism can be calculated as follows:

$$\frac{d[CO]}{dt} = -k_f[CO][O_2] + k_r[CO_2][O] - k_f[CO][OH] + k_r[CO_2][H]$$

The reaction rate "constants" are not constant but are functions of reaction temperature, usually modeled as:

$$k = AT^n \; e^{-E/RT}$$

where the variables are the pre-exponential factor or frequency factor *A*, reaction order *n* and activation energy *E*.

Many species (i.e. CH, OH, HO_2) that are present in elementary reaction are unstable and do not exist in normal situations and do not last for a long time and will be destroyed or converted to stable species. These species usually play an important role in the formation or destruction rate of final product.

Combustion of a specific fuel with air has its own set of elementary reactions which is called the *Combustion Mechanism* of that fuel. As the fuel molecule becomes more complex with higher Carbon number, more intermediate species get involved in the process that increases the number of elementary reactions and makes the combustion mechanism more complex; thus, it is hard to model the complete combustion mechanism for these types of fuels. The solution is to lump the couple of first initial elementary reactions that are responsible of breaking fuel molecule to smaller ones (Pyrolysis process) into a few global chemical equations. In this approach, the molecules that have available combustion mechanism are chosen as the smaller molecules to make it possible to combine the pyrolysis global equations with known combustion mechanism of smaller molecules to model the combustion mechanism of the fuel itself.

Besides the difficulty of modeling the combustion mechanism of pure fuels with high Carbon number, there exists another problem associated with the fuels that are being used in industry. Most of the hydrocarbon based fuels that are being used (including aviation fuels) are derivative of petroleum and are mixture of different species. To make the matter worse, the percentage of different species present in these fuels are not fixed and changes for different oil wells, refineries or time of the year. For example, aviation fuels consist of more than 300 components which makes it difficult (if not impossible) to model its physical or chemical properties. In order to reduce the number of components to a manageable size (10 to 15), a *surrogate model* can be created that mimics the same physical and chemical properties and distillate curve (Figure 48) of the actual fuel as much as possible while its has much less components than the original fuel. The surrogate model can be used in the modeling of the flow field or combustion inside combustor Table 14 shows surrogate model of JP-4 that consists of 14 pure components.

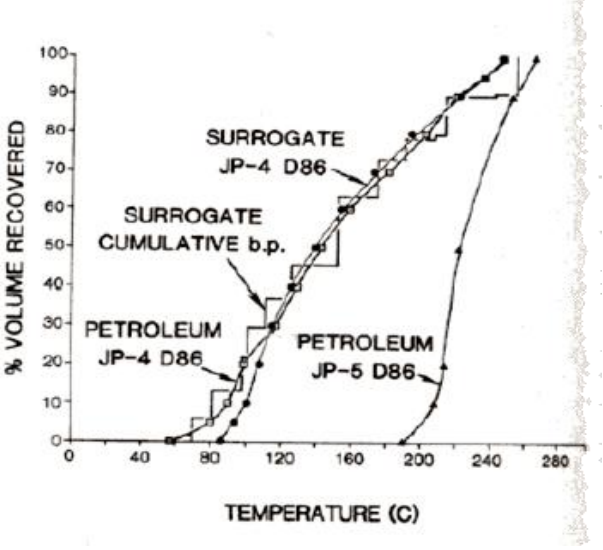

Figure 48: Distillate Curve of JP-4 [60]

Table 14 : Surrogate model of JP-4 [60]

Compound Class	Petroleum JP-4 vol%	Surrogate JP-4 vol%	Surrogate Components
Paraffin	61.2	61.5	n-Hexane n-Heptane n-Octane n-Nonane n-Decane n-Dodecane n-Tetradecane
Monocycloparaffins	24.2	24.0	Cyclohexane Methylcyclohexane Cyclo-octane
Dicycloparaffins	4.9	5.0	Decalin
Alkyl benzenes	8.2	8.0	Toluene
Indans and Tetralins	1.1	1.0	Tetralin
Indenes and Dihydronaphtalenes	0.0	0.0	-
Naphthalene	0.4	0.5	1-Methylnaphthalene
Total Paraffin	90.3	90.5	
Total Aromatics	9.7	9.5	
	100%	100%	

Although in such a surrogate model the number of components has been reduced dramatically, considering the current computational ability, it is still difficult to model the combustion mechanism for practical combustion analysis. Also there are not enough data about the reaction path and reaction rates of hydrocarbon fuels with such a complex structure.

Since the major constituents of aviation fuel (namely JP-8 or Jet-A) are Paraffins and Aromatics; it is possible to create a very simple model using a mixture of one Alkane and one aromatic that exhibits the similar chemical structures. For Jet-A ($C_{12}H_{23}$), Lindstedt and Maurice [30, 34] suggested using 89-mol% n-Decane ($C_{10}H_{22}$) representing Alkane and 11-mol% aromatic fuel. The aromatic fuel can be Benzene (C_6H_6), Toluene ($C_6H_5CH_3$), Ethyl-Benzene ($C_6H_5C_2H_5$) or Ethyl-Benzene ($C_6H_5C_2H_5$) /Naphtalene ($C_{10}H_8$). Benzene is not a good choice for the aromatic component since it does not give a good prediction of the aromatic concentration in the flame. Any of the others might be selected for the aromatic based on the availability of data. [35]

To simplify the model even more, aviation fuel can be represented by the components that have the highest percentage in the mixture and using its combustion mechanism. In the case of aviation fuel $C_{10}H_{22}$ or $C_{12}H_{24}$ is often used. Another approach is to create the combustion mechanism of the fuel using pyrolysis of a representative formula of aviation fuel (typically $C_{12}H_{23}$). [41, 50]

Pollutant Formation Mechanisms

There are certain elementary reactions and reaction paths that are present in all hydrocarbon fuel combustion mechanisms with little difference and they are responsible for the pollutant formation. A brief description of each of these pollutant formation mechanisms follows:

Thermal NO Formation (Zeldovich) Mechanism[28]
The Thermal NOx mechanism is the main formation mechanism of NO and is produced by the oxidation of atmospheric nitrogen in the high temperature region of the flame and in post flame gases. Zeldovich proposed the following elementary reactions for it:

$$O+N_2 <==> NO+N$$
$$N+O_2 <==> NO+O$$

By adding the following reaction, the mechanism is called extended Zeldovich mechanism

$$N+OH <==> NO+H$$

Prompt NO Formation (Fenimore) Mechanism [28]
Particularly important in rich combustion, Prompt NO formation is related to the interaction of atmospheric nitrogen with hydrocarbon radicals in the early stage of flame region which makes it totally different from the Thermal formation mechanism. It was discovered by Fenimore when studying the laminar premixed flame. Interaction of atomic nitrogen with HC radicals creates amines and cyano compounds and they converted to some intermediate compounds that ultimately will be turned into NO. Although the formation mechanism of Prompt NO is not as simple as Thermal NO due to the presence of a high number of hydrocarbon radicals and different reaction paths that depend on the combustion condition, the complexity can be reduced by considering the HC radical as the main radical interacting with nitrogen and ignoring the process that ends up to the formation of HC. The following reactions initiate the Prompt NO formation mechanism:

$$CH+N_2 <==> HCN+N$$
$$C+N_2 <==> CN+N$$

After this point, the mechanism depends on the equivalence ratio. For equivalence values less than 1.2, NO formation is based on following reaction [59].

$$HCN+O <==> NCO+H$$
$$NCO+H <==> NH+CO$$
$$NH+H <==> N+H_2$$
$$N+OH <==> NO+H$$

For higher equivalence ratios the mechanism becomes complex and its discussion is beyond the scope of this report.

Nitrous Oxide (N_2O) Intermediate Formation Mechanism

This mechanism is important in fuel-lean and low temperature conditions and consists of three steps as follows. [59]

$$O+N_2+M <==> N_2O+M$$
$$H+N_2O <==> NO+NH$$
$$O+N_2O <==> NO+NO$$

Nitrogen Dioxide Formation Mechanism
A significant part of the NO that is produced by the above mentioned mechanisms is converted to NO_2 in low temperature regions of combustion; hence, at the combustor exit there is a mixture of NO and NO_2 which is called NOx. The reactions responsible for NO_2 formation or destruction are given below:

$$NO+HO_2 <==> NO_2+OH$$
$$NO_2+H <==> NO+OH$$
$$NO_2+O <==> NO+O_2$$

The first reaction, which is responsible for NO_2 production, is significant at low temperature while next two reactions, responsible of NO_2 destruction, are significant at high temperature.

Carbon Monoxide (CO) Oxidation Mechanism
Unlike the NOx formation mechanisms, which do not produce a significant amount of heat and can be separated from the other chemical reactions present in the combustor, CO oxidation is the main source of heat release in combustion of hydrocarbon fuels. In simplified view, hydrocarbon fuel combustion can be divided in two steps which are CO formation based on fuel and air chemical interaction and CO oxidation to CO_2 in which the presence of water or hydrogen significantly enhances the oxidation rate. The first step has a complex mechanism which is fuel specific and sometimes not completely known to the researcher; however, the second step is simple and can be modeled by the following reactions with water as a source of hydrogen:

$$CO+O_2 ==> CO_2+O$$
$$O+H_2O ==> OH=OH$$
$$CO+OH==> CO_2+H$$
$$O_2+H ==> OH+O$$

In the presence of hydrogen the following reactions also have to be considered:

$$O+H_2 ==> OH+H$$
$$OH+H_2 ==> H_2O+H$$

Full Combustion Mechanisms

The calculation of many aspects of combustion, including performance and especially pollutant emissions, requires a realistic representation of chemistry interactions to model the underlying chemistry. Aviation fuels are comprised by complex mixtures of several hundreds of hydrocarbons such as alkanes, cycloalkanes, aromatics, and cyclic compounds. Detailed

chemical-kinetic mechanisms describing the combustion process of many of these components are not available, and thus detailed modeling of jet fuel remains as a real challenge. The study of the combustion process of aviation fuels, however, requires a defined composition. An approach to this problem is based on developing surrogates of these fuels. Surrogate fuels have been proposed as blends of a limited number of hydrocarbons for which their detailed chemistry is known. The blend components are determined to replicate the physical and chemical properties of the combustion of the fuel of interest.

Unlike combustion of single molecule fuels such as hydrogen, methane, and propane for which detailed mechanisms comprised of relatively small number of species and reactions are already available [4, 25, 55], for aviation fuels detailed mechanisms of surrogates are few and they are becoming increasingly complex, containing hundreds of species and thousands of elementary reactions. The first aviation fuel surrogate was given by Schulz [54] who proposed a 12-component mixture for JP-8. Other complex blends for aviation-type fuels were given by Dagaut [15, 16], Lindstedt and Maurice [30], and Patterson [42]. A comprehensive review of surrogates, experimental data, and kinetic schemes can be found in the survey by Dagaut and Cathonnet [14]. More recent detailed surrogates were given by Luche et al. [31], and Honnet et al. [23].

Detailed chemical-kinetic mechanisms of surrogate fuel are essential to understand the fundamental chemistry of the combustion process; however, their use is precluded by the high computational cost. In order to address this problem, some simpler models have been developed. For instance, a surrogate for kerosene TR0 composed of 89% n-decane, and 11% toluene, and containing 167 reactions and 63 species was developed by Elliot et al [19]. More recently, Strelkova et al [57] developed a surrogate for Jet A which is composed of 72.7 wt% decane, 9.1 wt% hexane, and 18.2 wt% benzene, involving 38 reactions and 24 species. These more compact mechanisms are capable of reproducing reasonably results of more detailed mechanisms. For instance, Figure 49 and Figure 50 show perfectly stirred reactor (PSR) calculations for the Elliot and Strelkolva mechanisms. Calculations for a detailed mechanism by Luche et al. [31] are also shown for comparison. The conditions of these calculations are those corresponding to the CFM56-7B engine take-off condition, i.e., 429.27 Psi, and 1453.08 R. The residence time is 2 ms and was chosen so that calculations were performed in the stable combustion branch of the 'S' curve. As shown by the temperature and CO profiles, good agreement with the detailed mechanism was obtained. Although these mechanisms are more affordable computationally, their main drawback is that they do not include NO chemistry, and therefore are not suitable for emission predictions. Another approach to address affordability and emissions is the use of mechanism reduction along with steady state approximation. This approach was used by Lepinette et al. [29] to predict NO and CO emission for methane mixtures for lean premixed combustion. Luche et al. [31] have also developed reduced mechanisms for kerosene combustion using the aforementioned approach.

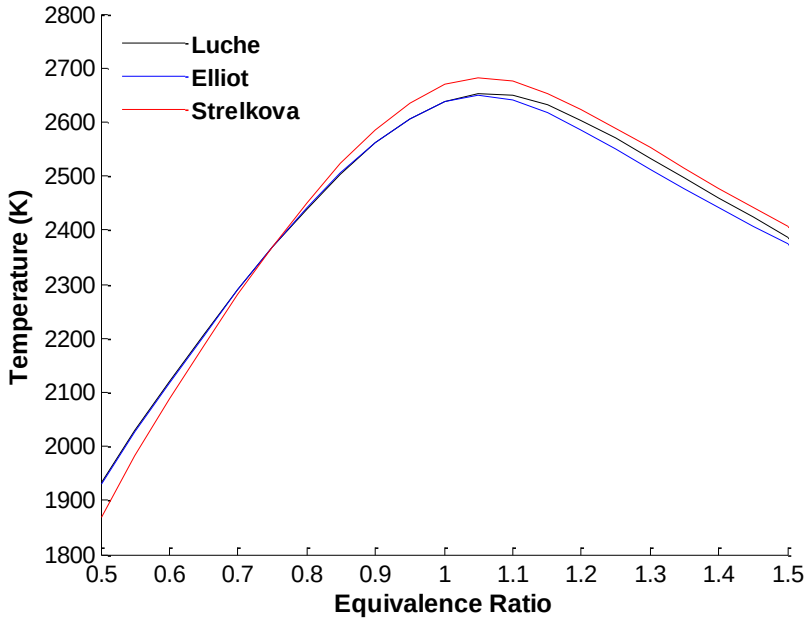

Figure 49: Reactor temperature calculations for a single PSR

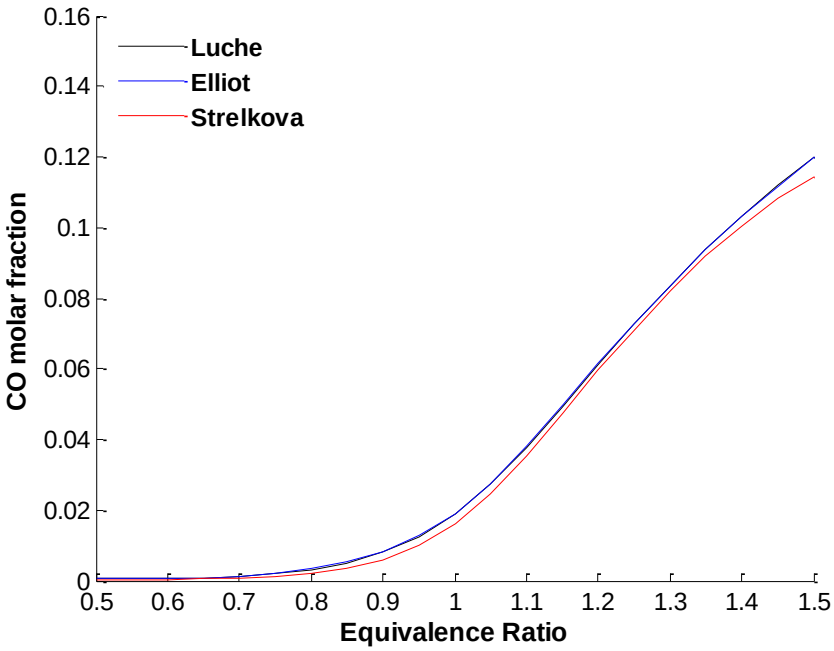

Figure 50: CO molar fraction calculations for a single PSR

Reduced Mechanisms

Similar to computational fluid dynamics in which the use of detailed mechanism is prohibited due to the computational overhead, early stages of design requires a high number of evaluations of the design tools that make the use of detailed chemistry unaffordable. Therefore, a tradeoff between accuracy and affordability is needed. A few of the more commonly encountered reduced mechanisms for Jet fuel are described below:

Kollrack Mechanism

The Kollrack mechanism is the simplest of the mechanisms considered. A 30-step mechanism created by Reiner Kollrack in 1976 for combustion of Jet-A fuel is a mixture of different hydrocarbons with the Carbon to Hydrogen ratio of 12/23 or the representative formula of $C_{12}H_{23}$. [32] It consists of 21 species and 30 reactions and includes the production of UHC, NOx and CO (Table 15). The first two steps are not elementary reactions but are global reactions representative of a great number of complex elementary reactions in the pyrolysis of the fuel molecules to smaller molecules. In this mechanism, the reaction rate coefficient is defined as:

$$k = 10^{B} T^{N} \; e^{-T_{activation}/T} \quad \text{(SI units: Kmole, m}^3\text{, k, s)}$$

Thus in order to use the mechanism in CHEMKIN format, the first term (10^B) must be considered as the pre-exponential factor *A*.

Table 15: Kollrack combustion Mechanism of Jet-A [32]

REACTION	B	N	$T_{REACTION}$
$C_{12}H_{23}+O_2 \Rightarrow 5C_2H_4+C_2H_3+O_2$	4.48	1.5	7900
$C_{12}H_{23}+OH \Rightarrow 6C_2H_4+O$	7.3	1.0	4500
$C_2H_4+H \Rightarrow C_2H_3+H_2$	10.48	0.0	9500
$H+H+M \Rightarrow H_2+M$	12.30	-1.0	0.0
$O+O+M \Rightarrow O_2+M$	11.0	-1.0	0.0
$H+OH+M \Rightarrow H2O+M$	13.85	-1.0	0.0
$H+O_2 \Rightarrow OH+O$	11.35	0.0	8400
$O+H_2 \Rightarrow OH+H$	10.24	0.0	4730
$CO+OH \Rightarrow CO_2+H$	-14.75	7.0	-7000
$H+H_2O \Rightarrow OH+H_2$	10.92	0.0	10050
$CH_3+O_2 \Rightarrow CH_2O+OH$	9.0	0.0	4000
$HO_2+M \Rightarrow H+O_2+M$	12.32	0.0	23000
$HO_2+H \Rightarrow OH+OH$	9.89	0.0	950
$CH_2O+OH \Rightarrow H_2O+HCO$	10.90	0.0	2120
$O+H_2O \Rightarrow OH+OH$	10.76	0.0	9000
$N_2+O \Rightarrow NO+N$	9.00	0.0	25000
$N+O_2 \Rightarrow NO+O$	5.00	1.0	2000
$N+OH \Rightarrow NO+H$	9.00	0.0	0.0
$HCO+O_2 \Rightarrow HO_2+CO$	10.48	0.0	7000
$HCO+OH \Rightarrow H_2O+CO$	10.30	0.0	0.0
$C_2H4+OH \Rightarrow C_2H_3+H_2O$	9.78	0.0	1750
$CH_2O+HO_2 \Rightarrow HCO+OH+OH$	9.0	0.0	4500
$C_2H_2+HO_2 \Rightarrow HCO+CH_2O$	9.30	0.0	5500
$C_2H_3+O_2 \Rightarrow C2H_2+HO_2$	9.23	0.0	5000
$NO+HO_2 \Rightarrow NO_2+OH$	3.00	1.0	0.0
$C_2H_4+O \Rightarrow CH_3+HCO$	9.93	0.0	1500
$C_2H_4+HO_2 \Rightarrow CH_3+HCO+OH$	9.90	0.0	5000
$H_2+CH_3 \Rightarrow CH_4+H$	7.0	-1.5	7140
$C_2H_2+OH \Rightarrow CH_3+CO$	8.2	0.0	2500
$CH_3+O \Rightarrow CH_2O+H$	11.11	0.0	1000

n-Decane Mechanism

In some publications the average carbon number of aviation fuels is assumed to be close to 10; consequently it is concluded that n-Decane and aviation fuels might have similar combustion characteristics and mechanism. Also a mixture of some aromatics and n-Decane has chemical characteristics close to Kerosene. But a complete and detailed mechanism of n-Decane is not entirely known, so it is modeled based on the observed n-Heptane pyrolysis and H-atom abstraction. [30] This mechanism appears capable of predicting the formation and destruction of benzene and aromatics in flames, which is essential for predicting soot formation and pollutant prediction in combustion. The published mechanism [30] consists of 193 species and 1085 elementary reactions.

n-Dodecane Mechanism

The n-Dodecane mechanism was used by L. Q. Maurice [30] and consists of 177 chemical species and 1138 elementary reactions. It contains sub-mechanism of molecules up to C_{12} and aromatics. Also the Nitrogen sub-mechanism consists of 3 main NOx formation mechanism of Zeldovich (thermal), Fenimore (prompt) and N_2O as well as NO and NO_2 chemistry.

Examination of Kollrack Mechanism

In the present work, the chosen kinetic mechanism is the one given by Kollrack [27, 49]. This mechanism was developed for $C_{12}H_{23}$/air combustion and involves the breakdown of the fuel molecule in two-stages. The NO chemistry includes thermal NO by the extended Zeldovich reactions, and prompt NO by the superquilibrium of oxygen molecules. It is composed of 21 species and 30 chemical reactions.

Figure 51 through Figure 53 show comparisons between the Kollrack and Luche mechanisms for PSR calculations. The conditions for the reactor are those for take-off as described above. Temperature, CO, and NO molar fraction are plotted as a function of residence time for stochiometric mixtures. It can be noticed that the Kollrack mechanism under-predicts temperature for small residence times; however, for residence times greater than 0.5ms the values show good agreement with those given by the Luche mechanism. Similarly, CO is under-predicted for small residence times. The agreement, however, is better for values greater than 1 ms. Unlike temperature and CO, NO is certainly under-predicted by almost half over the entire range of residence time.

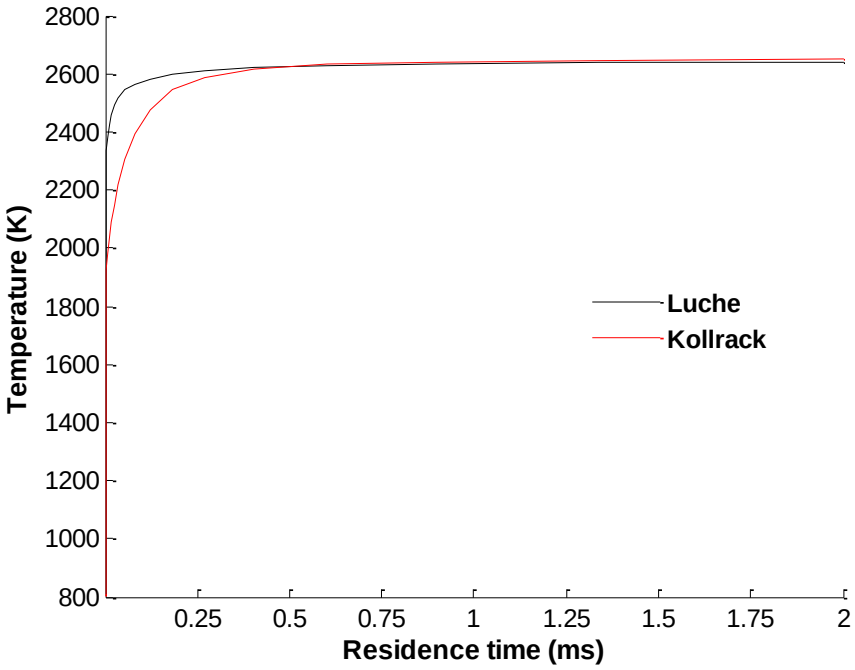

Figure 51: Reactor Temperature

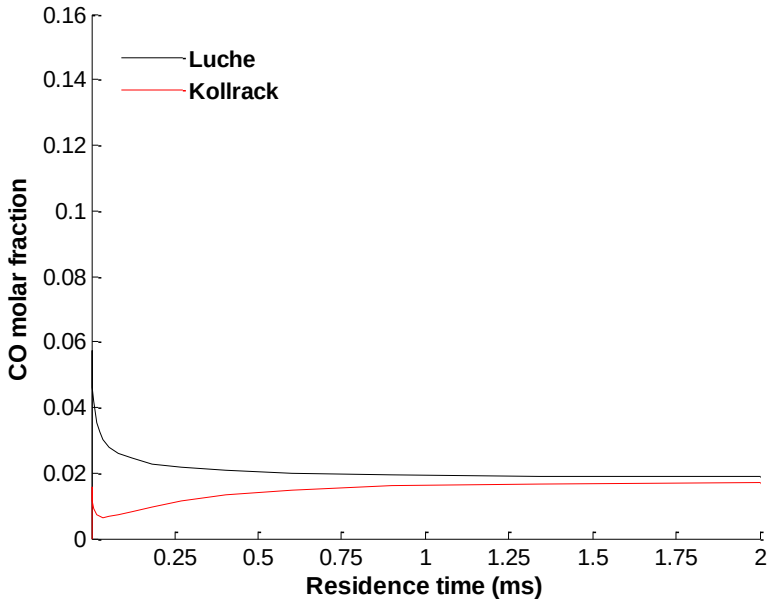

Figure 52: CO molar fraction

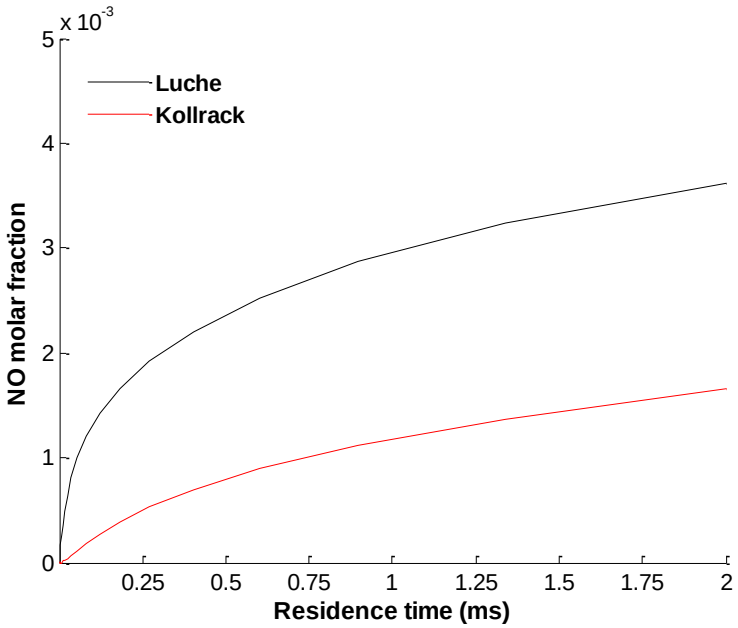

Figure 53: NO molar fraction

The behavior of the Kollrack mechanism with equivalence ratio was investigated and it is shown in Figure 54 through Figure 56. The residence time of the reactor was set to 2ms to ensure calculations at the stable combustion branch, and the conditions are the same as in the previous figures. The temperature was found to agree well in the considered range. The CO also shows good agreement; however, the CO prediction departs at equivalence ratio of 1.2 and thus CO values are likely to be under-predicted for richer mixtures. The NO is under-predicted for intermediate values, the agreement, however, is better for lean and rich mixtures.

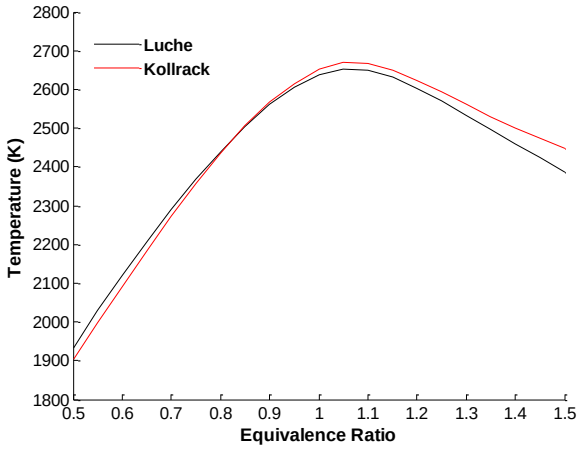

Figure 54: Reactor temperature

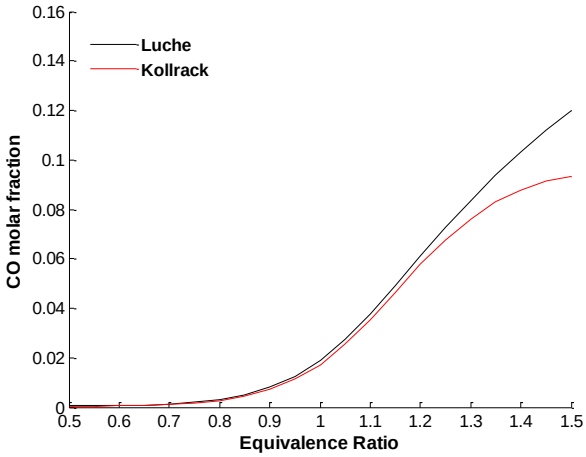

Figure 55: CO molar fraction

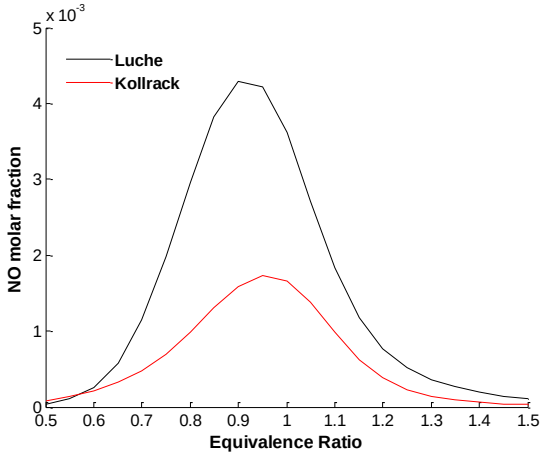

Figure 56: NO molar fraction

The above comparisons have shown that the Kollrack mechanism was found to give reasonable agreement for temperature as well as major species. Accurate prediction of emissions, however, depends on the conditions. For instance, at small residence times the mechanism is likely to fail due to the lack of chemical step for ignition. The under-prediction of NO suggests the importance of other paths for NO production that are not included in the Kollrack mechanism. In spite of this drawback, the Kollrack mechanism is chosen due to its balance between computational cost and accuracy.

Appendix B: Equations for SAC Model

Appendix B contains a list of flowcharts giving the logic of the on-design procedure of each element of the NPSS code for the SAC model and the calculations derived for the geometry.

Diffuser.int

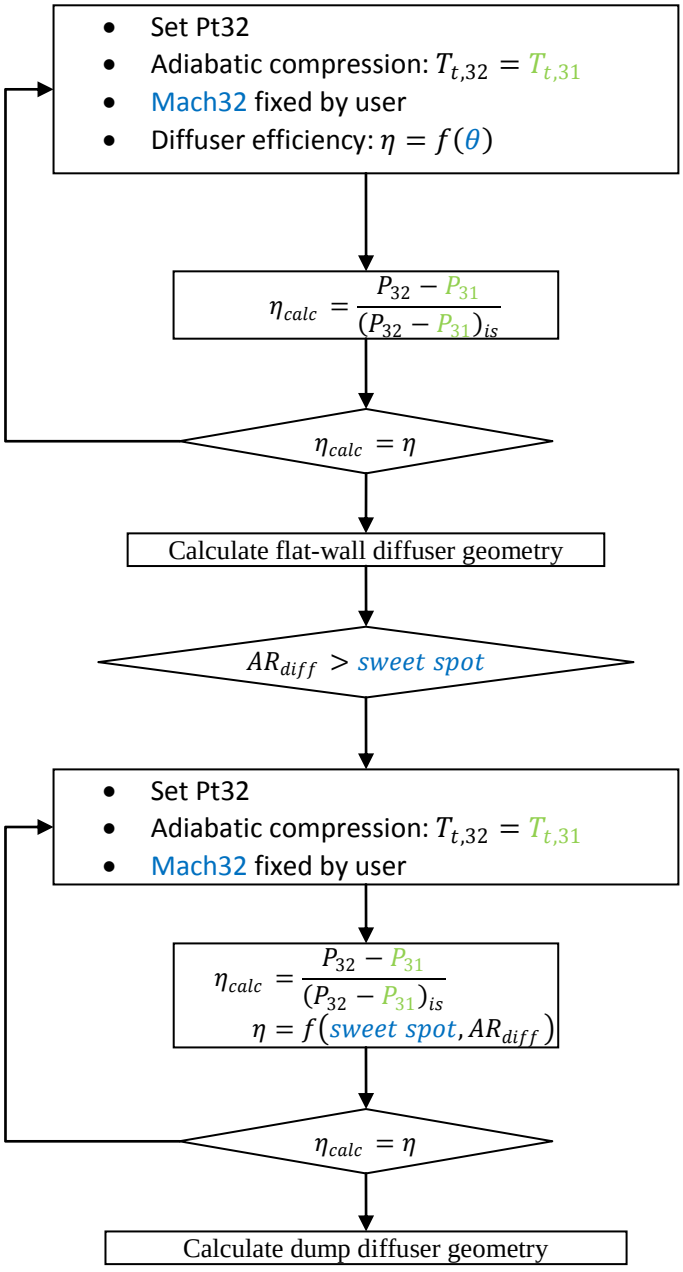

User inputs

passage_number	Number of passages
θ	Passage half-angle
Mach32	Mach number station 32
sweet_spot	Max aspect ratio for flat_wall diffuser

	Comp1 output
	User input

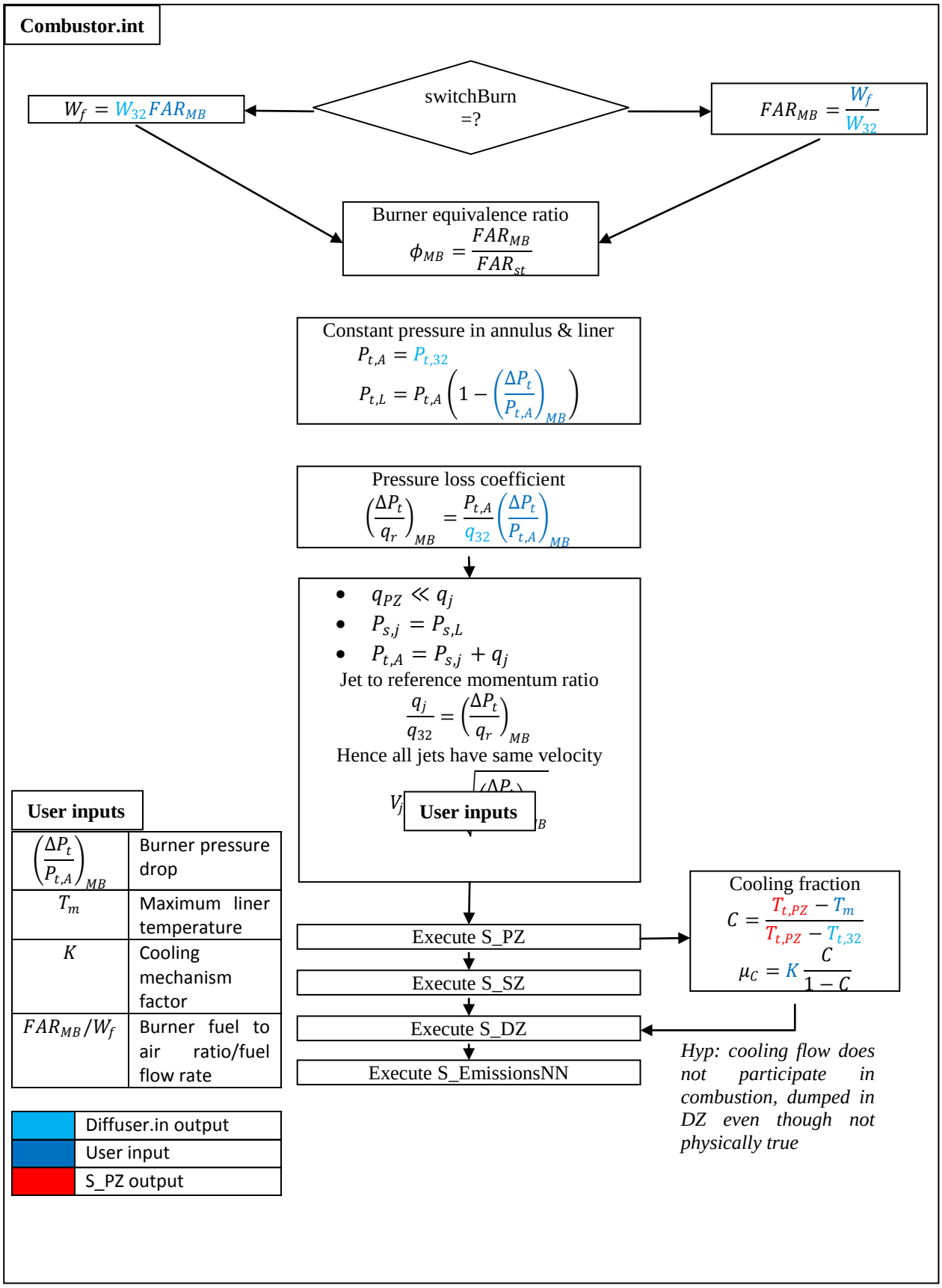
Combustor.int
$W_f = W_{32} FAR_{MB}$
switchBurn =?
$FAR_{MB} = \frac{W_f}{W_{32}}$
Burner equivalence ratio
$\phi_{MB} = \frac{FAR_{MB}}{FAR_{st}}$
Constant pressure in annulus & liner
$P_{t,A} = P_{t,32}$
$P_{t,L} = P_{t,A}\left(1 - \left(\frac{\Delta P_t}{P_{t,A}}\right)_{MB}\right)$
Pressure loss coefficient
$\left(\frac{\Delta P_t}{q_r}\right)_{MB} = \frac{P_{t,A}}{q_{32}}\left(\frac{\Delta P_t}{P_{t,A}}\right)_{MB}$
$q_{PZ} \ll q_j$
$P_{s,j} = P_{s,L}$
$P_{t,A} = P_{s,j} + q_j$
Jet to reference momentum ratio
$\frac{q_j}{q_{32}} = \left(\frac{\Delta P_t}{q_r}\right)_{MB}$
Hence all jets have same velocity
V_j
User inputs
Execute S_PZ
Execute S_SZ
Execute S_DZ
Execute S_EmissionsNN
Cooling fraction
$C = \frac{T_{t,PZ} - T_m}{T_{t,PZ} - T_{t,32}}$
$\mu_C = K\frac{C}{1-C}$
Hyp: cooling flow does not participate in combustion, dumped in DZ even though not physically true
User inputs
$\left(\frac{\Delta P_t}{P_{t,A}}\right)_{MB}$ Burner pressure drop
T_m Maximum liner temperature
K Cooling mechanism factor
FAR_{MB}/W_f Burner fuel to air ratio/fuel flow rate
Diffuser.in output
User input
S_PZ output

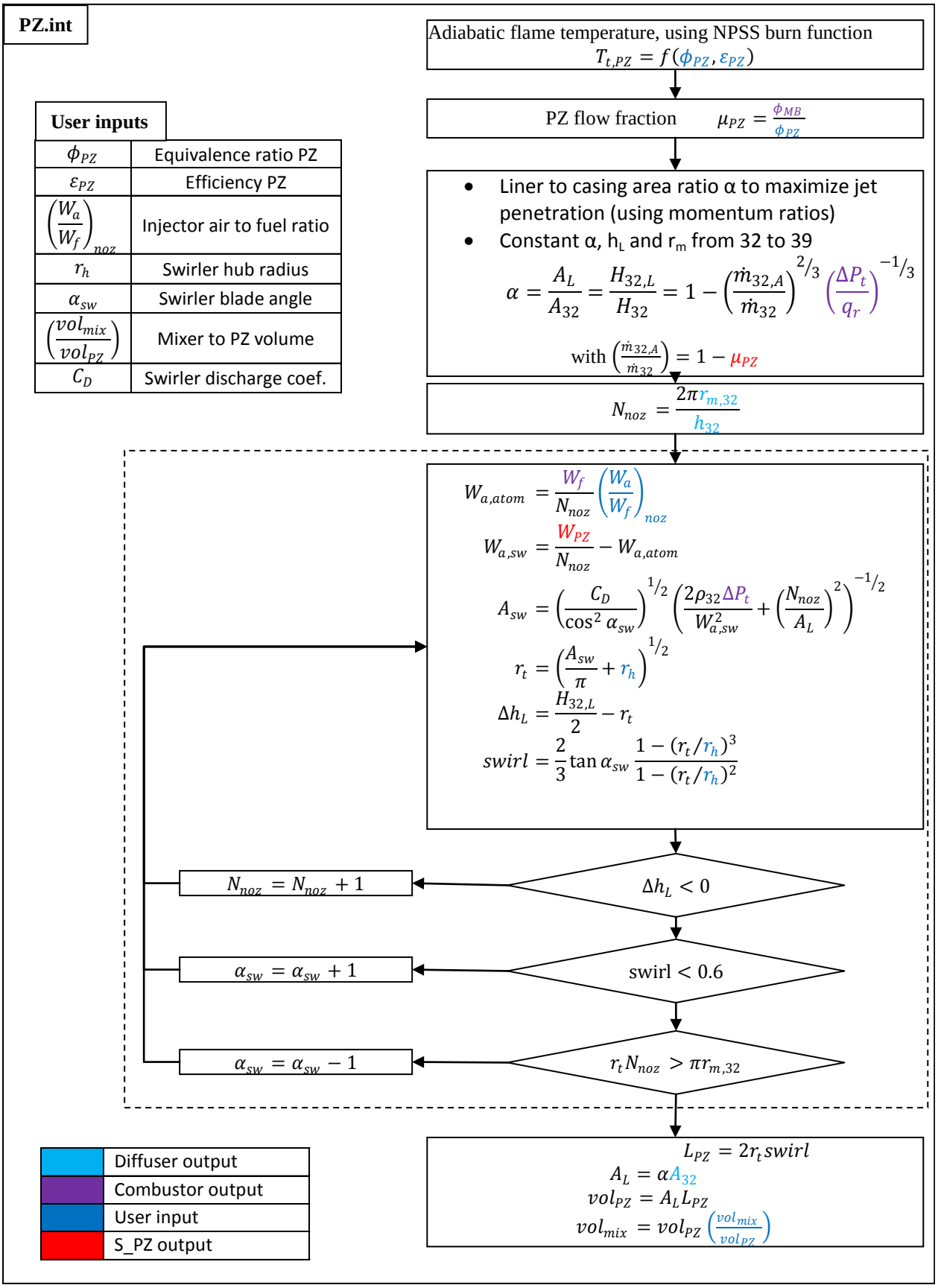
PZ.int
Adiabatic flame temperature, using NPSS burn function
$T_{t,PZ} = f(\phi_{PZ}, \varepsilon_{PZ})$
PZ flow fraction $\mu_{PZ} = \frac{\phi_{MB}}{\phi_{PZ}}$
Liner to casing area ratio α to maximize jet penetration (using momentum ratios)
Constant α, h_L and r_m from 32 to 39
$\alpha = \frac{A_L}{A_{32}} = \frac{H_{32,L}}{H_{32}} = 1 - \left(\frac{\dot{m}_{32,A}}{\dot{m}_{32}}\right)^{2/3} \left(\frac{\Delta P_t}{q_r}\right)^{-1/3}$
with $\left(\frac{\dot{m}_{32,A}}{\dot{m}_{32}}\right) = 1 - \mu_{PZ}$
$N_{noz} = \frac{2\pi r_{m,32}}{h_{32}}$
$W_{a,atom} = \frac{W_f}{N_{noz}} \left(\frac{W_a}{W_f}\right)_{noz}$
$W_{a,sw} = \frac{W_{PZ}}{N_{noz}} - W_{a,atom}$
$A_{sw} = \left(\frac{C_D}{\cos^2 \alpha_{sw}}\right)^{1/2} \left(\frac{2\rho_{32}\Delta P_t}{W_{a,sw}^2} + \left(\frac{N_{noz}}{A_L}\right)^2\right)^{-1/2}$
$r_t = \left(\frac{A_{sw}}{\pi} + r_h\right)^{1/2}$
$\Delta h_L = \frac{H_{32,L}}{2} - r_t$
$swirl = \frac{2}{3} \tan \alpha_{sw} \frac{1 - (r_t/r_h)^3}{1 - (r_t/r_h)^2}$
$\Delta h_L < 0$
$N_{noz} = N_{noz} + 1$
swirl < 0.6
$\alpha_{sw} = \alpha_{sw} + 1$
$r_t N_{noz} > \pi r_{m,32}$
$\alpha_{sw} = \alpha_{sw} - 1$
$L_{PZ} = 2 r_t swirl$
$A_L = \alpha A_{32}$
$vol_{PZ} = A_L L_{PZ}$
$vol_{mix} = vol_{PZ} \left(\frac{vol_{mix}}{vol_{PZ}}\right)$
User inputs
ϕ_{PZ} Equivalence ratio PZ
ε_{PZ} Efficiency PZ
$\left(\frac{W_a}{W_f}\right)_{noz}$ Injector air to fuel ratio
r_h Swirler hub radius
α_{sw} Swirler blade angle
$\left(\frac{vol_{mix}}{vol_{PZ}}\right)$ Mixer to PZ volume
C_D Swirler discharge coef.
Diffuser output
Combustor output
User input
S_PZ output

SZ.int

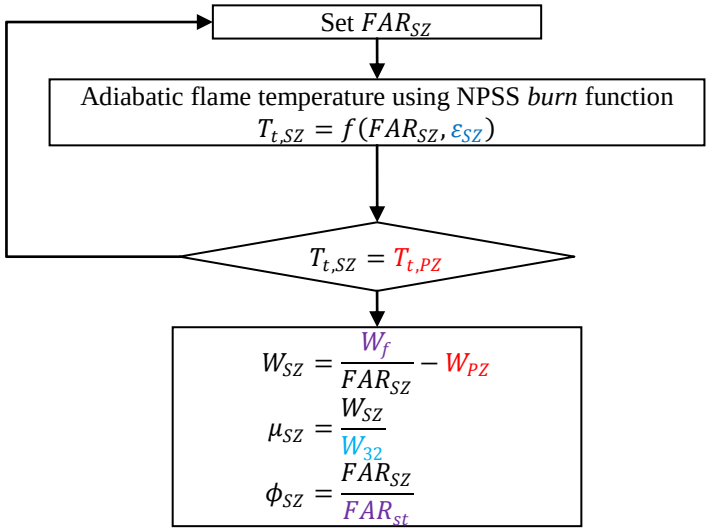

- mass conservation:

$$\frac{q_{A,SZ}}{q_{32}} = \left(\frac{1 - \mu_{PZ} - \mu_{cool}}{1 - \alpha}\right)^2$$

- Boussinesq assumption: $\frac{\rho_{PZ}}{\rho_{32}} = \frac{T_{t,32}}{T_{t,PZ}} = \frac{1}{\tau_{PZ}}$

  + mass cons.

$$\frac{q_{PZ}}{q_{32}} = \tau_{PZ}\left(\frac{\mu_{PZ}}{\alpha}\right)$$

- Conservation of momentum :

$$\sin^2\theta_{SZ} = 1 - \frac{q_{A,SZ}}{q_j}$$

- Regression (Lefebvre) :

$$\frac{Y_{max}}{d_{j,SZ}} = 1.15\sqrt{\frac{q_j}{q_{32}}\left(\frac{q_{PZ}}{q_{32}}\right)^{-1}}\sin\theta_{SZ}$$

- Using assumed jet penetration ratio:

$$d_{h,SZ} = C_{D,SZ}\left(\frac{Y_{max}}{H_{L,33}}\right)H_{L,33}\left(\frac{Y_{max}}{d_{j,SZ}}\right)^{-1}$$

- Using mass conservation:

$$N_{h,SZ} = \mu_{SZ}\left(\frac{4A_{32}}{\pi d_{j,SZ}^2}\right)\frac{U_{32}}{V_j}$$

$$L_{SZ} = \left(\frac{L_{SZ}}{H_{33,L}}\right)H_{33,L}$$
$$vol_{SZ} = A_L L_{SZ}$$

User inputs

$\left(\frac{Y_{max}}{H_{L,33}}\right)$	SZ jets penetration ratio	$\left(\frac{L_{SZ}}{H_{33,L}}\right)$	SZ aspect ratio
ε_{SZ}	Efficiency SZ	$C_{D,SZ}$	SZ holes discharge coef.

DZ.int

Mass conservation

$$\mu_{DZ} = 1 - \mu_{PZ} - \mu_{SZ} - \mu_{cool}$$
$$W_{DZ} = \mu_{DZ} W_{32}$$

- mass conservation:

$$\frac{q_{A,DZ}}{q_{32}} = \left(\frac{\mu_{DZ}}{1-\alpha}\right)^2$$

- Boussinesq assumption: $\frac{\rho_{PZ}}{\rho_{32}} = \frac{T_{t,32}}{T_{t,PZ}} = \frac{1}{\tau_{PZ}}$

  + mass cons.

$$\frac{q_{SZ}}{q_{32}} = \tau_{PZ}\left(\frac{\mu_{PZ} + \mu_{SZ}}{\alpha}\right)$$

- Conservation of momentum :

$$\sin^2\theta_{DZ} = 1 - \frac{q_{A,DZ}}{q_j}$$

- Regression (Lefebvre) :

$$\frac{Y_{max,DZ}}{d_{j,DZ}} = 1.15\sqrt{\frac{q_j}{q_{32}}\left(\frac{q_{SZ}}{q_{32}}\right)^{-1}}\sin\theta_{DZ}$$

- Using assumed jet penetration ratio:

$$d_{h,DZ} = C_{D,DZ}\left(\frac{Y_{max,DZ}}{H_{L,34}}\right)H_{L,34}\left(\frac{Y_{max,DZ}}{d_{j,DZ}}\right)^{-1}$$

- Using mass conservation:

$$N_{h,DZ} = \mu_{DZ}\left(\frac{4A_{32}}{\pi d_{j,DZ}^2}\right)\frac{U_{32}}{V_j}$$

Adiabatic flame temperature using NPSS *burn* function

$$T_{t,40} = f(\phi_{MB}, \varepsilon_{DZ})$$

$$A_{40} = f(M_{40}, T_{t,40}, P_{t,L}, W_{32})$$

$$L_{DZ} = \left(\frac{L_{DZ}}{H_{34,L}}\right)H_{34,L}$$
$$L_{tr} = \left(\frac{L_{tr}}{H_{34,L}}\right)H_{34,L}$$
$$vol_{DZ} = A_L L_{DZ} + \frac{1}{2}(A_L + A_{40})L_{tr}$$

User inputs

$\left(\frac{Y_{max}}{H_{L,34}}\right)$	DZ jets penetration ratio
ε_{DZ}	Efficiency DZ
$\left(\frac{L_{DZ}}{H_{34,L}}\right)$	DZ aspect ratio
$C_{D,DZ}$	DZ holes discharge coef.
Mach40	Mach number at station 40
rm_{40}	Mean radius at station 40
$\left(\frac{L_{tr}}{H_{34,L}}\right)$	Transition duct aspect ratio

	Diffuser output
	Combustor output
	User input
	S_PZ output
	S_SZ output

Geometry calculations

Note : in these flowcharts, « tilted » stations FS31t and FS39t and denoted with a prime « ' » for easier reading

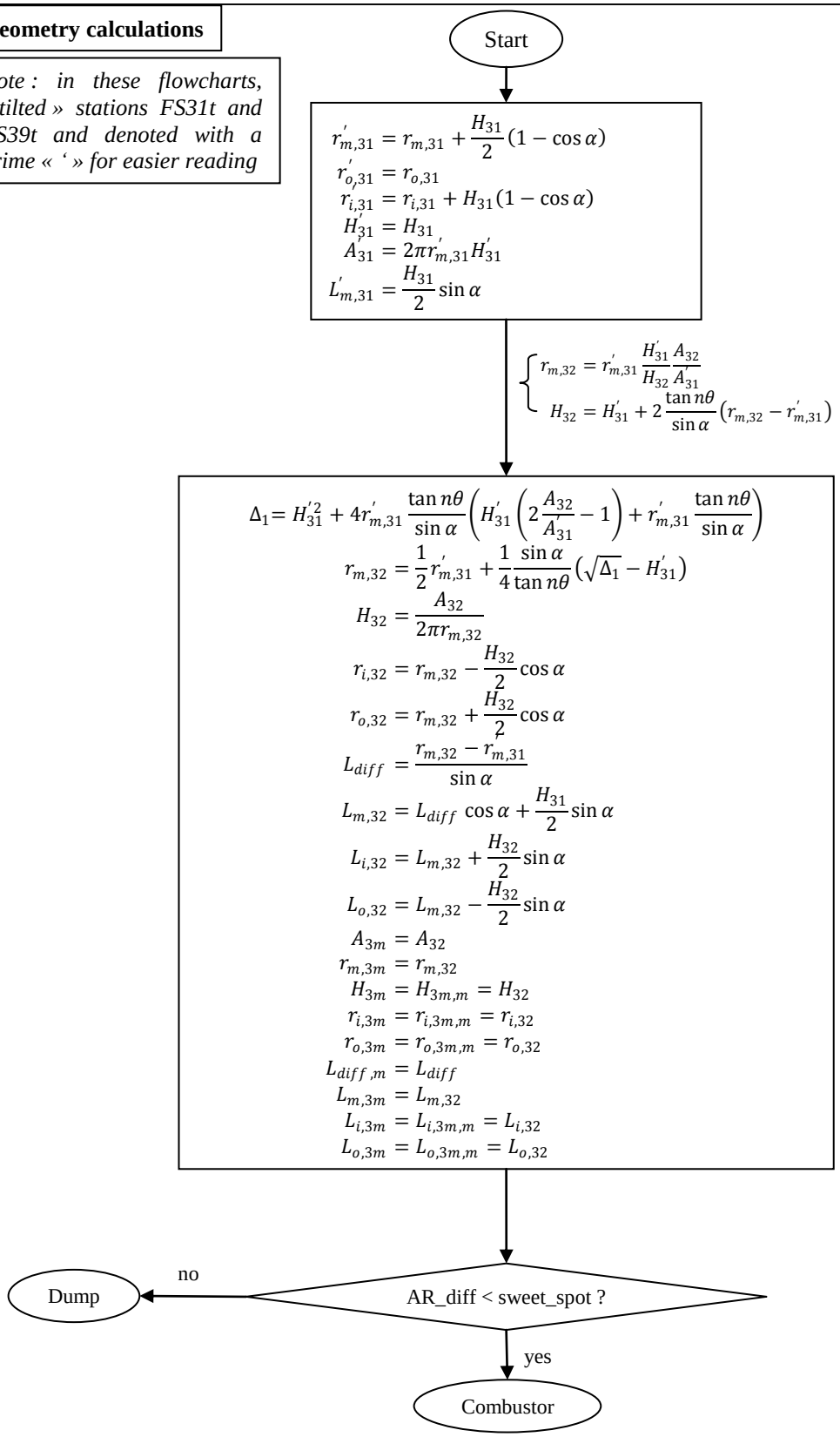

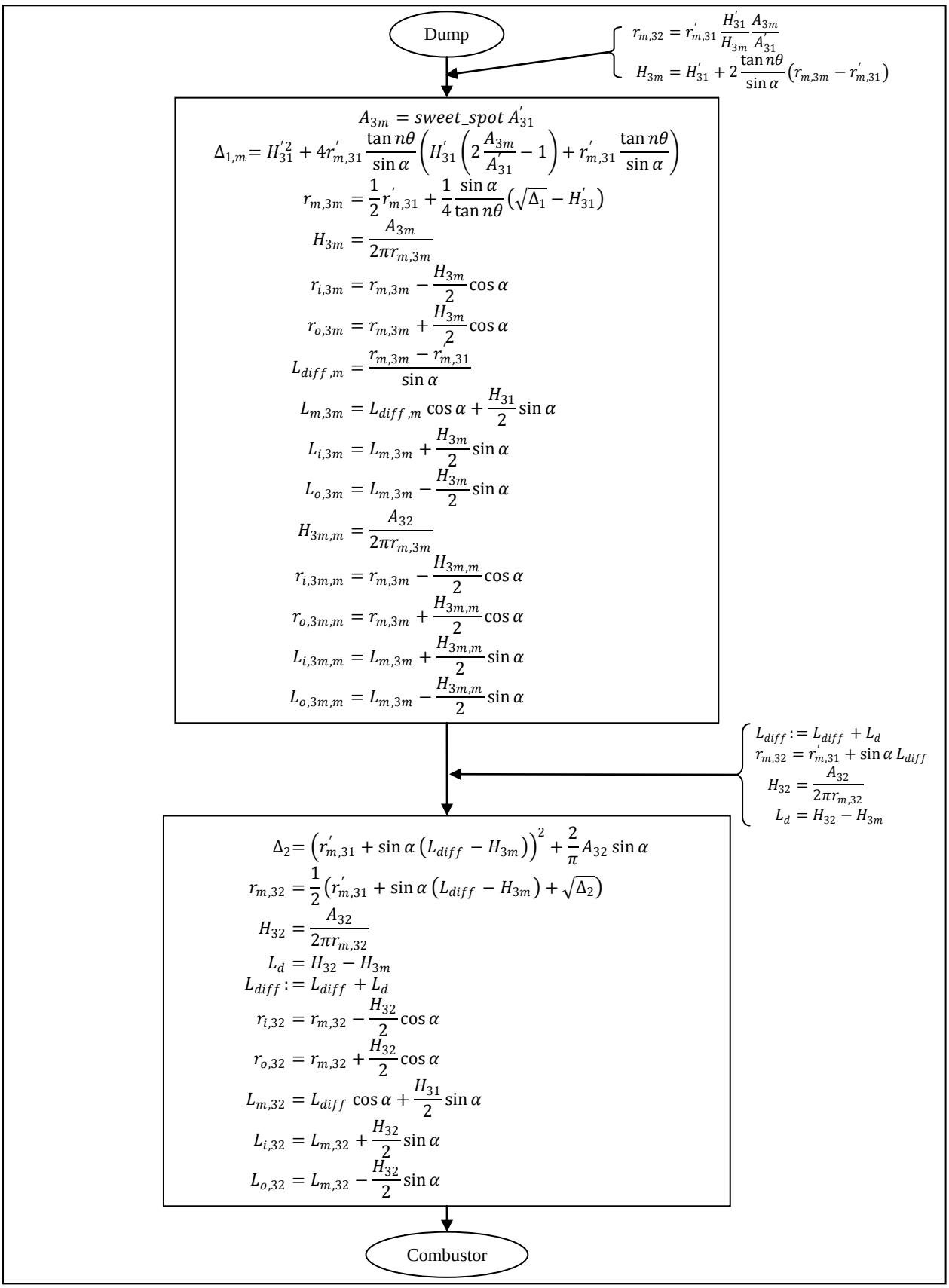
Dump
$r_{m,32} = r'_{m,31}\frac{H'_{31}}{H_{3m}}\frac{A_{3m}}{A'_{31}}$
$H_{3m} = H'_{31} + 2\frac{\tan n\theta}{\sin\alpha}(r_{m,3m} - r'_{m,31})$
$A_{3m} = sweet\_spot\ A'_{31}$
$\Delta_{1,m} = H'^{2}_{31} + 4r'_{m,31}\frac{\tan n\theta}{\sin\alpha}\left(H'_{31}\left(2\frac{A_{3m}}{A'_{31}} - 1\right) + r'_{m,31}\frac{\tan n\theta}{\sin\alpha}\right)$
$r_{m,3m} = \frac{1}{2}r'_{m,31} + \frac{1}{4}\frac{\sin\alpha}{\tan n\theta}(\sqrt{\Delta_1} - H'_{31})$
$H_{3m} = \frac{A_{3m}}{2\pi r_{m,3m}}$
$r_{i,3m} = r_{m,3m} - \frac{H_{3m}}{2}\cos\alpha$
$r_{o,3m} = r_{m,3m} + \frac{H_{3m}}{2}\cos\alpha$
$L_{diff,m} = \frac{r_{m,3m} - r_{m,31}}{\sin\alpha}$
$L_{m,3m} = L_{diff,m}\cos\alpha + \frac{H_{31}}{2}\sin\alpha$
$L_{i,3m} = L_{m,3m} + \frac{H_{3m}}{2}\sin\alpha$
$L_{o,3m} = L_{m,3m} - \frac{H_{3m}}{2}\sin\alpha$
$H_{3m,m} = \frac{A_{32}}{2\pi r_{m,3m}}$
$r_{i,3m,m} = r_{m,3m} - \frac{H_{3m,m}}{2}\cos\alpha$
$r_{o,3m,m} = r_{m,3m} + \frac{H_{3m,m}}{2}\cos\alpha$
$L_{i,3m,m} = L_{m,3m} + \frac{H_{3m,m}}{2}\sin\alpha$
$L_{o,3m,m} = L_{m,3m} - \frac{H_{3m,m}}{2}\sin\alpha$
$L_{diff} := L_{diff} + L_d$
$r_{m,32} = r'_{m,31} + \sin\alpha\, L_{diff}$
$H_{32} = \frac{A_{32}}{2\pi r_{m,32}}$
$L_d = H_{32} - H_{3m}$
$\Delta_2 = \left(r'_{m,31} + \sin\alpha\left(L_{diff} - H_{3m}\right)\right)^2 + \frac{2}{\pi}A_{32}\sin\alpha$
$r_{m,32} = \frac{1}{2}\left(r'_{m,31} + \sin\alpha\left(L_{diff} - H_{3m}\right) + \sqrt{\Delta_2}\right)$
$H_{32} = \frac{A_{32}}{2\pi r_{m,32}}$
$L_d = H_{32} - H_{3m}$
$L_{diff} := L_{diff} + L_d$
$r_{i,32} = r_{m,32} - \frac{H_{32}}{2}\cos\alpha$
$r_{o,32} = r_{m,32} + \frac{H_{32}}{2}\cos\alpha$
$L_{m,32} = L_{diff}\cos\alpha + \frac{H_{31}}{2}\sin\alpha$
$L_{i,32} = L_{m,32} + \frac{H_{32}}{2}\sin\alpha$
$L_{o,32} = L_{m,32} - \frac{H_{32}}{2}\sin\alpha$
Combustor

Hyp: *constant annulus & liner areas in combustor*

Combustor

$$A_{39} = A_{33} = A_{34} = A_{32}$$
$$A_L = \beta A_{32}$$
$$H_{32/33/34/39,L} = \beta H_{32/33/34/39}$$
$$L_{SZ/DZ} = \left(\frac{L_{SZ/DZ}}{H_{33/34,L}}\right) H_{33/34,L}$$
$$r_{m,33/34/39} = r_{m,32/33/34} + L_{PZ/SZ/DZ} \sin\alpha$$
$$H_{33/34/39} = \frac{A_{33/34/39}}{2\pi r_{m,33/34/39}}$$
$$r_{i,33/34/39} = r_{m,33/34/39} - \frac{H_{33/34/39}}{2}\cos\alpha$$
$$r_{o,33/34/39} = r_{m,33/34/39} + \frac{H_{33/34/39}}{2}\cos\alpha$$
$$r_{i,33/34/39,L} = r_{m,33/34/39} - \frac{H_{33/34/39,L}}{2}\cos\alpha$$
$$r_{o,33/34/39} = r_{m,33/34/39} + \frac{H_{33/34/39,L}}{2}\cos\alpha$$
$$L_{PZ/SZ/39,axial} = L_{PZ/SZ/DZ}\cos\alpha$$
$$L_{i,33/34/39} = L_{PZ/SZ/DZ,axial} + \frac{H_{33/34/39,L}}{2}\sin\alpha$$
$$L_{o,33/34/39} = L_{PZ/SZ/DZ,axial} - \frac{H_{33/34/39,L}}{2}\sin\alpha$$
$$L_{i,33/34/39,L} = L_{PZ/SZ/DZ,axial} + \frac{H_{33/34/39,L}}{2}\sin\alpha$$
$$L_{o,33/34/39,L} = L_{PZ/SZ/DZ,axial} - \frac{H_{33/34/39,L}}{2}\sin\alpha$$
$$vol_{PZ/SZ/DZ} = A_L L_{PZ/SZ/DZ}$$

$$\beta = \frac{H_L}{H_{ref}} = \frac{A_L}{A_{ref}}$$

$$H'_{39} = H_{39,L}$$
$$r'_{m,39} = r_{m,39} + \frac{H_{39,L}}{2}(1-\cos\alpha)$$
$$r'_{i,39} = r_{i,39}$$
$$r'_{o,39} = r'_{m,39} + \frac{H'_{39}}{2}$$
$$A'_{39} = 2\pi r'_{m,39} H'_{39}$$
$$L'_{39,axial} = \frac{H'_{39}}{2}\sin\alpha$$
$$L_{DZ,axial} = L_{39,axial} + L'_{39,axial}$$

$$r_{m,40,calc} = r'_{m,39}$$
$$H_{40} = \frac{A_{40}}{2\pi r_{m,40,calc}}$$
$$r_{i,40} = r_{m,40,calc} - \frac{H_{40}}{2}$$
$$r_{o,40} = r_{m,40,calc} + \frac{H_{40}}{2}$$

$\left|\frac{r'_{m,40,calc} - r_{m,40}}{r_{m,40}}\right| < 0.01$?

no

Start

Modify α

yes

$$L_{tr} = \left(\frac{L_{tr}}{H'_{39}}\right) H'_{39}$$
$$L_{total,axial} = L_{diff,axial} + L_{PZ,axial} + L_{SZ,axial} + L_{DZ,axial} + L_{tr}$$

Appendix C: Equations for RQL Model

Appendix C describes the equations used in each element of the NPSS code for the RQL model where they differ from those used by the SAC model.

Mixing and Dilution Zone Hole Sizing

The sizes of the Mixing and Dilution zone holes are important in order to have adequate mixing, to achieve the required temperature profile and to achieve the correct jet penetration. Small diameters provide jets with low momentum that are unable to penetrate deep enough into the Mixing and Dilution zones to mix well with the hot gases. Large diameters, on the other hand may result in too much jet penetration, leading to uneven temperature distribution.

Equation (1) shows the relationship between the orifice area and flow coefficient and the total mass flow. The mass density and total pressure drop are assumed to be the same for all the orifices.

$$\dot{m}_{ref} = \sum_{i=1}^{n} \rho V_i c_D A_i = \sum_{i=1}^{n} \rho \sqrt{\frac{2\Delta P_t}{\rho}_t} c_D A_i = \sum_{i=1}^{n} \sqrt{2\rho.\Delta P_t} c_D A_i = \sqrt{2\rho.\Delta P_t} \sum_{i=1}^{n} c_D A_i = \rho V_{ref} A_{ref} \quad (1)$$

Unlike in the SAC, the RQL combustor may use variable geometry; therefore the assumption of constant pressure drop coefficient (total pressure drop over dynamic pressure, dP/Q) cannot be used, because the pressure drop coefficient is a function of the size of the orifices. From Equation (2) one can obtain the pressure drop coefficient to be as follows:

$$\frac{\Delta P_{tot}}{Q} = \frac{\Delta P_{tot}}{\frac{1}{2}\rho V_{ref}{}^2} = \left(\frac{A_{ref}}{\sum_{i=1}^{n} c_D A_i} \right)^2 = \left(\frac{A_{ref}}{c_{D_{SW}} A_{sw} + c_{D_{MZ}} A_{MZ} + c_{D_{DZ}} A_{DZ} + c_{D_{cool}} A_{cool}} \right)^2 \quad (2)$$

The above equation shows that changing the swirler area in the variable geometry RQL combustor would change the pressure drop coefficient. After finding the pressure drop coefficient at a given power setting, the amount of flow that passes through the orifices of interest can be determined using the following equation:

$$frac_{jet} = \frac{\dot{m}_{jet}}{\dot{m}_{ref}} = \frac{c_D A_{Orifices}}{A_{ref}} \sqrt{\frac{\Delta P_{tot}}{Q}} \quad (3)$$

Atomizer and Swirler

To improve atomization in the RQL combustor an integrated high shear swirler may be used. However, for simplicity, in this report the conventional pressure-swirl Simplex atomizer with single axial swirler will be used. The following equation may be used to determine the amount of the flow that passes through the swirler to the Rich zone at a given power setting.

$$\dot{m}_{swirler} = \sqrt{\frac{2\rho\Delta P_t}{K_{sw}\left(\sec\theta / \alpha.A_{sw}\right)^2 - \frac{n_{inj}}{A_{liner}^2}}} \quad (4)$$

The total pressure drop is calculated from the pressure drop from equation (2). The variable α is the swirler area coefficient used when the variable geometry swirler area is used and n_{inj} is the number of injectors.

Rich Zone

The Rich zone component is almost the same as the Primary zone component for the SAC model. In the RQL, after determining the pressure drop coefficient and consequently the absolute burner pressure drop, the amount of the flow that goes to the Rich zone is determined using equation (4).

An additional feature is added to the Rich zone model which is the configuration option. Since some of the validation cases are performed for the a tubular type RQL combustor, it became necessary to include the tubular option (in addition to already available option of annular configuration) to the Rich zone, Mixing zone, Lean zone and Dilution zone models. The major difference between these two configurations is in the equation used to calculate the liner and casing heights for each component (Equations 5 and 6).

$$H_{annular} = \frac{Area_{crosssectiob}}{2\pi r_{mean}} \quad (5)$$

$$H_{tubular} = \sqrt{\frac{4Area_{CrossSection}}{\pi}} \quad (6)$$

Mixing Zone

The Mixing zone is specific to the RQL combustor, where the annulus air should mix quickly with the fuel rich hot gases coming out from the rich zone section. As described previously, there are different mixing methods, but this research is limited to the use of the wall-jet mixing method.

The first thing to be determined is the fraction of the air that should be added to the hot gases to bring it from the rich regime to the lean regime. At design condition (Take-Off or Super-Sonic cruise) this fraction is determined from the Lean equivalence ratio:

$$\frac{\dot{m}_{MZ}}{\dot{m}_{ref}} = \frac{\dot{m}_{fuel}}{far_{st}.\varphi_{LZ}} - n_{inj}.\dot{m}_{swirler} \quad (7)$$

At off-design conditions, the fraction is obtained from a different formula based on the quench orifices size and pressure drop that is provided later in this sub-section.

After obtaining the amount of air needed for quenching, the next step is to design the quench orifices and determine their number and size. The design of the quench orifice is very important as it will determined the quality of mixing and speed of quenching the rich zone hot gases. In the

wall-jet method, the number of the quench orifices for the can or tubular type configuration is shown in the equation below [28, 52]:

$$n = \frac{\pi\sqrt{2J}}{C} \tag{8}$$

where n is the optimum number of quenching orifices, J is the momentum flux ratio and C is an empirical constant (equal to 2.5 for the tubular configuration). The orifices are of circular shape. The momentum flux ratio is determined similar to the method described for the conventional SAC combustor.

For an annular configuration the optimum distance between orifices (S) is found by [28, 52].

$$\frac{S}{H} = \frac{C}{\sqrt{J}} \tag{9}$$

where H is the mixing zone height. The empirical constant (C) is 1.25 for in-line orifices configuration and 5 for staggered orifices configuration.

The following equation provides the maximum amount of penetration in the mixing zone in presence of multiple jets [52].

$$\frac{Y_{\max}}{d_j} = 1.25\sqrt{J}\,\frac{\dot{m}_{core}}{\dot{m}_{core} + \dot{m}_{jet}} \tag{10}$$

It should be noted that the wall-jet method results in larger mixing jets and lower efficiency in the mixing process. That is, the size of the large energy-containing eddies are bigger than those more advanced mixing concepts, in which case eddies with a larger range of size and turn-over time can create local areas of mixture with stoichiometric fuel- air ratio that create high levels of thermal NO_x. In other words, the poor quality of macro-mixing contributes to local stoichiometric burning.

Another important aspect of mixing in the mixing zone is the micro-mixing. After mixing of the quench air with core gases in macro-scales, the quality of the micro-mixing determines the flame temperature and emission levels. If one wants to model the whole macro and micro mixing process, then the turbulent modeling and chemical kinetic/flow interaction modeling is inevitable which is outside of the scope of the current research. To simplify the model, a characteristic mixing time is defined as the following equation.

$$\tau_{mix} = \frac{H_{MZ}^3}{\rho_{MZ}.\dot{m}_{MZ}} \tag{11}$$

To assess the mixing quality in the Mixing zone, an unmixedness parameter is defined as [8]:

$$unmixedness = \frac{\left\langle \tilde{f}''\tilde{f}'' \right\rangle}{\left(1 - \left\langle \tilde{f} \right\rangle\right)\left\langle \tilde{f} \right\rangle} \tag{12}$$

The unmixedness value ranges between 0 and 1, zero representing perfect mixing (where residence time is much longer than the mixing time) and one represents segregated mixture (very long mixing time).

The following equation relates the unmixedness to mixing time (τ_{mix}) and residence time(τ_{res}) [8].

$$unmixedness = \frac{1}{1 + C_{\phi}\,\tau_{res}/\tau_{mix}} \qquad (13)$$

where C_{φ} is a constant that is 1/3 for the Modfied Curl model.

Variable Geometry Off-Design

To account for the variable swirler geometry, which changes the pressure drop coefficient (dP/Q) of the burner section, the equivalent swirler effective area based on equation (4) is:

$$A_{swirler-effective} = \sqrt{K_{sw}\left(\sec\theta/\alpha.A_{sw}\right)^2 - \frac{n_{inj}}{A_{liner}^2}} \qquad (14)$$

Having the values from the on-design Rich zone model and given the swirler area multiplier (α) from a user-specified swirler area change schedule, one can determine the effective area of the swirler at any given off-design condition. Having the pressure drop coefficient calculated at off-design condition, the burner pressure drop is determined and then all objects are executed to determine the zone temperature, flow fractions and flow station properties.

Mixing Zone Off-Design

The Mixing zone component is linked to the Rich zone component through the flow station FS33. Similar to the Rich zone, the configuration may be “Annular” or “Tubular”. The cross section area at the mixing zone is reduced by the user-defined factor “MZtoPZ_areaRatio”. The number and size of the orifices at design condition is calculated using equations (8) and (9) and the maximum penetration is determined using equation (10). At Off-Design condition, the amount of the flow going through the mixing orifices is determined by the equations below.

$$\frac{\dot{m}_{MZ}}{\dot{m}_{tot}} = \frac{n_{MZ\_orifices}.\pi.D_{jet}^2.V_{jet}}{4.Area_{MZ}.V_{MZ}} \qquad (15)$$

$$V_{jet} = V_{ref}\sqrt{\frac{\Delta P}{Q}} \qquad (16)$$

For determining the Mixing zone exit temperature, the “Burn” function is not used. Assuming the ideal case of the perfect mixing and absence of any reaction, the exit temperature of the Mixing zone is simply the sum of the sensible enthalpies of air and core flows divided the total flow (Equation 17). The more accurate exit temperature will be determined later in the Chemical Reactor Network model.

$$T_{t\,MZ} = \frac{\dot{m}_{MZ}.h_{sensair}(T_{t\,ref}) + \dot{m}_{RZ}.h_{senscore}(T_{t\,RZ})}{\dot{m}_{MZ} + \dot{m}_{RZ}} \qquad (17)$$

Finally parameters related to the PaSR (Partially Stirred Reactor) model are calculated: the residence time of the Mixing zone:

$$\tau_{MZ\,residence} = \frac{Vol_{MZ}/2}{Area_{MZ}.V_{MZ}} \quad (18)$$

In equation (18), the volume is divided by two because the mixing flow is assumed to enter the MZ at the half-way point of the Mixing zone. The simulation time should be long enough so the solution of the PaSR reaches the steady state condition but not so long as to make the simulation very slow. It is defined to be 5 times of the residence time:

$$\tau_{MZ\,simulation} = 5.\tau_{MZ\,residence} \quad (19)$$

The mixing time in the Mixing zone and corresponding unmixedness value are determined using Equations (11) and (12). The time step of statistical samples that is required in the Monte Carlo simulation in the PaSR is set to one tenth of the Mixing zone residence time:

$$dt_{MCS\,MZ} = \frac{\tau_{MZ\,residence}}{10} \quad (20)$$

CreateCHEMKINInputs Object

The significant difference in the CreateCHEMKINInputs object relative to the SAC model is the additional equation to take into account the unmixedness in the Mixing zone. A simplified model is developed to model the macro-mixing and its quality in the mixing zone. The micro-mixing model is accounted for in the PaSR reactor of the CRN model.

The assumption for developing this model is that the perfectly mixed model (zero unmixedness) will burn in the Lean zone at the Lean zone equivalence ratio (which is well below one). As the Mixing zone unmixedness increases from zero to one, more and more of the mixture will burn at the unity equivalence ratio and the rest will burn at an equivalence ratio that is determined by the reamining air and fuel. The unmixedness value is an input from the Mixing zone object. A linear relationship is assumed between the Mixing zone unmixedness value and the equivalence ratio. The result is the equation which is shown below:

$$\dot{m}_{MZ\,un\text{-}mixed} = \frac{\dot{m}_{fuel}}{(far_{st} - far_{LZ}).(unmixedness_{MZ} - 1) + far_{st}} - \dot{m}_{RZ} \quad (21)$$

$$\dot{m}_{MZ\,mixed} = \dot{m}_{MZ} - \dot{m}_{MZ\,un\text{-}mixed} \quad (22)$$

References

1. Allaire, D.L., A Physics-Based Emissions Model for Aircraft Gas Turbine Combustors, Master's Thesis, Massachusetts Institute of Technology, May 2006
2. Andreini & Facchini, Gas Turbines Design and Off-Design Performance Analysis with Emissions Evaluation, Journal of Engineering for Gas Turbines & Power 126:83-91 (2004)
3. Bae, J.H. and C.T. Avedisian, Jet fuel droplet combustion with and without the convection, in 37th Intersociety Energy Conversion Engineering Conference (IECEC). 2002, IECEC: Washington, WA, USA.
4. Balakrihnan, G., and Williams, F.A., "Turbulent Combustion Regimes for Hypersonic Propulsion Employing Hydrogen-Air Diffusion Flames," Journal of Propulsion and Power, Vol. 10, No. 3, 1993, pp. 434-436.
5. Burrus, D., Sabla, P.E., and Bahr, D.W., Energy Efficient Engine Component Development and Integration Single-Annular Combustor Technology Report, NASA CR-159685, June 1980
6. Cai, Jeng & Tacina, The Structure of a Swirl-Stabilized Reacting Spray Issued from an Axial Swirler, AIAA paper 2005-1424
7. Chemkin software 4.1.1, Theory Manual, Chapter 9, 2007
8. Chen, J., Stochastic modeling of partially stirred reactors. Combustion Science and Technology, 1997. 122(1): p. 63-94.
9. Chen, R.H. The role of the recirculation vortex in improving fuel-air mixing within swirling flames. in Symposium(International) on Combustion, 22 nd. 1988. Seattle, WA: The Combustion Institute.
10. Chigier, N., Energy, combustion, and environment. 1981: McGraw-Hill Companies.
11. Chigier, N.A. and J.M. Beer. Velocity and static-pressure distributions in swirling air jets issuing from annular and divergent nozzles. in ASME Meeting FE-8, May 18-21 1964. 1964. New York, NY, United States: American Society of Mechanical Engineers (ASME).
12. Coordinating Research Council, Handbook of Aviation Fuel Properties. 1983, Society of Automotive Engineers (SAE): Atlanta, Ga. p. 113.
13. Correa, S.M., "Turbulence-chemistry interactions in the intermediate regime of premixed combustion," Combustion and Flame, Vol. 93, Issues 1-2, Pp 41-60 (April 1993)e
14. Dagaut, P., and Cathonnet, M., "The ignition, oxidation and combustion of kerosene: A review of experimental and kinetic modeling," Progress in Energy and Combustion Science, Vol.32, 2006, pp. 48-92.
15. Dagaut, P., Reuillon, Cathonnet, M. , and Voisin, D., " High Pressure Oxidation of Normal Decane and Kerosene in dilute from low to high temperature," Journal of Chemical Physics., Vol. 92, 1995, pp. 47-76.
16. Dagaut, P., Reuillon, M., Boettner, J.-C., and Cathonnet, M. , " Kerosene Combustion at Pressures up to 40 atm.: Experimental Study and Detailed Chemical Kinetic Modeling," Proceedings of the Combustion Institute., Vol. 25, 1994, pp. 919-926.
17. Dodds, W., Twin Annular Premixing Swirler (TAPS) Combustor, The Roaring 20th Aviation Noise & Air Quality Symposium, 2005
18. Dopazo, C., "Probability density function approach for a turbulent axisymmetric heated jet Centerline evolution" Physics of Fluids, vol.18, pp397 (1975).
19. Elliot, L., Ingham, D.B., Kyne, A.G., N.S. Mera, Pourkashanian, M., and Wilson, C.W.,"A novel approach to mechanism reduction optimization for aviation fuel/air reaction mechanism using a genetic algorithm," Proceedings of ASME Turbo Expo 2004, June 14-17, 2004.
20. Gogineni, S., et al., Combustion Air Jet Influence on Primary Zone Characteristics for Gas Turbine Combustors. Journal of Propulsion and Power, 2002. 18(2): p. 407-416.
21. Grisch, F., Orain, M., Rossow, B., Jourdanneau, E., and Guin, C., Simultaneous Equivalence Ratio and Flame Structure Measurements in Multipoint Injector Using PLIF, AIAA 2008-4868.

22. Heywood, J.B. and T. Mikus, Parameter Controlling Nitric Oxide Emissions from Gas Turbine Combustors, in AGARD Propulsion and Energetic Panel 41st Meeting on Atmospheric Pollution by Aircraft Engines. 1973: London, England.
23. Honnet, S., Seshadri, K., Niemann, U., and Peters, N.,"A surrogate fuel for kerosene," Proceedings of the Combustion Institute, Vol.32, 2009, pp. 485-492.
24. http://commons.wikimedia.org/wiki/File:Combustor_diagram_airflow.png
25. Jachimowski, C.J., "An Analytical study of the Hydrogen-Air Reaction Mechanism with Application to Scramjet Combustion" , NASA TP-2791, 1988.
26. Janicka, J., Kolbe, W. and Kollmann,W., Journal of Non-equilibrium Thermodynamics 4:47-(1979).
27. Kollrack, R., "Model calculations of the combustion product distribution in the primary zone of a gas turbine combustor," ASME Winter Annual Meeting, Paper No. 76-WA/GT, 1976.
28. Lefebvre, A.H., Gas Turbine Combustion. 2 ed. 1999, Philadelphia, PA: Taylor & Francis.
29. Lepinette, A., Linan, A., and Lazaro, B., "Reduced kinetics and coupling functions for calculating CO and NO emissions in gas-turbine combustion," Combustion Science and Technology, Vol. 177, 2005, pp. 907-931.
30. Lindstedt, R. P. and Maurice, L. Q., "A Detailed Chemical-Kinetic Model for Aviation Fuels", AIAA Journal of Propulsion and Power, Vol. 16, No. 2, 2000, p. 187.
31. Luche, J., Reuillon, M., Boettner, J.-C., and Cathonnet, M., "Reduction of large detailed kinetic mechanism: Application to kerosene/air combustion," Combustion Science and Technology, Vol. 176, 2004, pp. 1935-1963.
32. Mattingly, J. D. et al., "Aircraft Engine Design", AIAA Education Series. New York, 1987.
33. Matuszewski, L., Dupoirieux, F., Guin, C., and Grisch, F., "Numerical calculation of the NO formation in a multi-point combustion chamber and results of the associated validation experiments,", ONERA. Same as 6!
34. Maurice, L. Q. et al., "Emissions from Combustion of Hydrocarbons in a Well-Stirred Reactor", AIAA 99-1038, 1999.
35. Mawid, M. A. and Park, T. W., "Development of a Detailed Chemical Kinetic Mechanism for Combustion of JP-7 Fuel", AIAA-2003-4939, 39th AIAA/ASME/SAE Joint Propulsion Conference and Exhibit, Hutsville, Alabama, July 2003
36. McKinney, R.G., et al., The Pratt & Whitney TALON X Low Emissions Combustor: Revolutionary Results with Evolutionary Technology,2007
37. Mellor, A.M., Design of Modern Turbine Combustors. 1990, San Diego, CA: Academic Press.
38. Mongia, H., GE Aviation Low Emissions Combustion Technology Evolution, AIAA, 2008
39. Mongia, H., TAPS – A 4th Generation Propulsion Combustor Technology for Low Emissions, AIAA 2003-2657
40. Mongia, H.C., Aero-thermal design and analysis of gas turbine combustion systems - Current status and future direction in 34th AIAA/ASME/SAE/ASEE Joint Propulsion Conference and Exhibit, . 1998, AIAA: Cleveland, OH.
41. Montgomery, C. J. et al.' "Reduced Chemical kinetic Mechanism for Hydrocarbon Fuels", AIAA Journal of Propulsion and Power, Vol. 18, No. 1, 2002, p. 192.
42. Patterson, P.M., Kyne, A.G., Pourkashanian, M., Williams, A., and Wilson, C.W., "Combustion of Kerosene in Counterflow Diffusion Flames," Journal of Propulsion and Power, Vol.16, 2000, pp. 453-460.
43. Pope,S.B., Combustion Science and Technology 25:159-174 (1981)
44. Pratt & Whitney and General Electric, Critical Propulsion Components Volume 2: Combustor, NASA CR-2005-213584, 2005
45. Rizk & Mongia, Emissions Predictions of Different Gas Turbine Combustors, AIAA 94-0118
46. Rizk & Mongia, Semianalytical Correlations for NOx, CO, and UHC Emissions, Journal of Engineering for Gas Turbines & Power 115:612-19 (1993)
47. Rizk & Mongia, Three-Dimensional NOx Model for Rich/Lean Combustion, AIAA 93-0251

48. Rizk, N.K. et al, Predictions of Nox Formation Under Combined Droplet and Partially Premixed Reaction of Diffusion Flame Combustors, Journal of Engineering for Gas Turbines and Power, Vol. 124, January 2002, pp. 31-38
49. Roberts, R., Aceto, L.D., Kollrack, R., Texeira, D.P., and Bonnell, J.M., "An analytical model for nitric oxide formation in a gas turbine combustor," AIAA journal, Vol. 19, No. 6. 1972, pp. 820-826.
50. Roberts, Richard. et al, "An Analytical Model for Nitric oxide formation in a gas turbine combustor", AIAA Journal, Vol. 10, No. 6, June 1972, pp 820-826
51. Rosfjord, T.J., Aviation-fuel property effects on combustion. 1984, NASA Center.
52. Samuelson, S., Rich Burn, Quick-Mix, Lean Burn (RQL) Combustor, in The Gas Turbine Handbook, National Energy Technology Laboratory, Editor. 2006, U.S. Department of Energy, Office of Fossil Energy.
53. Sazhin, S.S., et al., Models for droplet transient heating: effects on droplet evaporation, ignition, and break-up. Int J Thermal Science, 2005. 44: p. 610–622.
54. Schulz, W., ACS petrol. Chem. Div. Preprints 37 (2), 1991, pp. 383-392.
55. Smith, G.P., et al, "GRI mech 3.0", http://www.me.berkeley.edu/gri_mech/
56. Smith, R., et al., Advanced Low Emissions Subsonic Combustor Study. 1998, NASA Center: Glenn Research Center.
57. Strelkova, M.I., Kirilov, I.A., Potapkin, B.V., Safonov, A.A., Sukhanov, L.P., Umanskiy, S.Ya, Deminsky, M.A., Dean, A.J., Varatharajan, B., and Tentner, A.M., "Detailed and reduced mechanism of jet A combustion at high temperatures", Combustion science and technology, Vol. 180, 2008, pp. 1788-1802.
58. Sturgess, G.J., et al, Emissions Reduction Technologies for Military Gas Turbine Engines, AIAA Journal of Propulsion and Power, Vol. 21, No. 2, March-April 2005
59. Turns, S.R., An introduction to combustion. 2 ed. 1996, New York: McGraw-Hill
60. Wood, McDonell, "Development and Application of a Surrogate Distillate Fuel", AIAA Journal of P&P, Vol4 (5), pp399, 1989